Journal Name

Crossmark
RECEIVED
dd Month yyyy
REVISED
dd Month yyyy

PAPER

From Circuits to Hardware: Benchmarking Standard and Qubit-Efficient Quantum Optimization on Real Hardware

Monit Sharma[1] and Hoong Chuin Lau[1,2*]

[1]School of Computing and Information Systems, Singapore Management University, Singapore
[2]Institute of High Performance Computing, A*STAR, Singapore
*Author to whom any correspondence should be addressed.

E-mail: monitsharma,hclau@smu.edu.sg

Keywords: quantum optimization, benchmarking, variational quantum eigensolver, QAOA, qubit-efficient encoding, combinatorial optimization, NISQ

Abstract
Despite rapid progress in quantum optimization, the field lacks broad real-hardware benchmarks comparing multiple algorithmic families across diverse classically hard combinatorial problems under one protocol. We present a hardware-aware benchmark of gate-based quantum optimization across four NP-hard problems: the multi-dimensional knapsack problem (MDKP), maximum independent set (MIS), quadratic assignment problem (QAP), and market-share problem (MSP), spanning variational methods (VQE, CVaR-VQE), standard, multi-angle, and warm-start QAOA, and qubit-efficient encodings (PCE, QRAO), executed on IBM Heron r1/r2 processors under resilience-level-2 mitigation. To our knowledge this includes the first real-hardware QRAO results and the first multi-problem PCE hardware benchmark.
Across 247 method–instance combinations we report transpiled circuit size, an independent-error gate-count fidelity proxy F_{est}, and hardware outcomes. An empirical operating point near $F_{\text{est}} \approx 0.1$ ($\sim$770 two-qubit gates at the median Heron-r2 CZ error rate) marks the transition to noise-dominated execution in the MDKP and MIS regimes. Two limitations emerge. QAP couples dense one-hot encodings with an exponentially sparse feasible manifold (feasible fraction $10!/2^{100}$ at n=10); no tested hardware method returns a feasible assignment. The tested QAOA-family circuits become noise-dominated after compilation, and a matched uniform-random control shows most feasible low-fidelity outcomes lie within the random range, with one MIS warm-start result reported as a finite-sample exception. A compilation counterfactual (SWAP-aware, fractional-gate, Nighthawk-topology) reduces two-qubit counts but moves no circuit above $F_{\text{est}} = 10^{-3}$; conclusions therefore apply to the tested implementations, not QAOA in general. Qubit-efficient methods extend runnable instance sizes but gain only within the empirical fidelity budget.[1]

1 Introduction

Benchmarking quantum optimization methods under realistic execution conditions remains an open challenge [1]. Although gate-based quantum algorithms such as the Variational Quantum Eigensolver (VQE) [2], Conditional Value-at-Risk VQE (CVaR-VQE) [3], and the Quantum Approximate Optimization Algorithm (QAOA) [4] have been widely studied for combinatorial optimization, existing evaluations are often limited to a single problem class, a single algorithm family, or simulator-based settings that do not fully reflect the practical constraints of present-day quantum hardware. As a result, it remains difficult to assess how different quantum optimization strategies compare under a unified protocol when compilation overhead, qubit connectivity, gate noise, and execution variability are taken into account.

This limitation is particularly important because the empirical performance of quantum optimization methods depends on more than the nominal algorithm alone. In practice, performance is shaped by a layered interaction between problem formulation, encoding strategy,

[1]Code available at: https://github.com/SMU-Quantum/quantum-optimization-benchmarks

arXiv:2607.11637v1 [quant-ph] 13 Jul 2026

circuit structure, transpilation overhead, and backend-specific noise processes. Methods that appear competitive before transpilation may degrade substantially after routing and compilation, while approaches that reduce algorithm-level circuit width may introduce different costs in circuit depth, classical post-processing overhead, or hardware robustness. A meaningful comparison therefore requires a benchmark that goes beyond idealized resource estimates and instead evaluates methods under realistic execution conditions.

These issues are especially relevant for comparisons between standard variational methods and qubit-efficient approaches. Variational energy-minimization methods such as VQE and CVaR-VQE operate directly on problem Hamiltonians, while QAOA-style methods exploit structured alternating operators. In contrast, encoding or reduction techniques such as Pauli Correlation Encoding (PCE) [5] and Quantum Random Access Optimization (QRAO) [6] aim to compress the problem representation or transform it into a more hardware-manageable form. Such methods can expand the range of instances that are runnable on current devices by reducing algorithm-level circuit width, but the practical value of this compression depends on whether the resulting circuits remain executable after transpilation and whether the recovered solutions remain robust under hardware noise.Consequently, qubit count alone is not a sufficient indicator of practical performance.

Despite growing interest in quantum optimization benchmarks [1, 7, 8, 9, 10, 11, 12, 13], broad real-hardware comparisons across multiple hard combinatorial problems (such as [14, 15, 16]) and multiple algorithmic families remain limited. Much of the existing literature focuses either on a single optimization method, a narrow benchmark family, or simulator-based assessments that do not expose the full gap between algorithmic design and hardware-realized behavior. This makes it difficult to separate algorithmic effects from encoding effects, and to determine when qubit-efficient formulations offer a genuine practical advantage rather than only a nominal reduction in width. It also limits the ability of the community to compare methods using consistent metrics and reproducible evaluation criteria.

In this work, we present a hardware-aware benchmarking study of gate-based quantum optimization methods across four classically hard combinatorial optimization problem classes: the Multi-Dimensional Knapsack Problem (MDKP) [17], Maximum Independent Set (MIS) [18], Quadratic Assignment Problem (QAP) [19], and Market Share Problem (MSP) [20]. These problems were chosen to span structurally diverse binary optimization regimes, including packing-type constraints, graph-based independence structure, strongly coupled quadratic assignment structure, and application-driven balancing constraints. Our benchmark includes variational energy-minimization methods (VQE and CVaR-VQE), QAOA-style approaches, and qubit-efficient encoding or reduction methods, including PCE and QRAO. Rather than focusing only on final objective values, we evaluate a broader set of metrics that affect performance on current hardware, including qubit requirements, transpiled circuit depth, total and two-qubit gate counts, compilation overhead, feasibility of execution, and execution robustness across real quantum processors.

The goal of this study is not to claim a practical quantum advantage, but to establish a systematic empirical baseline for assessing quantum optimization methods under realistic constraints. In particular, we seek to understand three questions: how different algorithmic families behave across structurally different hard problem classes, how algorithmic resource savings translate into hardware-realized behavior after transpilation, and how strongly simulator-based expectations align with real-device outcomes. This perspective is important for near-term benchmarking because conclusions drawn from idealized simulations may not persist once routing overhead and backend noise are taken into account.

Our empirical results show that practical performance is strongly shaped by the interaction between encoding choice and hardware constraints. Across the tested problems and backends, lower qubit count does not consistently imply better final performance on hardware. In several cases, qubit-efficient methods extend the range of runnable instances, but the resulting gains are partly offset by transpilation overhead, increased effective circuit depth, or degraded robustness during execution. Conversely, methods that are competitive in simulation may become substantially less effective after mapping to hardware-native gate sets and coupling graphs. These findings reinforce the need for benchmark protocols that report not only solution quality but also the compilation and execution characteristics that determine whether a method is practically deployable on current devices.

The main contributions of this paper are as follows:

- We present the first unified benchmark of multiple gate-based quantum optimization families (variational, QAOA-style, and qubit-efficient) evaluated across four structurally distinct

NP-hard combinatorial optimization problems under a common consistent experimental protocol. This breadth enables direct cross-family and cross-problem comparison that has not previously been reported in the literature.

- We evaluate these methods under a hardware-aware protocol that goes beyond solution quality to include qubit requirements, transpiled circuit depth, gate counts, compilation overhead, and execution robustness on real quantum hardware (IBM Heron processors). By treating these compilation and execution characteristics as primary benchmark dimensions rather than engineering footnotes, we provide a more complete picture of practical deployability on current devices.
- We provide a quantitative noise model derived from backend calibration data and use it to establish an empirically grounded fidelity threshold that distinguishes signal-preserving from noise-dominated execution. This threshold clarifies when qubit-efficient encodings provide genuine practical benefit and when compilation overhead erodes their advantage, yielding actionable guidance for method selection on near-term hardware.
- We establish a fully reproducible empirical baseline, namely software stack, backend metadata, transpilation policy, and per-instance execution diagnostics, for future benchmarking studies of quantum optimization on realistic devices. All code and benchmark instances are publicly available, enabling direct comparison with methods developed as hardware continues to improve.

The remainder of the paper is organized as follows. Section 2 reviews the relevant quantum optimization methods and benchmarking context. Section 3 describes the benchmark problems, evaluation metrics, and experimental protocol. Section 4 presents the optimization methods, encodings, and hardware execution workflow. Section 5 reports the benchmark results on simulators and real quantum hardware. Section 6 discusses the main empirical insights and their implications for near-term quantum optimization. Section 7 concludes the paper.

2 Background and Related Work

2.1 Gate-based quantum optimization methods

Gate-based quantum optimization for combinatorial problems is commonly studied through variational hybrid algorithms, where a parameterized quantum circuit prepares candidate states and a classical optimizer updates the circuit parameters based on measurement outcomes. Among the most widely used approaches are the Variational Quantum Eigensolver (VQE) and the Quantum Approximate Optimization Algorithm (QAOA), together with several variants designed to improve robustness, trainability, or sampling quality [2, 4, 21, 22].

In the optimization setting, the goal is to prepare low-energy states of a problem Hamiltonian whose ground-state structure encodes high-quality classical solutions. VQE typically uses a hardware-efficient or structured ansätze and minimizes the expectation value of the Hamiltonian through iterative classical optimization. This formulation is flexible and can be applied across a wide range of problems, but its empirical behavior depends strongly on the chosen ansätze, optimizer, measurement budget, and hardware noise [23, 24].

QAOA adopts a more structured strategy based on alternating applications of a problem Hamiltonian and a mixing Hamiltonian [4, 22]. Its problem-informed circuit structure has made it one of the central methods in quantum optimization, particularly for graph and constraint-based binary problems. Several variants have been proposed to improve practical performance, including warm-start approaches, multi-angle parameterizations, and risk-sensitive objectives such as Conditional Value-at-Risk (CVaR) optimization [3, 25, 26]. In practice, however, both VQE- and QAOA-style methods face similar near-term limitations: circuit depth grows under transpilation, two-qubit gates dominate hardware error, and performance can degrade substantially when mapped to sparse-connectivity devices.

A key point for benchmarking is that these methods should not be compared only at the level of idealized pre-transpiled circuits. Their practical behavior depends on how the encoded Hamiltonian interacts with ansätze structure, routing overhead, hardware-native gate sets, and sampling noise. This motivates the hardware-aware perspective adopted in this work.

2.2 Qubit-efficient encodings and reduction strategies

Alongside standard variational approaches, a growing line of work studies qubit-efficient encodings and reduction methods that attempt to make larger optimization problems accessible on current

hardware by reducing qubit requirements [5, 6]. Two representative examples considered in this paper are Pauli Correlation Encoding (PCE) and Quantum Random Access Optimization (QRAO).

PCE reformulates the original binary optimization problem into a reduced quantum representation by embedding binary decision structure into correlations among Pauli observables, typically after an intermediate reduction to a related quadratic form such as weighted Max-Cut [5]. The central motivation is to trade algorithm-level circuit width against more involved encoding, correlator reconstruction, rounding, and classical post-processing. QRAO follows a related compression philosophy, using quantum random access codes to encode multiple classical bits into fewer qubits and then recover approximate classical solutions through rounding procedures [6]. These approaches are attractive for near-term hardware because qubit availability remains a dominant bottleneck. Their practical value, however, must be assessed through the full execution stack, including encoding, compilation, measurement, correlator reconstruction or QRAC rounding, feasibility checks, and any method-specific local search.

For this reason, qubit-efficient methods are evaluated using the same practical criteria as standard variational methods: final objective quality, backend eligibility, transpiled circuit size, compilation overhead, and execution robustness. A central purpose of the present benchmark is to assess these trade-offs empirically across multiple problem classes.

2.3 Benchmarking quantum optimization

Contemporary efforts to establish broader benchmarks for quantum optimization fall into three complementary categories. First, instance-library initiatives such as the Quantum Optimization Benchmarking Library (QOBLIB) [7] have assembled curated collections of classically hard combinatorial problems to support reproducible cross-study comparison. Our benchmark draws on problem families consistent with QOBLIB but extends the evaluation to multiple method families executed on real quantum processors. Second, cross-platform hardware studies such as McDowall *et al.* [27] compare near-term quantum optimization algorithms across multiple processor architectures, focusing on how algorithmic performance depends on backend choice. Our study is complementary in scope: we focus on a single processor family (IBM Heron r1/r2) but span a wider range of method families and problem classes, and we additionally provide a quantitative noise model linking benchmark outcomes to backend calibration data. Method-specific benchmarking studies further show that reported VQA performance can depend materially on ansatz construction, hyperparameter selection, optimizer cost, and the choice of fixed-resource classical comparators. In particular, Turati *et al.* [28] benchmark adaptive VQAs and QAOA on QUBO instances, while Schwägerl *et al.* [29] study VQA performance for combinatorial optimization under fixed practical resource budgets relative to sampling and greedy baselines.

Third, protocol-level methodology work such as Abbas *et al.* [1] and Lubinski *et al.* [8] proposes evaluation standards for quantum optimization. The present study implements several of the practices these works advocate; backend metadata logging, transpiled resource accounting, shot-budget reporting, and feasibility tracking, and treats them as first-class benchmark dimensions rather than engineering details.

Despite these efforts, broad real-hardware comparisons across multiple hard combinatorial problems and multiple algorithmic families remain limited. Much of the existing literature focuses either on a single optimization method, a narrow benchmark family, or simulator-based assessments that do not expose the full gap between algorithmic design and hardware-realized behaviour. This makes it difficult to separate algorithmic effects from encoding effects, and to determine when qubit-efficient formulations offer a genuine practical advantage rather than only a nominal reduction in width. Relative to these efforts, the present paper contributes the deepest hardware-facing diagnostic analysis to date across multiple algorithmic families on structurally distinct NP-hard binary problems, tied to an explicit and reproducible process-fidelity model.

2.4 Position of the present work

The present paper is designed to address this gap through a unified, hardware-aware benchmark spanning multiple algorithmic families and multiple structurally distinct NP-hard problems. Rather than isolating one method or one problem class, we compare standard variational energy-minimization methods, QAOA-style methods, and qubit-efficient encodings within a common experimental protocol. Our emphasis is not only on solution quality, but also on the practical execution characteristics that determine whether a method is usable on current devices, including qubit requirements, transpiled depth, gate counts, compilation overhead, and execution robustness.

This perspective places the paper closer to a benchmarking and methodology contribution than to a single-algorithm performance study. In particular, it complements simulator-based comparative studies by quantifying the gap between algorithmic-level design and hardware-realized behavior, and it extends narrower hardware studies by broadening both the algorithmic and problem-level scope. The resulting benchmark is intended to serve as a reproducible baseline for future work on quantum optimization under realistic execution constraints.

3 Benchmark Design

3.1 Design objectives

The benchmark is designed to evaluate quantum optimization methods under a unified and hardware-aware protocol across multiple classes of hard binary optimization problems. Our objective is not merely to compare final objective values, but to assess how algorithmic families behave when differences in problem structure, encoding strategy, and hardware execution are taken into account. To this end, the benchmark was constructed around four design principles.

First, the selected problems should be classically hard and structurally diverse. A benchmark restricted to a single family may reflect problem-specific biases rather than general algorithmic behavior. We therefore include problem classes with substantially different constraint and interaction structure, ranging from packing-type constraints to graph-based exclusivity, strongly coupled quadratic assignment structure, and application-driven balancing constraints.

Second, the benchmark should include method families with distinct resource trade-offs. In particular, we compare standard variational methods, QAOA-style approaches, and qubit-efficient encoding or reduction strategies. This makes it possible to assess not only which methods perform well on a given problem, but also how algorithm-level width reduction interacts with compilation and noise.

Third, the evaluation should reflect realistic execution conditions. Metrics such as algorithmic-level circuit width and noiseless simulator objective value are informative, but insufficient for understanding performance on current devices. We therefore include hardware-facing diagnostics such as transpiled circuit depth, total and two-qubit gate counts, compilation overhead, backend eligibility, and execution robustness.

Fourth, the benchmark should support fair comparison across methods and problem instances. All methods are evaluated on common benchmark families with consistent reporting of solution quality, feasibility, and execution characteristics. This allows algorithmic and encoding effects to be interpreted within a shared experimental framework rather than through isolated case studies.

3.2 Terminology and reporting conventions

We use *algorithm-level circuit width*, to mean the number of circuit wires in the encoded circuit before hardware-aware transpilation. For direct QUBO formulations, number of qubits normally equals the number of encoded binary variables. For PCE and QRAO, it is the number of circuit wires after the respective compression mapping.

This quantity is not a fault-tolerant logical-qubit count and should not be interpreted as such. When a physical-qubit count is reported, it refers to the device qubits occupied by the transpiled layout and may differ from pre-transpiled qubits, because layout, routing, and ancillary wires can alter the hardware realization.

We use *classical post-processing* as the umbrella term for the method-specific operations that turn measurement outcomes into reported candidates. For direct VQE, CVaR-VQE, and QAOA-style methods, this consists of bitstring interpretation, original-problem scoring, and best-candidate selection. For PCE, the corresponding operation is correlator reconstruction; for QRAO, it is QRAC rounding. We use *feasibility repair* only when a procedure explicitly modifies a candidate to restore constraint satisfaction, and *local search* only for an explicit objective-improving neighborhood search. These operations are reported separately rather than being collectively called "decoding."

3.3 Benchmark problem classes and instance scope

We consider four NP-hard 0–1 combinatorial optimization problem classes: the Multi-Dimensional Knapsack Problem (MDKP) [17, 30], Maximum Independent Set (MIS) [18, 31], Quadratic Assignment Problem (QAP) [19, 32, 33], and Market Share Problem (MSP) [20, 34]. These problems were selected to cover complementary structural regimes: packing constraints, graph-induced exclusivity, dense assignment interactions, and target-allocation balancing. This diversity is important because near-term quantum optimization performance depends not only on

nominal problem size, but also on constraint density, interaction structure, encoding overhead, and compiled circuit complexity.

Multi-Dimensional Knapsack Problem (MDKP). MDKP generalizes the classical knapsack problem by imposing multiple resource constraints [17, 30, 35]. Given item profits and several capacity dimensions, the goal is to select a subset of items that maximizes total value while satisfying all resource limits. In this benchmark, MDKP represents a packing problem in which feasibility and constraint handling are central to performance evaluation.

Maximum Independent Set (MIS). MIS asks for the largest subset of mutually nonadjacent vertices in a graph [18, 31]. Its graph-induced exclusivity structure maps naturally to quadratic binary objectives and provides a contrast to capacity-constrained packing formulations such as MDKP.

Quadratic Assignment Problem (QAP). QAP assigns facilities to locations so as to minimize a quadratic flow-distance cost [19, 32, 33]. Its dense pairwise couplings and strict assignment structure make it the most demanding family in the benchmark from the standpoint of encoded Hamiltonian density and compiled circuit growth.

Market Share Problem (MSP). MSP is an application-driven binary optimization problem in which selected decisions must match prescribed market-share or allocation targets [20, 34]. It differs from the other three families because solution quality is naturally measured by target deviation rather than by a conventional profit or cost gap alone.

For each problem class, we select instances that are nontrivial relative to current quantum optimization methods while remaining within the executable regime of at least some compared approaches after encoding and compilation. The reference "Optimal" or "BKS" values reported in the result tables are taken from the corresponding benchmark sources [36, 37, 33, 34] and are used only as evaluation targets for gap or deviation reporting. This intermediate benchmark regime reveals how practical viability changes with encoded width, coupling density, transpilation burden, and hardware noise.

3.4 Compared method families

The benchmark includes three broad categories of gate-based quantum optimization methods.

Variational energy-minimization methods. These include VQE and CVaR-VQE, which optimize parameterized circuits with respect to the expectation value or a risk-sensitive tail objective derived from the measured energy distribution. These methods provide a flexible baseline and are representative of a large portion of near-term quantum optimization literature.

QAOA-style methods. This category includes standard QAOA, warm-start QAOA, and multi-angle QAOA. The benchmark evaluates these three concrete implementations under a fixed depth-selection, parameter-optimization, compilation, and hardware-execution protocol. The results should therefore not be interpreted as a universal statement about all QAOA variants. In particular, routing-specialized QAOA compilation, SWAP-network constructions, fixed-schedule linear-ramp QAOA, and spectral-gap-informed parameter schedules are distinct protocol families with different parameter-selection and compilation assumptions [38, 39, 40].

Qubit-efficient encodings and reductions. This category includes PCE and QRAO, which aim to reduce qubit requirements by compressing or reformulating the optimization problem before quantum execution. These methods are especially relevant in the present benchmarking regime because qubit availability is often the first practical bottleneck on current hardware.

The purpose of this classification is not to impose strict boundaries between all algorithmic variants, but to compare representative optimization strategies with meaningfully different width-depth-decoding trade-offs.

3.5 Evaluation metrics

To support a hardware-aware comparison, we report metrics from four complementary categories.

Solution quality. We evaluate the best solution obtained by each method relative to a classical reference, using feasibility status and a problem-appropriate quality metric. For MDKP, MIS, and QAP, solution quality is reported through the optimality gap to the best-known or classically certified reference value:

$$\mathrm{Gap}(\%) = 100 \times \frac{|z_{\mathrm{ref}} - z_{\mathrm{alg}}|}{|z_{\mathrm{ref}}|}, \tag{1}$$

where z_{ref} is the classical reference value and z_{alg} is the objective value recovered by the quantum method.

For the Market Share Problem (MSP), however, the classical optimal objectives are small integer deviation values. In this setting, percentage optimality gaps can be misleading or unstable: a change of only a few deviation units may produce a large percentage gap, even though the operational interpretation is better captured directly by the deviation from the target allocation. We therefore report MSP quality using the total absolute deviation

$$\mathrm{TDev} = \sum_i |A_i(\mathbf{x}) - T_i|\,, \tag{2}$$

where $A_i(\mathbf{x})$ denotes the achieved allocation for target category i under solution $\mathbf{x}$, and T_i is the corresponding prescribed target. Lower TDev indicates a better market-share match, with $\mathrm{TDev} = 0$ corresponding to an exact target match when such a solution is attainable. For MSP tables, we also report the maximum single-category deviation, denoted MDev, to indicate whether the total deviation is spread across many categories or concentrated in one large imbalance.

To permit comparison across MSP instances with different target scales, we additionally report the range-normalized TDev approximation ratio

$$\mathrm{AR}_{\mathrm{TDev}}(\mathbf{x}) = \frac{\mathrm{TDev}_I^{\max} - \mathrm{TDev}(\mathbf{x})}{\mathrm{TDev}_I^{\max} - \mathrm{TDev}_I^{\star}}. \tag{3}$$

where $\mathrm{TDev}_I^{\star}$ and $\mathrm{TDev}_I^{\max}$ are respectively the classically certified minimum and maximum TDev values over the original feasible decision domain for MSP instance I. Thus, $\mathrm{AR}_{\mathrm{TDev}} = 1$ denotes the certified minimum-TDev solution, whereas $\mathrm{AR}_{\mathrm{TDev}} = 0$ denotes the worst feasible target mismatch. TDev remains the primary application-level metric because the normalized ratio alone does not convey the absolute magnitude of the market-share deviation.

For constrained problems, feasibility is reported explicitly because near-optimal but infeasible solutions are not operationally comparable to feasible ones. Where relevant, additional measures of violation magnitude are also reported.

Algorithm-level circuit width. We record the algorithm-level circuit width, number of qubits, required by each encoding or method. This is the pre-transpilation width defined in Sec. 3.2, not a fault-tolerant logical-qubit count. It is particularly important when comparing standard formulations against qubit-efficient strategies, since reduced algorithm-level width is one of the main claimed advantages of encoding-based methods.

Compiled circuit characteristics. Algorithm-level resource counts alone do not capture hardware difficulty. We therefore also report post-transpilation metrics, including circuit depth, total gate count, and two-qubit gate count after mapping to the target backend. These quantities provide a more realistic picture of execution cost and noise exposure.

Compiled circuit characteristics. Algorithm-level resource counts alone do not capture hardware difficulty. We therefore record both pre-transpilation and post-transpilation circuit metrics: algorithm-level depth and two-qubit-gate count before backend mapping, together with transpiled depth, total gate count, and two-qubit-gate count after routing, native-basis decomposition, and scheduling on the target processor. The difference between these two descriptions quantifies compilation expansion under hardware connectivity constraints. For the representative QAOA-family circuits shown in Figure 4, historical transpilation increases two-qubit-gate counts by a factor of 4.47–6.24 across all four problem families.

Execution robustness. Finally, we assess practical hardware behavior through metrics such as the number of successful jobs, evaluation counts, shot budgets, latency summaries, and overall execution stability across repeated runs. These diagnostics are important because current-device

benchmarking is affected not only by nominal circuit size, but also by queueing, job failures, and backend-specific variability.

Taken together, these metrics allow us to distinguish between methods that look attractive at the algorithm-level design stage and methods that remain competitive after compilation and hardware execution.

3.6 Fairness and comparison protocol

A central challenge in benchmarking quantum optimization methods is ensuring that comparisons remain meaningful across methods with different operating principles. In this work, fairness is enforced at the level of benchmark instances, evaluation criteria, quantum-evaluation budget, and final candidate-processing protocol rather than by forcing every method into an artificially identical parameterization.

All compared methods are evaluated on the same benchmark families and judged using the same core outcome measures: solution quality, feasibility, algorithm-level circuit width, compiled circuit characteristics, and execution robustness. Classical reference solutions are used to anchor performance interpretation. Where a method produces probabilistic outputs, the reported solution is obtained through the method-specific classical post-processing procedure defined in Sec. 3.2. This makes reconstruction, rounding, repair, and local-search stages explicit rather than conflating them under the single term "decoding."

At the same time, we avoid conflating fundamentally different notions of resource use. In particular, algorithm-level circuit width, transpiled gate counts, and execution success statistics are reported separately rather than merged into a single composite score. This makes it possible to identify the source of a method's strengths or limitations more precisely.

This distinction is important for qubit-efficient methods. PCE's correlator-sign reconstruction and QRAO's rounding rule are native decoding steps required to map their compressed quantum representations back to binary decision variables. They are distinct from the subsequent shared local-improvement routine. We therefore do not attribute the final performance of PCE or QRAO solely to their quantum circuits; the reported values reflect their complete documented pipeline, as do the results for all other method families.

At the same time, we avoid conflating fundamentally different notions of resource use. In particular, algorithm-level circuit width, transpiled gate counts, and execution success statistics are reported separately rather than merged into a single composite score.

3.7 Simulator and hardware scope

The benchmark includes both simulator-based and real-hardware evaluations, since the two provide complementary information. Simulators offer a controlled setting for comparing algorithmic behavior without device-specific noise, queueing, or availability effects, whereas hardware runs reveal how those expectations change after compilation, routing, and execution on present-day processors. This distinction is particularly important for width-reduction strategies, whose apparent advantages at the encoding level may weaken or change after transpilation.

The benchmark is therefore empirical in scope. It is not intended to establish asymptotic superiority among quantum optimization families or to claim practical quantum advantage over classical methods. Rather, it provides a reproducible baseline for characterizing the current operating regime of representative gate-based quantum optimization methods on classically hard benchmark problems, including executability, solution quality, and the simulator–hardware gap under realistic resource constraints.

4 Methods

4.1 Problem-to-QUBO workflow

All benchmark instances are first expressed as binary optimization models and then converted into Quadratic Unconstrained Binary Optimization (QUBO) form. This QUBO–Ising workflow follows the standard equivalence between binary quadratic optimization and Ising Hamiltonian formulations, which has become a common interface between combinatorial optimization and quantum optimization methods [41, 42]. This common representation enables the application of multiple gate-based quantum optimization methods within a unified pipeline. For constrained problems, the QUBO is obtained by incorporating constraint violations into the objective through quadratic penalty terms, yielding an unconstrained binary model whose low-energy states correspond to high-quality solutions of the original problem.

The use of a common QUBO representation serves two purposes. First, it standardizes the input format across structurally different benchmark problems, allowing multiple algorithmic

Table 1. Compact structural profile of the benchmark QUBOs. N_Q is QUBO width, ρ_Q is coupling density, R_Q is the coefficient dynamic range, and R_λ is the penalty-to-objective scale ratio. R_Q is reported as an across-instance range; ρ_Q and R_λ are reported as family medians. Full per-instance values are provided in Appendix A.

Problem	Inst.	N_Q range	Median ρ_Q	R_Q range	Median R_λ	Dominant encoded structure
MDKP	12	45–122	0.678	8.53×10^3–6.75×10^5	4.78	Capacity and slack-induced couplings
MIS	7	8–128	0.181	9–129	65.0	Sparse graph-induced edge couplings
QAP	11	100–144	0.818	1.07×10^5–2.21×10^{10}	389.3	Dense row–column one-hot assignment encoding
MSP	8	48–156	0.589	9.86×10^4–1.70×10^6	14.7	Target-allocation and balancing penalties

families to be compared within the same evaluation framework. Second, it enables a consistent transition from classical binary models to quantum Hamiltonians. Each QUBO is mapped to an Ising-type cost Hamiltonian, which is then used either directly in variational energy-minimization methods or indirectly through encoding and reduction techniques such as PCE and QRAO.

4.2 Structural descriptors of the benchmark QUBOs

The common QUBO–Ising workflow produces structurally different optimization landscapes across the four benchmark families. Table 1 therefore reports the QUBO width, coupling density, coefficient dynamic range, and penalty-to-objective scale ratio for the actual encoded instances. Here, ρ_Q denotes the fraction of nonzero off-diagonal QUBO couplings, R_Q is the ratio of the largest to smallest absolute nonzero QUBO coefficient, and R_λ is the ratio between the largest penalty scale and the largest objective-term magnitude. Exact definitions and full instance-level structural records are provided in Appendix A.

The families occupy distinct structural regimes. MIS remains comparatively sparse because its couplings are inherited from the input graph. In contrast, MDKP and MSP acquire moderate-to-high density through capacity, slack, and target-balancing penalties. QAP is the most restrictive case: its direct one-hot assignment encoding combines dense interactions, the broadest coefficient ranges, and an extremely small feasible permutation manifold. For the selected $n = 10$ QAP instances, only $10!/2^{100} \approx 10^{-23.54}$ of binary strings encode valid assignments; for the $n = 12$ instances, this fraction falls to $12!/2^{144} \approx 10^{-34.67}$. These descriptors are not universal hardness scores, but they identify formulation-level features that influence variational conditioning, compilation overhead, and feasibility recovery.

4.3 Constraint penalties and coefficient scaling

All constrained benchmark instances are converted to QUBO form using quadratic penalties generated by the Qiskit Optimization converter pipeline. Let the pre-penalty binary objective be written as

$$f(x) = f_{\text{lin}}(x) + f_{\text{quad}}(x), \tag{4}$$

and let the converted equality or slack-expanded inequality constraints be represented by integer-valued residuals $g_r(x, s)$. The resulting penalized QUBO has the generic form

$$E_\lambda(x, s) = f(x) + \lambda \sum_r g_r(x, s)^2. \tag{5}$$

For every benchmark instance, the penalty coefficient was selected before any quantum execution by the Qiskit automatic-bound rule

$$\lambda = 1 + (U_{\text{lin}} - L_{\text{lin}}) + (U_{\text{quad}} - L_{\text{quad}}), \tag{6}$$

where L_{lin}, U_{lin}, L_{quad}, and U_{quad} are lower and upper bounds on the linear and quadratic pre-penalty objective contributions at the converter stage. This construction is analytical rather than hardware-tuned or grid-tuned. Because the binary and slack-expanded constraint residuals are integer valued, any violation has $g_r(x, s)^2 \geq 1$. The selected penalty therefore exceeds the pre-penalty objective bound range used by the converter and makes a unit constraint violation energetically more expensive than the full modeled objective range.

The resulting penalty construction differs by problem family only through the constraint residual. For MDKP, binary-expanded integer slack variables enforce capacity inequalities,

$$E_{\text{MDKP}}(x, s) = -\sum_i p_i x_i + \lambda_{\text{K}} \sum_k \left(\sum_i w_{ki} x_i + s_k - C_k \right)^2. \tag{7}$$

Table 2. Penalty construction summary for the benchmark QUBOs. All penalties are selected by the automatic pre-penalty objective-bound rule in Eq.(6); they are fixed before quantum execution, shared across all converted constraints of an instance, and not normalized before Hamiltonian construction. Full instance-level structural metrics and penalty scales are reported in Appendix B.

Problem	Constraint representation	Penalty symbol	Tested penalty range	Selection basis
MDKP	Capacity inequalities with binary slack	λ_{K}	4,022–182,685	Automatic objective-bound rule
MIS	Edge-conflict inequalities	λ_{MIS}	9–129	Automatic objective-bound rule; $\lambda_{\mathrm{MIS}} = \lvert V\rvert + 1$
QAP	Row and column one-hot equalities	λ_{Q}	1.07185×10^5–1.102967×10^{10}	Automatic objective-bound rule
MSP	Target-allocation equalities with binary deviation variables	λ_{M}	1,963–20,613	Automatic objective-bound rule

For MIS, edge-conflict inequalities are penalized as

$$E_{\mathrm{MIS}}(x) = -\sum_{i\in V} x_i + \lambda_{\mathrm{MIS}} \sum_{(i,j)\in E} x_i x_j. \tag{8}$$

For the unit-weight MIS instances, the automatic bound gives $\lambda_{\mathrm{MIS}} = |V|+1$, which is conservative: any $\lambda_{\mathrm{MIS}} > 1$ is sufficient to prefer removing an endpoint of a violating edge over retaining the conflict penalty. For QAP, the direct assignment encoding uses row and column one-hot penalties,

$$E_{\mathrm{QAP}}(x) = \sum_{i,k}\sum_{j,l} f_{ik} d_{jl} x_{ij} x_{kl} + \lambda_{\mathrm{Q}} \left[\sum_i \left(1 - \sum_j x_{ij}\right)^2 + \sum_j \left(1 - \sum_i x_{ij}\right)^2 \right]. \tag{9}$$

For MSP, target-allocation equalities are enforced after binary expansion of the deviation variables,

$$E_{\mathrm{MSP}}(x,s) = f_{\mathrm{TDev}}(x,s) + \lambda_{\mathrm{M}} \sum_g \left(A_g(x) + s_g - T_g\right)^2, \tag{10}$$

where $A_g(x)$ is the allocation expression, s_g is the corresponding binary-expanded deviation variable, and T_g is the target.

No coefficient normalization is applied after QUBO conversion. The resulting penalized QUBO is passed directly to `to_ising()` for VQE- and QAOA-family methods or to the subsequent PCE and QRAO encodings. Thus, all methods begin from the same instance-specific penalized QUBO, preserving the relative objective-to-penalty scale through the common construction stage; method-specific differences arise only during encoding, variational optimization, sampling, and post-processing. The resulting family-level structural and coefficient scales are summarized in Table 1. Appendix A defines the structural descriptors and reports the detailed QAP instance-level analysis, while Appendix B documents the instance-specific penalty values, automatic selection rule, and representative penalty-sensitivity audit.

4.4 Method instantiation details

The compared method families are defined in Sec. 3.4. Here we specify only their experimental instantiations. The variational family consists of VQE and CVaR-VQE, with CVaR evaluated using the fixed confidence level $\alpha = 0.25$. The QAOA-style family consists of standard QAOA together with warm-start QAOA and multi-angle QAOA. The qubit-efficient family consists of PCE and QRAO, which differ from the direct formulations through problem compression and method-specific classical recovery structure rather than through ansätze choice alone. Additional ansätze, optimizer, and encoding settings are reported in the following subsections.

4.5 Variational optimization and candidate-selection protocol

All method–instance configurations were compared under a common nominal shot-based variational-optimization protocol. The direct variational methods use their native parameterized circuits and objectives: VQE and CVaR-VQE use hardware-efficient ans"atze, while QAOA, MA-QAOA, and WS-QAOA use layered cost–mixer constructions at method- and instance-dependent algorithmic depth p. QRAO likewise uses a parameterized hardware-efficient circuit after its compressed encoding, whereas PCE uses a correlation-encoding circuit comprising

single-qubit rotations and entangling R_{XX} layers. These method-specific representations determine the circuit and parameterization, but all methods are evaluated within the same nominal optimizer budget, shot allocation, and candidate-selection framework. The additional encoding and native recovery steps for PCE and QRAO are specified in Section 4.4.

The benchmark protocol uses COBYLA through `scipy.optimize.minimize` in SciPy 1.15.3, with a maximum of 200 optimizer iterations and 200 objective evaluations. Each objective evaluation uses 1,000 shots. Final candidate sampling also uses 1,000 shots where a distinct final-sampling record is retained. For runs with recorded initialization metadata, variational parameters are initialized independently and uniformly over $[0, 2\pi]$. The runner retains the parameter vector associated with the best observed objective value and then applies the method-specific reconstruction or rounding step, followed by the common feasibility-preserving local-improvement procedure described in Section 3.6.

The 200-evaluation specification is an upper bound, rather than a requirement that every execution consume exactly 200 objective evaluations. To document realized execution behaviour, we audited 262 retained benchmark records. Among these, 149 reached the planned evaluation cap and 113 returned an `optimizer_success` status before reaching the cap. The retained records do not contain explicit function, parameter, or gradient tolerance values. We therefore use `optimizer_success` only as the status returned by the optimization framework; it is not interpreted as evidence of tolerance-based convergence, local optimality, or global optimality.

The benchmark reports one primary protocol execution for each method–instance configuration. It is consequently a fixed-protocol comparison rather than an exhaustive hyperparameter sweep or an estimate averaged over all possible random initializations. A reduced simulator study nevertheless shows that decoded quality can be materially initialization-sensitive for selected nontrivial VQE and warm-start-QAOA cases. No additional method-specific tuning or re-optimization was introduced after inspection of individual headline outcomes. The reported values should therefore be interpreted as outcomes of the stated common-budget protocol, not as optimizer-independent best-case performance for each algorithmic family.

Table 25 in Appendix C summarizes the recovered optimizer, shot-budget, stopping-status, and realized-evaluation information, while Table 26 reports the reduced initialization-sensitivity analysis. Problem-wise compiled circuit depths, gate counts, and trainable-parameter counts are reported in Appendices J–M.

4.6 Method-specific encoding settings

Qubit-efficient methods require additional compression choices beyond the ansätze selection. For QRAO, we use compression parameter $k = 3$, corresponding to the highest compression level in the QRAC-based formulation used here [6], and the highest level that remained practically usable under our circuit-depth constraints.. This configuration yields substantial qubit savings while avoiding the more severe depth growth associated with stronger compression. For PCE, we use two-body Pauli correlations, corresponding to quadratic compression [5]. Higher-order compression is possible in principle, but it requires deeper circuits and was not practical within the present execution regime.

For PCE, we employ a QUBO-based cost formulation together with controlled perturbation and correlator-sign reconstruction from the compressed Pauli-correlation representation. The recovered benchmark artifacts indicate that the reported PCE runs use a single-pass COBYLA protocol with a planned upper bound of 200 objective evaluations and no recursive multi-round re-optimization.

After correlator-sign reconstruction, the PCE candidate receives the same single one-pass feasible local-improvement routine applied to every quantum method after its native decoding or rounding step. Thus, the reported PCE values represent the prescribed end-to-end hybrid quantum–classical pipeline under the common fixed-budget and common post-processing protocol, rather than the strongest attainable performance of a recursively tuned PCE procedure or of a PCE-exclusive local-search procedure. PCE's method-specific contribution is its compressed encoding and native correlator reconstruction; the subsequent local refinement is shared across VQE, CVaR-VQE, QAOA, MA-QAOA, WS-QAOA, PCE, and QRAO, as described in Section 3.6.

Realized evaluation counts, termination statuses, and replayability metadata are reported in Appendix C. Full mathematical details of the PCE formulation, correlator reconstruction, and shared post-processing protocol are reported in Appendix D.

4.7 Simulator environment and MPS validation

Simulator-based experiments were conducted with Qiskit Aer 0.17.2 using the `matrix_product_state` method in double precision on CPU. Production runs used adaptive uncapped bond dimension (`matrix_product_state_max_bond_dimension=None`) with truncation

enabled at threshold 10^{-16}. The simulations were executed on an Apple M3 Pro system with 12 CPU cores and 36 GB physical memory; no GPU acceleration was used. Shot-based execution was retained in simulation to preserve the sampling, candidate-selection, and post-processing workflow used for hardware experiments.

To test whether MPS truncation affects the MDKP simulator reference, we performed a targeted fixed-final-parameter stability audit on two large VQE-family circuits that contribute to the negative MDKP simulator–hardware gap discussed in Section 5.8: a 99-qubit CVaR-VQE circuit for `pet2` and a 60-qubit VQE circuit for `hp1`. For each circuit, the final parameter vector, QUBO formulation, circuit construction, final-shot budget, and decoding procedure were held fixed. The only changed variables were the MPS bond-dimension cap and truncation threshold. Each setting used the same 20 independent sampling seeds, with 1,000 shots per seed.

For the 99-qubit CVaR-VQE circuit, the production uncapped run reached maximum observed bond dimension $\chi_{\text{obs}} = 64$. Explicit caps of 64 and 128 reproduced the production empirical output distribution and decoded solution quality exactly. For the 60-qubit VQE circuit, the production run reached $\chi_{\text{obs}} = 66$; explicit caps of 128 and 256 likewise reproduced the production result. Relaxing the truncation threshold from 10^{-16} to 10^{-12} produced no change in either case. At threshold 10^{-8}, the empirical output-distribution change remained small and the decoded solution quality was unchanged. In contrast, deliberately restrictive bond caps produced measurable distribution deviations, confirming that the audit is sensitive to harmful bond restriction. Full settings and results are reported in Appendix E.

4.8 Quantum hardware execution

To complement simulation-based results, we re-ran the benchmarking pipeline on real quantum processors accessed through provider-supported runtime interfaces. Hardware experiments are treated as execution-realistic evaluations rather than as noisy replications of simulator runs. Accordingly, backend identity, execution window, and job-level status information were recorded as part of the experimental context.

A fully controlled campaign in which every method–instance combination is executed on one fixed processor was not practical within the available hardware access window. Queue times and backend availability varied substantially during the campaign, so runs were submitted to compatible IBM backends when they were available rather than being delayed indefinitely for a single device. This choice was made to complete the planned benchmark under realistic access constraints; it was not intended to treat the available processors as interchangeable noise sources.

Backend heterogeneity can contribute to observed differences because processor topology, calibration state, native gate set, routing overhead, and execution window affect the realized circuit. We therefore do not interpret cross-backend hardware differences as controlled estimates of an isolated algorithmic effect. Instead, they are reported as end-to-end hardware-realized outcomes under the stated practical access protocol. Each result is tied to its backend identity, execution window, transpiled resource metrics, and available calibration metadata in the appendix, so that backend context remains visible rather than being absorbed into an algorithm-only comparison.

4.9 Hardware configuration and software stack

The hardware experiments reported in this study were executed on superconducting quantum processors accessed through provider-supported runtime interfaces. Across the reported runs, the primary IBM backends were `ibm_fez`, `ibm_torino`, and `ibm_marrakesh`. Backend identity, transpiled circuit resources, and execution-level diagnostics for each reported method–instance configuration are provided in the problem-wise hardware-diagnostics appendices, Appendices J–M. These processors were treated as distinct execution environments rather than interchangeable noise sources, since differences in processor family, qubit count, topology, calibration state, and routing overhead can materially affect realized circuit performance. Multiple backends were used because queue times and device availability prevented a practical single-backend campaign across the full benchmark; consequently, the hardware results are not presented as a same-device controlled ranking of algorithm families.

For each backend used in the benchmark, we recorded the processor identity, total available qubit count, connectivity structure, and native gate basis exposed by the backend configuration at execution time. Compilation targeted the backend's native one- and two-qubit gate set and coupling map supplied through the provider interface. When available, we additionally logged representative backend property summaries during the experimental window, including readout error and two-qubit gate error information, so that observed degradation can be interpreted in the context of hardware state rather than attributed solely to the optimization method.

Table 3. Execution and mitigation pipeline. Compilation, Estimator mitigation, raw final sampling, and classical recovery are distinct stages of the reported benchmark protocol.

Stage	Primitive / configuration	Role in reported result
Circuit compilation	Transpiler `optimization_level=3`	Backend-aware mapping, decomposition, routing, and circuit optimization; not error mitigation
Variational objective evaluation	EstimatorV2, `resilience_level=2`	Runtime-managed mitigation applied to expectation-value estimates used by COBYLA
Final candidate sampling	Separate SamplerV2, raw/default options	Unmitigated/default bitstring distribution used for decoding and candidate selection
Decoding and local refinement	Classical post-processing	Method-specific reconstruction, feasibility checking, and shared one-round local improvement

Because calibration values drift over time, hardware performance is not treated as a timeless property of a named backend. Instead, each hardware result is tied to an execution window and backend-specific metadata. We therefore report backend identity in the main benchmark tables and provide backend-facing circuit and execution summaries in the appendix.

All reported experiments were implemented in Qiskit [43], with the exact software versions fixed throughout the benchmarking campaign. Unless otherwise stated, hardware circuits were transpiled using a fixed compilation policy with transpiler optimization level 3. Compilation maps each pre-transpilation circuit to the backend's native gate set and coupling graph, thereby determining the realized depth, two-qubit gate count, physical-qubit layout, and routing overhead. Runtime resilience and error mitigation are applied after this mapping stage and are reported separately.

4.10 Execution and mitigation pipeline

The hardware workflow separates compilation, expectation-value estimation, final bitstring sampling, and classical solution recovery. Transpiler `optimization_level=3` is used for backend-aware mapping, gate decomposition, routing, and circuit optimization before execution. This is a compilation setting, not an error-mitigation setting.

Variational objective evaluations use IBM Runtime EstimatorV2 with `resilience_level=2`. No custom TREX, ZNE noise-factor, extrapolator, twirling, or dynamical-decoupling options were manually configured or retained as part of the benchmark protocol. The managed Runtime preset is therefore treated as a provider-controlled mitigation setting for expectation-value estimates, rather than as a fully specified custom mitigation protocol.

Final candidate bitstrings are obtained through separate SamplerV2 jobs with raw/default options and no custom sampler noise-management settings. These SamplerV2 outputs are then passed to the method-specific decoding procedure, original-problem feasibility checks, and the shared one-round local refinement. Consequently, runtime-managed mitigation affects the Estimator expectation values used by the COBYLA objective evaluations; it does not directly mitigate the final bitstrings used to decode the reported solutions. Table 3 summarizes the four-stage execution path and distinguishes the backend-aware compilation step, Runtime-managed mitigation of Estimator objective evaluations, raw/default final sampling, and the subsequent classical recovery procedure.

Runtime-managed mitigation can increase Estimator execution cost through additional internally managed circuit ensembles, but the exact overhead was not isolated from backend queue time, calibration variation, and ordinary runtime variability. The complete execution provenance is reported in Appendix O.2.

4.11 Compilation and transpilation protocol

Compilation is treated as a first-class component of the benchmarking stack. For each circuit–backend pair, we transpile the parameterized circuit using the backend-native gate basis and coupling map under the fixed compilation policy described in Section 4.9. This mapping stage determines the realized circuit after layout selection, routing, native-basis decomposition, and transpiler optimization. Pre-transpilation circuit descriptions can therefore differ substantially from the backend-native circuits ultimately executed on the processor.

For every evaluated circuit–backend configuration, we record both algorithm-level and post-transpilation resource characteristics. The algorithm-level description captures the circuit implied by the selected problem encoding and ansatz before backend mapping. The transpiled description records the circuit depth, total gate count, two-qubit gate count, and backend identity

after routing and native-gate decomposition. This distinction is necessary because connectivity constraints can induce substantial routing overhead, including SWAP insertion, and can amplify depth and two-qubit-gate burden even when the original encoded circuit is relatively compact.

The complete backend-specific transpilation records are reported in the problem-wise hardware-diagnostics appendices, Appendices J–M. These records provide problem- and method-level circuit-resource information together with the associated execution context. Representative empirical evidence of the resulting pre-/post-transpilation expansion for bound QAOA-family circuits is presented later in Figure 4 and discussed in Section 5.7.

We therefore treat transpiled circuit statistics as primary evaluation metadata rather than as secondary implementation details. They quantify the backend-native execution burden relevant to noise exposure and hardware deployability, whereas algorithm-level resource counts describe only the abstract problem encoding and ansatz construction.

Runtime resilience and error-mitigation settings are not folded into these transpilation statistics. Compilation, Runtime-managed Estimator mitigation, raw/default final sampling, and classical candidate recovery are reported as separate stages of the hardware-execution protocol.

4.12 Sampling and objective estimation

All quantum evaluations use shot-based primitives. Simulator and hardware protocols use the shot budgets recorded in the execution artifact. For hardware runs, EstimatorV2 evaluations are used to obtain expectation-value objectives during variational optimization, while final candidate bitstrings are obtained separately from raw/default SamplerV2 jobs.

For expectation-based methods, the Estimator output defines the objective supplied to the optimizer. For CVaR-based methods, the objective is computed from the lower tail of the measured energy distribution using the fixed confidence level $\alpha = 0.25$.

The final reported solution is not decoded from the mitigated Estimator expectation value. Instead, it is reconstructed from the separate SamplerV2 bitstring distribution and then evaluated in the original combinatorial problem domain. This distinction is important: runtime-managed Estimator mitigation may alter the optimization landscape seen by COBYLA, but it does not directly correct the bitstrings used for final decoding, feasibility assessment, or local refinement.

4.13 Hardware noise model and process fidelity estimation

The quantum processors used in this study are IBM Heron-family superconducting transmon devices: `ibm_fez` and `ibm_marrakesh` (Heron r2, 156 qubits) and `ibm_torino` (Heron r1, 133 qubits). All three use a heavy-hexagonal lattice topology with fixed-frequency transmon qubits and tunable couplers, operating near 15 mK in dilution refrigerators. The native two-qubit gate is CZ, with basis gate set $\{\mathrm{CZ}, \mathrm{ID}, \mathrm{RZ}, \mathrm{SX}, \mathrm{X}\}$ on Heron r2 and $\{\mathrm{CZ}, \mathrm{RZZ}, \mathrm{ID}, \mathrm{RZ}, \mathrm{SX}, \mathrm{X}\}$ on Heron r1. Representative backend characteristics during the experimental window are summarized in Table 4.

Table 4. Representative calibration characteristics for the backends used in this study, consistent with published Heron-family specifications [44] and backend calibration snapshots during the experimental window. Exact per-job calibration values are logged in the reproducibility appendix.

Backend	Processor	Qubits	Topology	$\tilde{T}_1$ (μs)	$\tilde{T}_2$ (μs)	$\tilde{\varepsilon}_{2Q}$	$\tilde{\varepsilon}_{\mathrm{ro}}$
`ibm_fez`	Heron r2	156	heavy-hex	100–300	80–200	3×10^{-3}	1.45×10^{-2}
`ibm_marrakesh`	Heron r2	156	heavy-hex	100–300	80–200	3×10^{-3}	1.25×10^{-2}
`ibm_torino`	Heron r1	133	heavy-hex	100–300	80–200	4×10^{-3}	2.41×10^{-2}

The Heron r2 processors benefit from two-level system (TLS) mitigation circuitry that actively manages material defects contributing to decoherence, resulting in improved coherence stability relative to earlier generations [44]. Published Heron-family specifications report that updated calibration procedures introduced in 2024 reduced the median CZ error from approximately 5×10^{-3} to 3×10^{-3}, and that circuits with up to approximately 5 000 two-qubit gate operations remain within the signal-preserving regime on this architecture [44, 45]. These are the two quantities we use to build our noise model.

4.13.1 Process fidelity estimate. For a transpiled circuit with N_{2Q} two-qubit gates executed on a backend with median two-qubit gate error ε_{2Q}, we estimate the process fidelity as

$$F_{\mathrm{est}} \approx \left(1 - \varepsilon_{2Q}\right)^{N_{2Q}}. \tag{11}$$

This expression assumes independent, identically distributed depolarizing errors on each two-qubit gate and neglects coherent error accumulation, crosstalk, single-qubit gate errors, readout effects, and calibration drift. Accordingly, F_{est} is an independent-error gate-count proxy rather than a direct measurement of a circuit's process fidelity or final output distribution.

The proxy tracks the dominant two-qubit-noise contribution under the representative calibration conditions used in this study and provides a useful heuristic for distinguishing signal-preserving from strongly noise-dominated execution regimes. However, an extremely small value of F_{est} does not by itself prove that measured output samples are uniformly random: structured residual correlations, device-specific noise effects, and problem-dependent post-processing can remain relevant. The thresholds derived from F_{est} should therefore be interpreted as benchmark-specific diagnostic reference points rather than universal hardware thresholds.

Under this model, two reference values are informative for interpreting the Heron-family hardware outcomes:

- $F_{\text{est}} \approx 0.1$ (equivalently $N_{2Q} \approx 770$ at $\varepsilon_{2Q} = 3 \times 10^{-3}$): a benchmark-specific operating point at which the present data begin to show a transition toward strongly noise-dominated execution; see Figures 5 and 6. This value is not a universal ZNE threshold. ZNE estimates noiseless expectation values by evaluating deliberately amplified noise levels and extrapolating to zero noise [46, 47]; whether it is useful for a given circuit cannot be inferred from F_{est} alone.
- $F_{\text{est}} \approx 0.01$ (equivalently $N_{2Q} \approx 1540$): a more conservative reference value at which the independent-error proxy attenuates a unit-scale ideal signal to roughly one percent of its noiseless magnitude.

These numerical values are benchmark-specific diagnostic reference points, derived from the representative Heron-family calibration rate and the shot-budget regime used in this study; they would shift with different hardware, circuits, calibration windows, or shot budgets.

4.13.2 Representative fidelity estimates. Table 5 reports estimated process fidelity for representative method–instance–backend combinations from each benchmark family, chosen to span the signal-preserving and noise-dominated regimes. Full per-instance fidelity proxies, hardware outcomes, and simulator outcomes for all evaluated method–instance–backend combinations are reported in the master fidelity table in Appendix O, Table 96.

Table 5. Representative gate-count fidelity proxies by problem family. N_{2Q} is the transpiled two-qubit gate count from the hardware-diagnostics appendices; F_{est} is computed from Eq. (11) under the simplified independent-error model. It is an execution diagnostic rather than a direct measurement of the final output distribution. Sim gap and HW gap are the respective optimality gaps to BKS for MDKP, MIS, and QAP. For MSP, we report TDev instead of percentage optimality gap, as defined in Eq. (2), because MSP objectives are small integer target-deviation values for which percentage gaps are less informative. Feas: Y if the hardware run returned a feasible solution, N otherwise.

Problem	Method	Instance	N_{2Q}	F_{est}	Sim gap %	HW gap %	Feas
MDKP	VQE	hp1	180	5.8×10^{-1}	39.8	27.0	Y
MDKP	CVaR-VQE	pet2	347	2.5×10^{-1}	30.4	1.5	Y
MDKP	QAOA	hp1	22 501	4.4×10^{-30}	–	36.2	Y
MDKP	PCE	hp1	168	5.1×10^{-1}	20.9	13.3	Y
MDKP	QRAO	hp1	111	7.2×10^{-1}	–	5.9	Y
MIS	VQE	1tc.32	96	7.5×10^{-1}	8.3	–	N
MIS	QAOA	1dc.128	48 702	2.8×10^{-64}	–	–	N
MIS	PCE	1tc.16	6	9.8×10^{-1}	50.0	62.5	Y
QAP	VQE	chr12a	1 323	1.9×10^{-2}	–	–	N
QAP	QAOA	chr12a	84 111	1.8×10^{-110}	–	–	N
QAP	PCE	nug12	20	9.4×10^{-1}	36.0	–	N
MSP	VQE	ms20	144	6.5×10^{-1}	–	TDev=4	Y
MSP	QAOA	ms40	76 599	1.1×10^{-100}	–	TDev=42	Y
MSP	PCE	ms20	168	5.1×10^{-1}	–	TDev=45	Y

Three patterns stand out in Table 5. First, VQE and CVaR-VQE circuits remain in the proxy range 0.25–0.6 at the tested scales, consistent with their ability to return useful solutions on MDKP and MSP. Second, QAOA-style circuits have transpiled two-qubit gate counts exceeding 20 000 for all representative instances and therefore extremely small gate-count fidelity proxies.

This places them well inside the strongly noise-dominated regime, but does not by itself establish that their measured output distributions are uniform.

To test the practical consequence of this regime, we performed a matched uniform-random best-shot control over all 106 low-fidelity QAOA-family hardware runs. For each run, the control matches the decision-variable dimension, optimizer-trajectory candidate budget, batch-selection rule, within-batch tie-breaking rule, and shared one-round local refinement used by the hardware pipeline. Of the 106 runs, 43 hardware outputs are infeasible and are treated as feasibility-only comparisons. Among the remaining feasible runs with a finite matched random-quality distribution, 51 lie within the empirical random range and 11 are worse than the matched random baseline. One warm-start-QAOA MIS run returned a feasible candidate while none of the 300 matched random replicates did; this is reported as a finite-sample feasibility exception rather than as a direct optimality-gap comparison. Thus, the dominant low-fidelity QAOA-family pattern is compatible with best-of-budget random candidate selection under the benchmark protocol, while the feasibility exception shows that low F_{est} alone must not be treated as proof of fully uniform-random output. Full results are reported in Appendix N.

Third, for QAP, even the shallowest VQE ansätze at 144 qubits produces transpiled circuits exceeding 1 200 two-qubit gates, with estimated proxy below 0.02, consistent with the complete hardware infeasibility reported in Section 5.4. These patterns support the use of the benchmark-specific fidelity thresholds derived in Sec. 4.13 as diagnostic reference points rather than universal predictive laws.

Table 6. Compilation-only counterfactual summary for 12 representative bound QAOA-family circuits. Reductions are measured relative to reconstructed historical transpilation. The Nighthawk result uses topology-only compilation; the fractional-gate result is a gate-resource counterfactual and was not executed under the original resilience configuration. No audited circuit crosses $F_{\text{est}} \geq 10^{-3}$ or $F_{\text{est}} \geq 10^{-2}$ under any condition.

Compilation condition	Median transpiled N_{2Q}	Median change	Circuits with $F_{\text{est}} \geq 10^{-3}$
Historical compilation	31,025	–	0 / 12
SWAP-aware Heron surrogate	34,443	−12.0%	0 / 12
Fractional-gate Heron surrogate	29,411	+4.1%	0 / 12
SWAP-aware Nighthawk surrogate	24,866	+19.8%	0 / 12

4.13.3 Compilation counterfactuals for QAOA-family circuits. The negative QAOA-family hardware results should be interpreted at the level of the tested implementations rather than as a statement about QAOA in general. To assess whether plausible compilation improvements alone could move the reported circuits back into the signal-preserving regime, we performed a compilation-only counterfactual audit on 12 representative bound circuits: QAOA, MA-QAOA, and WS-QAOA for MDKP `hp1`, MIS `1tc.32`, QAP `tai10a`, and MSP `ms20`. The pre-transpilation circuits and final bound parameter vectors were fixed; no parameters were retrained and no additional hardware executions were performed.

Each circuit was compared under four conditions: (i) the reconstructed historical compilation recorded in the saved hardware artifacts; (ii) a connectivity-aware SABRE mapping and routing configuration on a Heron-like heavy-hex surrogate; (iii) a bound-circuit fractional-gate Heron counterfactual that preserves R_{ZZ} structure where possible; and (iv) the same connectivity-aware routing approach on a topology-only square-lattice Nighthawk surrogate. The latter is a topology study only and does not use Nighthawk calibration data or hardware execution.

Table 6 summarizes the results. The square-lattice Nighthawk surrogate produces the largest median reduction in transpiled two-qubit gates, 19.8%, followed by fractional-gate Heron compilation at 4.1%. The particular SWAP-aware Heron surrogate used here increases median two-qubit-gate count by 12.0% relative to the saved historical routes. This should not be interpreted as evidence that all routing-aware methods fail; rather, it shows that the historical routing was already competitive with this specific SABRE-based surrogate configuration.

Most importantly, none of the 12 representative bound circuits crosses either $F_{\text{est}} = 10^{-3}$ or $F_{\text{est}} = 10^{-2}$ under any tested counterfactual. The strongest topology-only reduction therefore remains insufficient to restore these circuits to the benchmark's signal-preserving regime. Fractional-gate results are reported only as gate-resource counterfactuals: they were not executed under the original runtime resilience configuration because that workflow is not directly compatible with the original ZNE/probabilistic-error-amplification setting.

The resulting conclusion is deliberately narrow. The historical standard QAOA, MA-QAOA, and WS-QAOA implementations remain strongly noise-dominated at the reported scales, even after

the examined compilation counterfactuals. This result does not exclude improved performance from other QAOA formulations, deeper architecture-specific compilation, alternative parameter schedules, different mixers, or future hardware generations.

4.14 Classical post-processing and solution recovery

The output of each quantum method is ultimately interpreted at the level of the original combinatorial optimization problem. For the direct QUBO-based methods (VQE, CVaR-VQE, QAOA, MA-QAOA, and WS-QAOA), each measured bitstring is treated directly as a candidate binary decision vector and scored in the original problem domain.

For PCE, measured Pauli correlators are converted into a binary candidate by correlator reconstruction, as defined in Appendix D. For QRAO, measurement outcomes are converted into a binary candidate through the QRAC rounding rule. These operations are distinct and are collectively referred to as method-specific classical post-processing.

After a candidate is obtained, its feasibility is checked against the original constrained problem rather than only against the unconstrained QUBO objective. When an explicit procedure modifies a candidate to restore constraint satisfaction, we call that procedure feasibility repair. The PCE pipeline also uses the separately reported, feasibility-preserving multi-bit local search described in Appendix D; this is classical improvement rather than measurement interpretation.

For each instance and method, the reported solution is the best candidate returned by the prescribed sampling and classical post-processing pipeline. This distinction is especially important for constrained benchmarks such as MDKP, QAP, and MSP, where a low penalized objective does not necessarily imply an operationally valid solution.

5 Results

5.1 Overview of the empirical comparison

We now report the benchmark results under the protocol described in Sections 3 and 4. Our goal is not only to compare final objective quality across method families, but also to assess how those comparisons change once realistic execution constraints are taken into account. Accordingly, we evaluate each method family both through problem-level solution metrics and through hardware-facing diagnostics such as algorithmic level width, transpiled circuit growth, and execution robustness.

To keep the discussion interpretable, we organize the main results around the four benchmark problems and compare three broad method families in each case: (i) VQE-style energy-minimization methods (VQE and CVaR-VQE), (ii) QAOA-style methods (QAOA, MA-QAOA, and WS-QAOA), and (iii) qubit-efficient encoding or reduction methods (PCE and QRAO). The main text focuses on benchmark-level patterns, while detailed circuit-compilation and execution-robustness summaries are reported in the appendix.

Across the full benchmark, performance is heterogeneous across problem classes and method families. The detailed cross-problem synthesis is given in Sec. 5.6; here we first examine each problem family separately.

5.2 MDKP: balanced comparison across all method families

MDKP is the most balanced family in the benchmark because all compared methods return feasible solutions on hardware, allowing a genuine comparison of solution quality under realistic execution constraints. The VQE-style results in Table 7 show that both VQE and CVaR-VQE remain feasible on all instances, with CVaR-VQE achieving the lower gap on most cases, including especially strong gains on `pet2`, `pb2`, `pb5`, `pet5`, and `pet6`. This indicates that the tail-focused objective can improve recovery of better samples for constrained packing instances, although the advantage is not uniform.

The QAOA-family results in Table 8 show that all three variants are also feasible on every tested instance, but the best variant is instance-dependent. MA-QAOA attains the lowest gap on several instances, including `hp1`, `hp2`, `pb1`, `pb4`, and `pet4`, whereas WS-QAOA is best on `pb2`, `pb5`, `pet2`, `pet5`, and `pet7`. Standard QAOA is occasionally best, for example on `pet3` and `pet6`, but is less consistently competitive than the structured variants. Thus, for MDKP, modifying the operator schedule or warm-start structure often improves performance relative to vanilla QAOA.

The encoding-based comparison in Table 9 reveals the clearest width–quality trade-off in the paper. PCE uses only 6–10 qubits across the tested instances, whereas QRAO uses 32–62 qubits and the direct formulations require substantially larger widths. This compression is substantial and materially expands the set of backends on which the problem can be executed. However, PCE is not uniformly best in objective quality: QRAO attains the lower gap on 8 of the 12 MDKP instances,

Table 7. Combined MDKP VQE and CVaR-VQE results summary across instances. Entries report the primary performance metrics (Optimal/BKS, Qubits, Feasibility, and Gap). The Qubits column is reported as VQE / CVaR-VQE when the two encodings require different algorithmic-level widths. The lower gap per instance is boldfaced.

Instance	**Optimal**	**Qubits**	**VQE**		**CVaR-VQE**	
			Feasible	**Gap (%)**	**Feasible**	**Gap (%)**
hp1	3418	60	Yes	**26.95**	Yes	33.85
hp2	3186	67	Yes	17.92	Yes	**15.88**
pb1	3090	59	Yes	22.62	Yes	**14.89**
pb2	3186	66	Yes	26.77	Yes	**11.93**
pb4	95168	45	Yes	**33.63**	Yes	34.97
pb5	2139	116	Yes	29.73	Yes	**18.14**
pet2	87061	99	Yes	16.98	Yes	**1.50**
pet3	4015	102	Yes	**32.38**	Yes	36.61
pet4	6120	107	Yes	44.69	Yes	**41.91**
pet5	12400	122	Yes	25.65	Yes	**13.83**
pet6	10618	86	Yes	20.24	Yes	**13.88**
pet7	16537	100	Yes	**23.28**	Yes	24.52

Table 8. Combined MDKP results for QAOA, MA-QAOA, and WS-QAOA across instances. Entries report the primary performance metrics (Optimal/BKS, Qubits, Feasibility, and Gap). The lower gap per instance among the three variants is boldfaced.

Instance	**Optimal**	**Qubits**	**QAOA**		**MA-QAOA**		**WS-QAOA**	
			Feas.	**Gap**	**Feas.**	**Gap**	**Feas.**	**Gap**
hp1	3418	60	Yes	36.22	Yes	**21.06**	Yes	23.61
hp2	3186	67	Yes	19.68	Yes	**15.66**	Yes	29.19
pb1	3090	59	Yes	36.67	Yes	**27.86**	Yes	28.45
pb2	3186	66	Yes	42.18	Yes	44.51	Yes	**33.93**
pb4	95168	45	Yes	37.53	Yes	**27.63**	Yes	43.13
pb5	2139	116	Yes	23.47	Yes	28.00	Yes	**20.80**
pet2	87061	99	Yes	14.70	Yes	30.97	Yes	**1.28**
pet3	4015	102	Yes	**20.05**	Yes	27.52	Yes	36.74
pet4	6120	107	Yes	33.33	Yes	**14.38**	Yes	25.65
pet5	12400	122	Yes	37.30	Yes	26.21	Yes	**13.79**
pet6	10618	86	Yes	**23.09**	Yes	39.87	Yes	30.45
pet7	16537	100	Yes	49.76	Yes	28.91	Yes	**27.62**

while PCE is best on the remaining 4. MDKP therefore provides a clear positive example of the benchmark thesis: qubit-efficient encodings improve executability, but the strongest compression does not by itself determine the best final hardware outcome. In particular, the benchmarked quadratic PCE configuration is competitive on several instances under the same shared one-pass local-improvement rule applied to all quantum methods. Its results should not be interpreted as an upper bound on what a more aggressive multi-pass or higher-order PCE variant might achieve.

The simulator results reported in the appendix provide a controlled reference for this comparison, while the hardware results show how the final ranking changes after compilation and execution. Taken together, MDKP is the clearest example in the benchmark where all method families remain viable and meaningful trade-offs between quality, width, and hardware overhead can be observed directly. Figure 1 contrasts the simulator and hardware gaps for these method families and shows that simulator-side rankings do not transfer uniformly to hardware.

5.3 MIS: a sharp feasibility threshold under hardware execution

The MIS results reveal a different behavior from MDKP. Rather than a balanced quality comparison across all methods, the dominant pattern is a sharp feasibility breakdown as instance size increases. The VQE-style results in Table 10 show that both VQE and CVaR-VQE solve the smallest instances well, with zero gap on `1tc.8` and near-optimal performance on `1tc.16`. However, this behavior does not persist: from `1tc.32` onward, feasibility begins to collapse, and by the 64- and 128-variable instances both methods become infeasible.

A similar pattern appears for the QAOA family in Table 11. The structured variants remain

Table 9. Combined MDKP results for PCE and QRAO across instances. Entries report Optimal/BKS, Qubits, shown as PCE/QRAO when the encodings differ, feasibility, and gap to BKS. The lower gap per instance is boldfaced.

Instance	Optimal	Qubits	PCE		QRAO	
			Feas.	Gap	Feas.	Gap
hp1	3418	7 / 38	Yes	13.25	Yes	**5.85**
hp2	3186	8 / 45	Yes	**14.56**	Yes	16.67
pb1	3090	7 / 37	Yes	22.78	Yes	**15.40**
pb2	3186	8 / 44	Yes	21.37	Yes	**13.65**
pb4	95168	6 / 32	Yes	**21.30**	Yes	21.71
pb5	2139	10 / 57	Yes	**17.72**	Yes	18.00
pet2	87061	9 / 44	Yes	1.69	Yes	**0.64**
pet3	4015	9 / 44	Yes	**7.97**	Yes	34.12
pet4	6120	9 / 47	Yes	20.42	Yes	**18.63**
pet5	12400	10 / 58	Yes	37.50	Yes	**25.52**
pet6	10618	9 / 52	Yes	19.92	Yes	**15.23**
pet7	16537	9 / 62	Yes	25.27	Yes	**16.79**

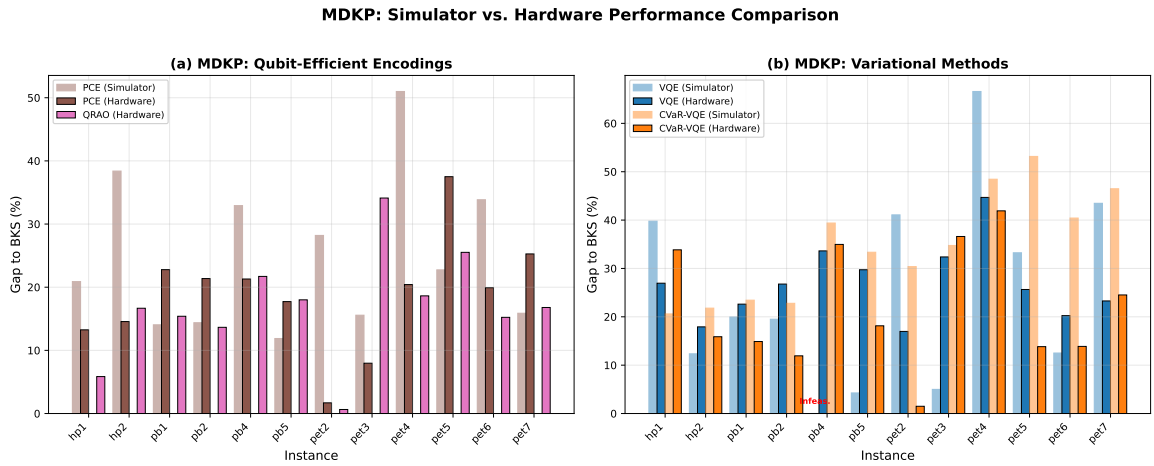

Figure 1. MDKP simulator versus hardware performance across qubit-efficient and variational methods. Panel (a) compares PCE and QRAO on MDKP instances using gap to the optimal solution, while panel (b) reports the corresponding comparison for VQE and CVaR-VQE. The figure shows that simulator-side rankings do not transfer uniformly to hardware: some methods retain moderate performance degradation, whereas others exhibit larger hardware-induced gap inflation or infeasibility on selected instances. Overall, the plot highlights a nontrivial simulator–hardware gap even at these small benchmark sizes and shows that hardware execution can materially change relative method quality.

strong on the smallest graphs, and WS-QAOA is the best-performing QAOA-style method on several of the larger feasible cases. Most notably, WS-QAOA remains feasible on `1tc.64`, where the other QAOA-style methods fail. Even so, the larger MIS instances still expose a clear feasibility cliff: performance deteriorates rapidly once the width and compiled circuit burden exceed what current hardware can support reliably.

The encoding-based MIS comparison in Table 12 confirms that compression helps, but only to a point. QRAO outperforms PCE on the smaller and intermediate feasible instances, achieving zero gap on `1tc.8` and better recovery than PCE on `1tc.16` and `1tc.32`. However, neither encoding family can maintain feasibility indefinitely as the instances grow. Thus, MIS does not simply reward lower width; rather, it exposes a practical boundary beyond which current hardware noise and compilation overhead dominate. The feasibility breakdown is summarized in Figure 2.

This makes MIS one of the most informative families in the benchmark from a hardware perspective. At small scale, several methods perform well and even reach zero gap. At moderate scale, the benchmark becomes sensitive to architecture and encoding choice. At larger scale, feasibility itself becomes the central issue. The main lesson from MIS is therefore not just that gaps worsen with size, but that backend-realized feasibility can collapse sharply even when the problem size still appears moderate.

Table 10. Combined MIS VQE and CVaR-VQE results across instances. Entries report the known optimum/BKS, Qubits, feasibility, and gap to BKS. The lower gap per instance among feasible methods is boldfaced; infeasible runs are reported with gap ∞.

Instance	**Optimal**	**Qubits**	**VQE**		**CVaR-VQE**	
			Feas.	**Gap**	**Feas.**	**Gap**
1tc.8	4	8	Yes	**0.00**	Yes	**0.00**
1tc.16	8	16	Yes	**0.00**	Yes	12.50
1tc.32	12	32	No	∞	Yes	**16.67**
1tc.64	20	64	No	∞	No	∞
1et.64	18	64	No	∞	No	∞
1dc.64	10	64	No	∞	No	∞
1dc.128	16	128	No	∞	No	∞

Table 11. Combined MIS results for QAOA, MA-QAOA, and WS-QAOA across instances. Entries report the known optimum/BKS, Qubits, feasibility, and gap to BKS. The lower gap per instance among feasible variants is boldfaced; infeasible runs are reported with gap ∞.

Instance	**Optimal**	**Qubits**	**QAOA**		**MA-QAOA**		**WS-QAOA**	
			Feas.	**Gap**	**Feas.**	**Gap**	**Feas.**	**Gap**
1tc.8	4	8	Yes	**0.00**	Yes	**0.00**	Yes	**0.00**
1tc.16	8	16	Yes	25.00	Yes	12.50	Yes	**0.00**
1tc.32	12	32	Yes	25.00	No	∞	Yes	**16.67**
1tc.64	20	64	No	∞	No	∞	Yes	**35.00**
1et.64	18	64	No	∞	No	∞	No	∞
1dc.64	10	64	No	∞	No	∞	No	∞
1dc.128	16	128	No	∞	No	∞	No	∞

5.4 QAP: the clearest negative result in the benchmark

QAP is the most structurally restrictive family in the study and provides the clearest negative result under real-hardware execution. The difficulty is not explained by circuit width alone. The benchmark uses standard QAPLIB instances in the $n = 10$–12 range; the smallest selected instances, `tai10a` and `tai10b`, already require 100 binary variables under the direct one-hot formulation. A valid assignment corresponds to a permutation, so only 10! of the 2^{100} binary strings are feasible:

$$\frac{10!}{2^{100}} \approx 10^{-23.54}. \tag{12}$$

For the $n = 12$ instances, the direct formulation contains 144 binary variables and the feasible fraction contracts to

$$\frac{12!}{2^{144}} \approx 10^{-34.67}. \tag{13}$$

This sparse permutation-feasible manifold is combined with dense flow-distance interactions and row-and-column one-hot penalties. Across the tested QAP instances, the median QUBO density is 0.818, the median interaction degree is 95.4, and coefficient dynamic range reaches as high as 2.21×10^{10}. Thus, even the smallest standard QAPLIB instances selected for this benchmark are already structurally very different from a 100-variable sparse graph or packing QUBO.

The VQE-style results in Table 13 show that both VQE and CVaR-VQE are infeasible on all tested QAP instances. The same conclusion holds for the QAOA family in Table 14, where QAOA, MA-QAOA, and WS-QAOA all fail to recover feasible solutions on the hardware-tested instances. Even the encoding-based methods in Table 15 do not resolve this difficulty: PCE and QRAO remain infeasible on the tested QPU runs.

This result is scientifically important and should not be treated as merely a failure case. QAP combines three adverse properties in the direct benchmark encoding: dense flow-distance interactions, strict row-and-column one-hot assignment constraints, and an exponentially sparse feasible subset of the binary search space. The resulting QUBOs have widths of 100–144 variables, median density 0.818, and coefficient dynamic ranges extending to 2.21×10^{10} across the tested instances.

The simulator results in Appendix I.3 provide an instructive contrast. VQE and CVaR-VQE remain infeasible on the tested QAP instances even under simulator execution, whereas PCE returns feasible candidates on several instances, albeit with large optimality gaps of approximately

Table 12. Combined MIS results for PCE and QRAO across instances. Entries report the known optimum/BKS, qubits used, feasibility, and gap to BKS. The lower gap per instance among feasible methods is boldfaced; infeasible runs are reported with gap ∞.

Instance	Optimal	PCE			QRAO		
		Qubits	Feas.	Gap	Qubits	Feas.	Gap
1tc.8	4	3	Yes	25.00	4	Yes	**0.00**
1tc.16	8	4	Yes	62.50	6	Yes	**12.50**
1tc.32	12	6	No	∞	13	Yes	**25.00**
1tc.64	20	8	No	∞	23	No	∞
1et.64	18	8	No	∞	24	No	∞
1dc.64	10	8	No	∞	18	No	∞
1dc.128	16	10	No	∞	46	No	∞

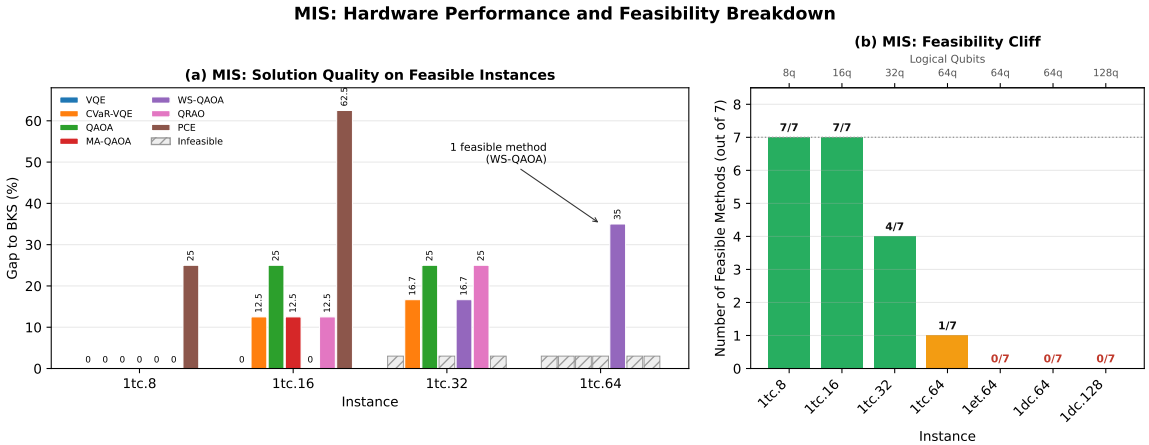

Figure 2. Hardware performance and feasibility breakdown for MIS. Panel (a) reports finite optimality gaps for feasible method–instance outcomes; hatched bars denote infeasible outcomes. WS-QAOA is the only feasible method on `1tc.64`. Panel (b) reports the number of feasible methods out of seven for each instance: 7/7, 7/7, 4/7, 1/7, 0/7, 0/7, and 0/7 from `1tc.8` through `1dc.128`. Feasibility therefore collapses sharply with problem size, even though an isolated feasible outcome remains at 64 algorithm-level qubits.

15%–235%. This indicates that compressed PCE reconstruction can retain partial access to the permutation-feasible manifold under noise-free execution, but does not remove the underlying structural difficulty of the dense QAP formulation.

The complete hardware infeasibility should therefore not be attributed to qubit count or compilation cost in isolation. The observed barrier reflects the combined effect of dense interactions, broad coefficient scales, one-hot penalty structure, a combinatorially sparse feasible assignment manifold, hardware compilation overhead, execution noise, and recovery sensitivity. QAP therefore serves as a stress test that separates partial representability in simulation from reliable feasible-solution recovery on current hardware. Figure 3 contrasts the feasible PCE simulator candidates with the uniform hardware infeasibility across all seven methods.

5.5 MSP: strong compression but weak recovered hardware quality

MSP exhibits a markedly different pattern from both MDKP and MIS. Here, the most important observation is that qubit-efficient encodings achieve the strongest compression, but not the best recovered hardware solution quality. The VQE-style results in Table 16 show that the relative performance of VQE and CVaR-VQE is instance-dependent. VQE is better on some instances, including `ms20`, `ms30`, `ms31`, `ms51`, while CVaR-VQE improves on others such as `ms40`, `ms50`, `ms21`, and `ms41`. Thus, unlike MDKP, there is no consistent advantage of the CVaR objective for MSP.

The QAOA-style results in Table 17 are again highly instance-dependent. QAOA is strongest on some cases, WS-QAOA is best on others, and MA-QAOA is competitive only on a subset. This reinforces that MSP has a different optimization structure from the graph-based or packing-based benchmarks and cannot be interpreted through the same intuition as MIS or MDKP.

The encoding-based results in Table 18 provide the most important benchmark message for MSP. PCE and QRAO compress the instances to only 7–11 qubits, which is a dramatic reduction relative to the 48–156 qubits required by the direct formulations. However, this compression comes

Table 13. Combined QAP VQE and CVaR-VQE results across instances. Entries report the known optimum/BKS, circuit width (Qubits), feasibility, and gap to BKS. The lower gap per instance among feasible methods is boldfaced; infeasible runs are reported with gap ∞.

Instance	Optimal	Qubits	VQE		CVaR-VQE	
			Feas.	Gap	Feas.	Gap
chr12a	9552	144	No	∞	No	∞
chr12b	9742	144	No	∞	No	∞
chr12c	11156	144	No	∞	No	∞
nug12	578	144	No	∞	No	∞
had12	1652	144	No	∞	No	∞
rou12	235528	144	No	∞	No	∞
scr12	31410	144	No	∞	No	∞
tai10a	135028	100	No	∞	No	∞
tai10b	1183760	100	No	∞	No	∞
tai12a	224416	144	No	∞	No	∞
tai12b	39464925	144	No	∞	No	∞

Table 14. Combined QAP results for QAOA, MA-QAOA, and WS-QAOA across instances. Entries report the known optimum/BKS, circuit width (Qubits), feasibility, and gap to BKS. The lower gap per instance among feasible variants is boldfaced; infeasible runs are reported with gap ∞. A dash indicates that the method was not run or not reported for that instance.

Instance	Optimal	Qubits	QAOA		MA-QAOA		WS-QAOA	
			Feas.	Gap	Feas.	Gap	Feas.	Gap
chr12a	9552	144	No	∞	No	∞	No	∞
chr12b	9742	144	No	∞	No	∞	No	∞
chr12c	11156	144	No	∞	No	∞	No	∞
nug12	578	144	No	∞	No	∞	No	∞
had12	1652	144	No	∞	No	∞	No	∞
rou12	235528	144	No	∞	No	∞	No	∞
scr12	31410	144	No	∞	No	∞	No	∞
tai10a	135028	100	No	∞	No	∞	No	∞
tai10b	1183760	100	No	∞	No	∞	No	∞
tai12a	224416	144	No	∞	No	∞	No	∞
tai12b	39464925	144	No	∞	No	∞	No	∞

at a substantial cost in recovered solution quality. Across all tested MSP instances, the gaps obtained by PCE and QRAO are much larger than those of the best full-width methods, often by one or more orders of magnitude. In addition, feasibility remains limited despite the compression, showing that low width alone does not guarantee robust recovery for balancing-type problems.

MSP is therefore the strongest counterexample in the benchmark to any simple "fewer qubits is better" narrative. The compressed methods make the instances far easier to fit on current devices, but the best hardware outcomes are generally obtained by full-width VQE/CVaR-VQE or QAOA-style methods, depending on the instance. This problem family most clearly demonstrates that qubit count should be treated as an important but incomplete metric of practical performance.

5.6 Cross-problem benchmark observations

When viewed together, the four benchmark families yield a problem-dependent picture of near-term quantum optimization. MDKP permits a balanced comparison across all method families, MIS exposes a sharp feasibility boundary, QAP is the most demanding dense-assignment case, and MSP shows that strong compression does not automatically imply strong recovered solutions. This variation justifies the use of multiple structurally distinct benchmark families rather than relying on a single canonical optimization problem.

The problem-wise hardware diagnostics in Appendices J–M show that these differences are closely tied to backend-native circuit growth, two-qubit-gate burden, and execution robustness. The dedicated QAOA-family pre-/post-transpilation audit in Appendix G further shows how routing, native-basis decomposition, and connectivity constraints can substantially increase the realized two-qubit-gate count relative to the algorithm-level circuit. Complete method–instance–backend fidelity and outcome records are provided in Appendix O, Table 96.

Methods that appear only modestly different at the algorithmic level can therefore diverge

Table 15. Combined QAP results for PCE and QRAO across instances. Entries report the known optimum/BKS, the number of qubits required by each encoding, feasibility, and gap to BKS. The lower gap per instance among feasible methods is boldfaced; infeasible runs are reported with gap ∞. A dash indicates that the method was not run or not reported for that instance.

Instance	Optimal	PCE			QRAO		
		Qubits	Feas.	Gap	Qubits	Feas.	Gap
chr12a	9552	11	No	∞	56	No	∞
chr12b	9742	11	No	∞	62	No	∞
chr12c	11156	11	No	∞	54	No	∞
nug12	578	11	No	∞	63	No	∞
had12	1652	11	No	∞	144	No	∞
rou12	235528	11	No	∞	132	No	∞
scr12	31410	11	No	∞	60	No	∞

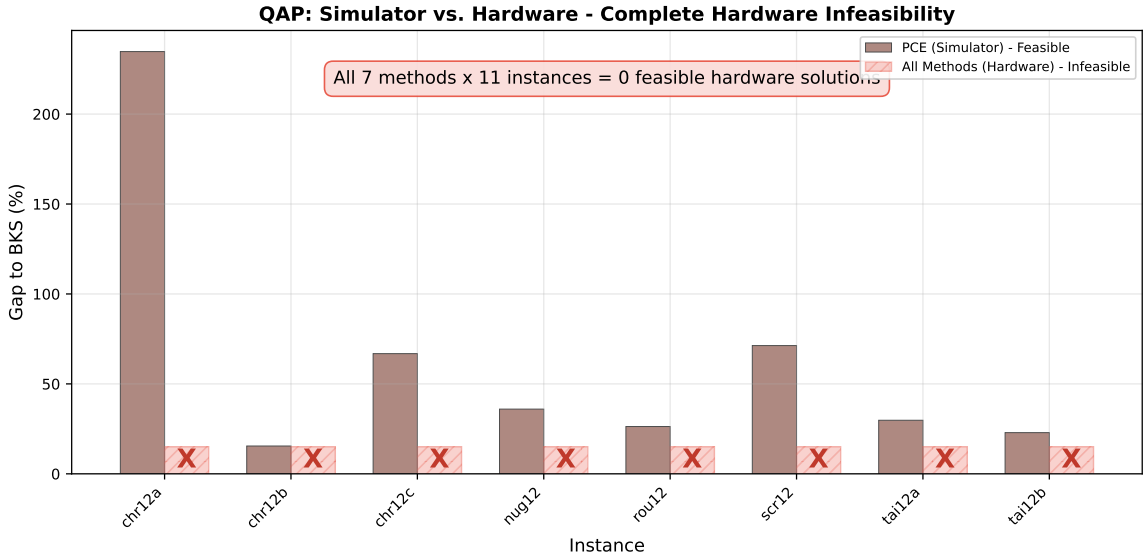

Figure 3. QAP simulator versus hardware comparison. The direct QAP encoding combines dense flow-distance couplings with row-and-column one-hot assignment constraints; for the tested $n = 10$ and $n = 12$ instances, valid assignments occupy approximately $10^{-23.54}$ to $10^{-34.67}$ of the full binary hypercube. PCE returns feasible simulator candidates on several instances, although with large optimality gaps, whereas none of the seven hardware-executed methods returns a feasible QAP assignment. The comparison therefore illustrates the interaction of restrictive QAP feasibility geometry with compilation overhead, execution noise, and recovery sensitivity.

substantially after transpilation, particularly when dense encoded interactions or nonlocal entangling patterns increase effective depth and two-qubit-gate burden. The benchmark should consequently be interpreted as a full-stack evaluation of encoding, compilation, execution, and solution recovery, rather than as a comparison of abstract encodings alone.

5.7 Connectivity-induced compilation expansion

The effect of hardware connectivity is most visible when comparing algorithm-level QAOA-family circuits with the backend-native circuits that are actually executed. Figure 4 reports this comparison for 12 representative bound depth-3 circuits: QAOA, MA-QAOA, and WS-QAOA on MDKP `hp1`, MIS `1tc.32`, QAP `tai10a`, and MSP `ms20`. The lower point in each row is the algorithm-level two-qubit-gate count before transpilation; the upper point is the two-qubit-gate count recorded after historical backend-native transpilation.

All 12 representative circuits expand substantially after transpilation, with post-transpilation to algorithm-level two-qubit-gate ratios ranging from 4.47 to 6.24. The family-level median expansion is 6.01× for MDKP, 4.49× for MIS, 5.52× for QAP, and 6.23× for MSP. The largest absolute burden occurs for QAP: the median representative QAOA-family circuit grows from 14,310 algorithm-level two-qubit gates to 79,027 transpiled two-qubit gates. The largest relative median expansion occurs for MSP, where the median count grows from 6,300 to 39,227.

The historical compilation artifacts also retain routing metadata. Median recorded SWAP counts are 5,030 for MDKP, 169 for MIS, 16,802 for QAP, and 8,876 for MSP. These values

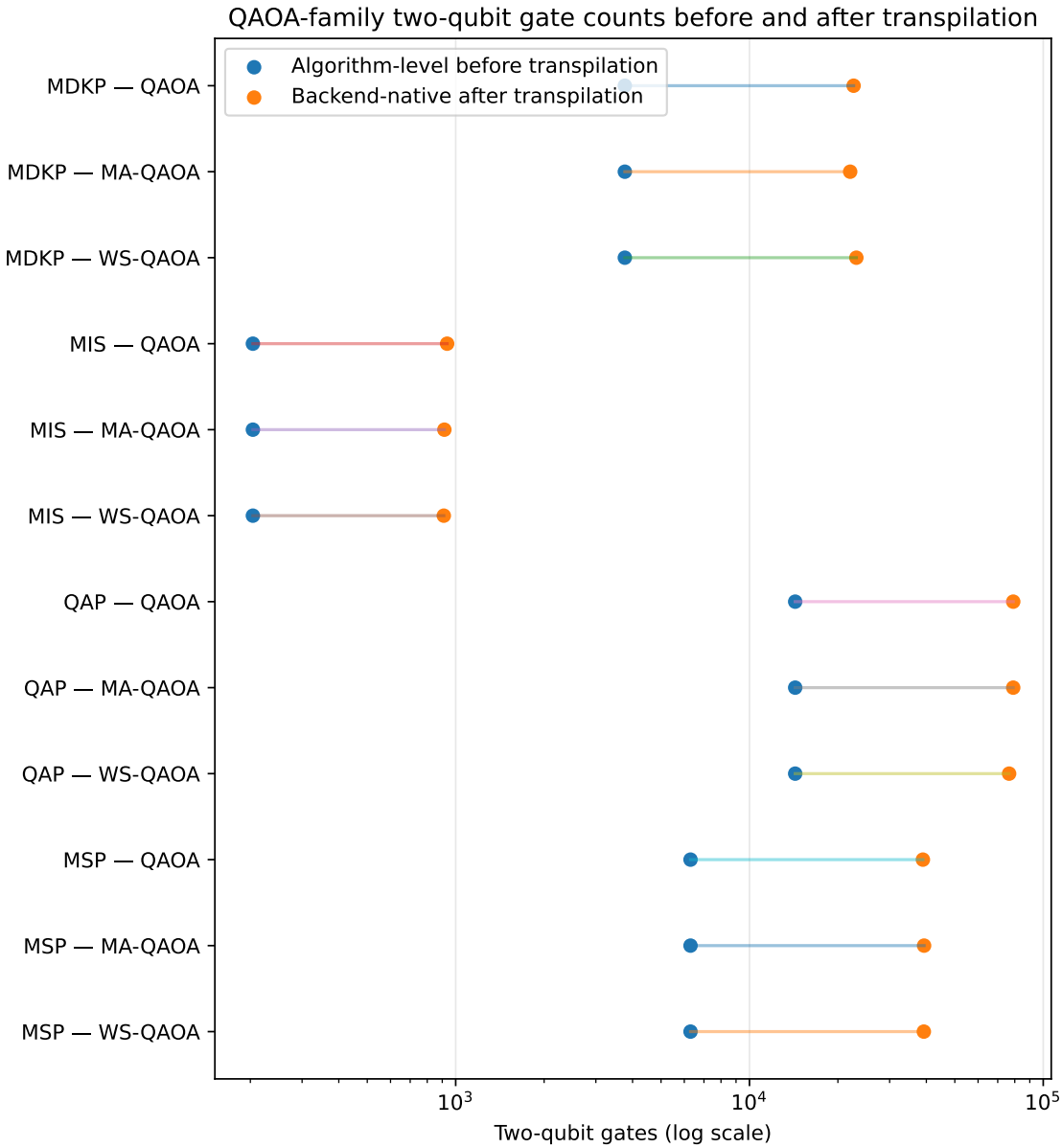

Figure 4. Historical QAOA-family two-qubit-gate counts before and after transpilation. Each row compares the same representative bound depth-3 circuit before backend mapping with the corresponding historically executed backend-native circuit. The four problem families are represented by MDKP `hp1`, MIS `1tc.32`, QAP `tai10a`, and MSP `ms20`. The horizontal axis is logarithmic. Expansion reflects the combined effects of routing, SWAP insertion, native-basis decomposition, scheduling, and post-routing circuit simplification; it should not be attributed to SWAP gates alone.

Table 16. Market Share results for VQE and CVaR-VQE. Because the classically certified MSP optima are small integers (0–3), percentage gaps are unstable and uninformative. We report total absolute deviation (**TDev**), maximum single-product deviation (**MDev**), and the range-normalized TDev approximation ratio ($\mathbf{AR}_{\mathrm{TDev}}$). TDev remains the primary application-level quality measure. No reported hardware run achieved an exact target match.

			VQE			CVaR-VQE		
Inst.	**Opt.**	**Q**	**TDev**	**MDev**	$\mathbf{AR}_{\mathrm{TDev}}$	**TDev**	**MDev**	$\mathbf{AR}_{\mathrm{TDev}}$
ms20	3	48	**4**	**2**	**0.998**	27	21	0.951
ms30	2	84	**127**	**89**	**0.919**	347	214	0.777
ms40	1	118	188	85	0.936	**150**	**91**	**0.949**
ms50	0	150	644	214	0.865	**476**	**165**	**0.900**
ms21	3	50	215	121	0.586	**9**	**7**	**0.988**
ms31	3	84	**12**	**7**	**0.994**	51	21	0.968
ms41	1	118	273	135	0.916	**48**	**16**	**0.985**
ms51	1	156	**439**	**152**	**0.915**	565	177	0.891

Table 17. Market Share results for QAOA, MA-QAOA, and WS-QAOA. **TDev**: total absolute deviation from target split. **MDev**: maximum deviation on any single product. $\mathbf{AR}_{\mathrm{TDev}}$: range-normalized TDev approximation ratio. No reported hardware run achieved an exact target match.

			QAOA			MA-QAOA			WS-QAOA		
Inst.	**Opt.**	**Q**	**TDev**	**MDev**	$\mathbf{AR}_{\mathrm{TDev}}$	**TDev**	**MDev**	$\mathbf{AR}_{\mathrm{TDev}}$	**TDev**	**MDev**	$\mathbf{AR}_{\mathrm{TDev}}$
ms20	3	48	21	15	0.963	**10**	**8**	**0.986**	41	34	0.922
ms30	2	84	**59**	**35**	**0.963**	203	101	0.870	296	121	0.810
ms40	1	118	**42**	**20**	**0.986**	619	213	0.790	901	285	0.694
ms50	0	150	846	287	0.822	2440	576	0.488	**318**	**92**	**0.933**
ms21	3	50	15	14	0.977	19	13	0.969	**9**	**7**	**0.988**
ms31	3	84	170	65	0.889	54	31	0.966	**36**	**26**	**0.978**
ms41	1	118	594	279	0.817	**85**	**60**	**0.974**	348	183	0.893
ms51	1	156	1242	317	0.759	**495**	**218**	**0.904**	1024	270	0.801

reinforce that sparse or structured processor connectivity materially affects the realized circuit burden. They are not used as an additive accounting identity because native-gate decomposition and later transpiler simplifications can change the relation between recorded SWAP operations and final two-qubit-gate count.

This evidence supports the interpretation that circuit feasibility and fidelity cannot be inferred from algorithm-level QAOA gate counts alone. The relevant hardware quantity is the post-transpilation circuit produced for the selected backend and execution protocol.

5.8 Noise-induced performance degradation: a quantitative analysis

The problem-wise hardware diagnostics in Appendices J–M, combined with the fidelity model of Section 4.13, enable a quantitative comparison between backend-native circuit burden, feasibility, and recovered hardware quality. Figure 5 separates this comparison into two views. Panel (a) plots feasible MDKP and MIS hardware outcomes as optimality gap to BKS against the transpiled two-qubit-gate count. Panel (b) shows all infeasible hardware outcomes in problem-family lanes, including QAP runs, for which no reported hardware execution returns a feasible assignment. Feasible MSP outcomes are not included in panel (a) because they are evaluated using total absolute deviation rather than percentage optimality gap.

Several observations emerge from Figure 5. First, feasible low-gate-count outcomes span a substantial range of optimality gaps, from near-zero values to roughly 45%. This spread shows that remaining solution-quality variation cannot be attributed to two-qubit-gate burden alone: ansatz choice, encoding, optimization trajectory, sampling, and classical recovery remain relevant within the lower-(N_2Q) regime. Second, the feasible QAOA-family outcomes at $N_{2Q} > 10^4$ lie in a markedly different backend-native circuit regime, with gate-count fidelity proxies below 10^{-30}. The matched uniform-random control shows that the dominant pattern among these feasible low-fidelity QAOA-family outcomes is compatibility with, or underperformance relative to, random candidate pools processed by the same trajectory-level selection and one-round local-refinement rule. This supports a best-of-budget sampling interpretation for most of the tested QAOA-family runs, while not establishing that every measured output distribution is fully uniform.

Third, panel (b) shows that infeasibility is not confined to a single two-qubit-gate threshold. MIS failures emerge across an expanding range of compiled circuit sizes, whereas QAP is infeasible throughout the reported hardware set despite substantial variation in its compiled resource burden. The QAP pattern is therefore consistent with a combined structural and execution barrier: dense

Table 18. Market Share results for PCE and QRAO. **TDev**: total absolute deviation from target split. **MDev**: maximum deviation on any single product. $\mathbf{AR}_{\mathrm{TDev}}$: range-normalized TDev approximation ratio. Despite substantial algorithm-level width reduction (7–11 qubits versus 48–156 for full-width methods), recovered deviations remain large. No reported hardware run achieved an exact target match.

		PCE				**QRAO**			
Inst.	**Opt.**	**Q**	**TDev**	**MDev**	$\mathbf{AR}_{\mathrm{TDev}}$	**Q**	**TDev**	**MDev**	$\mathbf{AR}_{\mathrm{TDev}}$
ms20	3	7	**45**	**31**	**0.914**	11	81	62	0.840
ms30	2	8	**167**	**82**	**0.893**	11	291	133	0.813
ms40	1	10	**296**	**95**	**0.900**	11	485	156	0.836
ms50	0	11	**822**	**207**	**0.827**	11	1120	301	0.765
ms21	3	7	**52**	**34**	**0.904**	11	99	71	0.812
ms31	3	8	**185**	**90**	**0.879**	11	310	145	0.797
ms41	1	10	**317**	**102**	**0.902**	11	509	164	0.843
ms51	1	11	**845**	**215**	**0.836**	11	1150	310	0.777

Table 19. Mean noise-induced gap inflation per method family and problem. The noise penalty is defined as (HW gap − Sim gap) for each instance where both are available; positive values indicate that hardware execution worsens the gap, negative values indicate that hardware execution improves on the simulator-measured gap. Reported errors are standard errors across instances.

Problem	Method family	N	Median N_{2Q}	Mean noise penalty (%)
MDKP	VQE-family	22	310	-7.1 ± 3.5
MDKP	Qubit-efficient	12	260	-6.3 ± 4.6
MIS	VQE-family	4	120	$+4.2 \pm 2.6$
MIS	Qubit-efficient	4	13	$+6.2 \pm 6.3$

assignment interactions, one-hot feasibility constraints, sparse feasible support, compilation overhead, and hardware noise all contribute to the observed failure of feasible-solution recovery.

Figure 6 presents the feasible MDKP and MIS hardware outcomes as a function of the independent-error gate-count fidelity proxy F_{est}. The figure separates the strongly noise-dominated regime, $F_{\mathrm{est}} < 10^{-3}$, in panel (a) from the signal-preserving regime, $F_{\mathrm{est}} \geq 10^{-3}$, in panel (b). This separation distinguishes the deeply compiled QAOA-family executions from the lower-depth variational and qubit-efficient circuits that remain within the higher-fidelity regime. The dashed reference lines in panel (b) mark the benchmark-specific values $F_{\mathrm{est}} = 0.01$ and $F_{\mathrm{est}} = 0.1$, which are used as diagnostic reference points rather than universal performance thresholds. MSP outcomes are excluded because they use total absolute deviation rather than percentage optimality gap, while QAP outcomes are excluded because no reported hardware QAP execution returns a feasible solution.

Table 19 reports the mean noise penalty, defined as the per-run difference between hardware gap and simulator gap, for each method family and problem where both gaps are available.

Two features of Table 19 warrant explicit discussion. First, the MIS noise penalty is small and positive, as expected: hardware execution on small MIS instances degrades solution quality relative to simulation. Second, the MDKP noise penalty is *negative*: under the fixed-shot and fixed-evaluation protocol, hardware runs obtain lower optimality gaps than the corresponding shot-based simulator runs on average.

This observation should not be interpreted as evidence that hardware noise is intrinsically beneficial or that it generically improves variational optimization. It may reflect a combination of finite-shot stochasticity, best-candidate selection, optimizer-trajectory variability, and backend-specific execution effects. To test whether MPS bond truncation could explain this pattern, we performed targeted stability checks on the 99-qubit CVaR-VQE `pet2` circuit and the 60-qubit VQE `hp1` circuit, both of which contribute to the negative MDKP gap. As reported in Appendix E, the production uncapped MPS results were reproduced by explicit converged and conservative bond caps, while relaxed truncation thresholds left decoded solution quality unchanged. Thus, for these representative VQE-family MDKP cases, we find no evidence that MPS bond-dimension truncation explains the negative simulator–hardware gap.

The result remains an empirical property of the present protocol rather than a causal demonstration of noise-assisted escape from local minima. The stability audit is deliberately scoped to the selected VQE-family cases. It does not separately validate a historical MDKP PCE result because the archived 182-parameter PCE circuit cannot be reconstructed exactly from the currently available 42-parameter implementation and no serialized legacy circuit artifact is available.

Figure 7 summarizes the feasibility landscape across the whole benchmark.

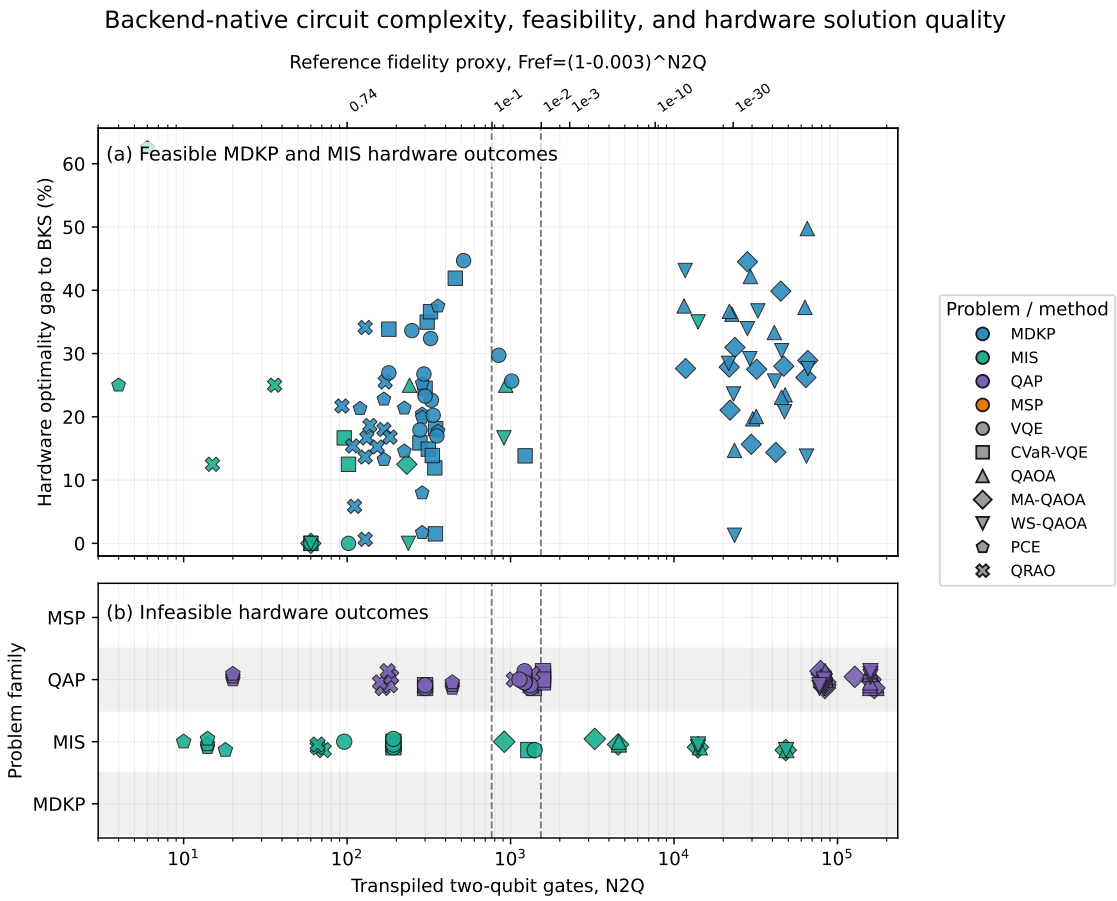

Figure 5. Backend-native circuit complexity, feasibility, and hardware solution quality. **(a)** Feasible MDKP and MIS hardware outcomes, plotted as optimality gap to BKS against the transpiled two-qubit-gate count N_{2Q}. **(b)** Infeasible hardware outcomes, grouped into shaded problem-family lanes; marker shape denotes method and color denotes problem family in both panels. MSP feasible outcomes are omitted from panel (a) because they use TDev rather than percentage optimality gap, but MSP infeasible outcomes are retained in panel (b). QAP appears only in panel (b) because all reported hardware QAP outcomes are infeasible. The lower x-axis shows backend-native N_{2Q}; the upper x-axis gives the common reference mapping $F_{\mathrm{ref}} = (1 - 0.003)^{N_{2Q}}$. This upper axis is a visual reference under the median Heron-r2 CZ error and is not a substitute for the backend-specific F_{est} values reported in the appendix. Vertical dashed lines mark the reference thresholds $F_{\mathrm{ref}} = 0.1$ and $F_{\mathrm{ref}} = 0.01$. The matched uniform-random control for low-fidelity QAOA-family runs is reported separately in Appendix N.

5.8.1 Implications. Taken together, the fidelity analysis, Figures 5–7, and Table 19 support four quantitative conclusions.

1. *The fidelity thresholds derived in Sec. 4.13 serve as useful empirical diagnostics within this benchmark.* They should be read as execution-aware reference points under the observed Heron calibration regime, not as first-principles predictive laws.

2. *QAP provides the clearest example of a structural feasibility barrier under current hardware constraints.* The direct QAP encodings combine 100–144 binary variables, dense quadratic interactions, row-and-column one-hot assignment penalties, broad coefficient ranges, and feasible subsets occupying only approximately $10^{-23.54}$ to $10^{-34.67}$ of the corresponding binary hypercubes. The QAP failure is therefore not attributable to gate count alone: restrictive feasibility geometry, dense compilation overhead, execution noise, and recovery sensitivity jointly place the tested end-to-end pipelines outside the reliable hardware operating regime.

3. *Deeply compiled QAOA-style methods are predominantly random-baseline-limited under the tested protocol.* Their compiled circuits fall far below the benchmark-specific gate-count fidelity regime identified above. Across the 106 low-fidelity QAOA-family hardware runs, matched uniform-random controls show that most feasible outcomes lie within the empirical random range or are worse than random best-shot selection under the same trajectory-level selection and one-round local-refinement procedure. This does not prove that every

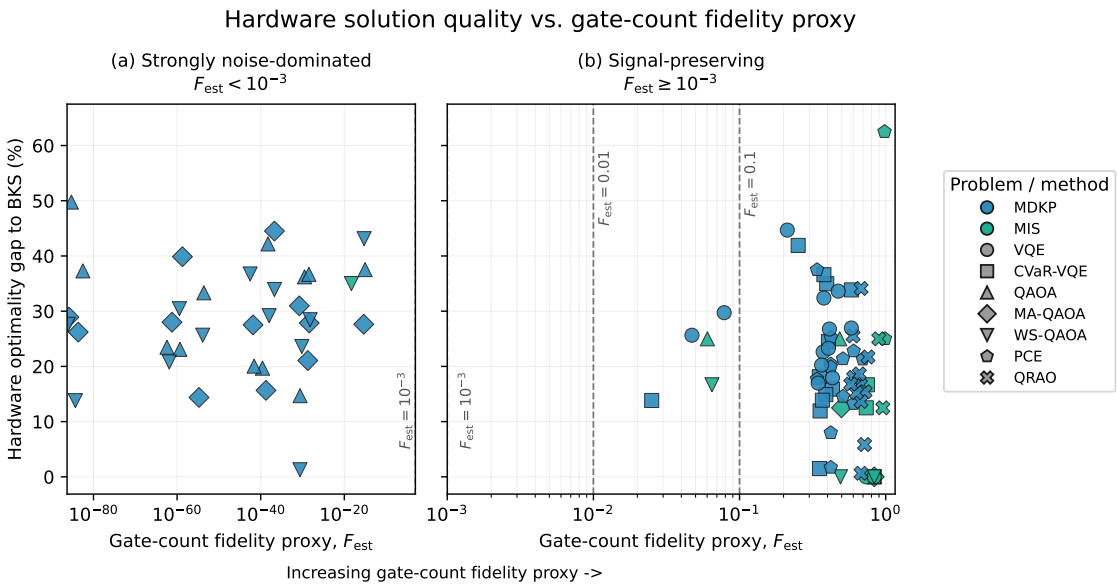

Figure 6. Feasible MDKP and MIS hardware outcomes versus the independent-error gate-count fidelity proxy F_{est}. **(a)** Strongly noise-dominated regime, $F_{\text{est}} < 10^{-3}$. **(b)** Signal-preserving regime, $F_{\text{est}} \geq 10^{-3}$. The panels are ordered from lower to higher fidelity to make the transition across the $F_{\text{est}} = 10^{-3}$ boundary visually continuous. The dashed lines in panel (b) mark the benchmark-specific heuristic reference values $F_{\text{est}} = 0.01$ and $F_{\text{est}} = 0.1$. MSP outcomes are omitted because they are evaluated using TDev rather than percentage optimality gap; QAP outcomes are omitted because no reported hardware QAP run is feasible. The matched uniform-random control for the low-fidelity QAOA-family subset is reported separately in Appendix N.

low-fidelity output distribution is uniform; one MIS warm-start-QAOA case is reported separately as a finite-sample feasibility exception.

4. *Qubit efficiency is beneficial only when compression survives compilation and decoding.* PCE gives short compiled circuits for MIS and MDKP, but the MSP results show that circuit width alone does not guarantee strong recovered solutions.

6 Discussion

6.1 Problem-dependent method performance

The problem-dependent variation summarized in Sec. 5.6 suggests that near-term quantum optimization benchmarks should be interpreted as problem–method–hardware triples rather than as method rankings alone. The qualitative behavior changes across MDKP, MIS, QAP, and MSP: different problem structures expose different bottlenecks in the quantum workflow, including constraint handling, graph structure, interaction density, and decoding sensitivity. As a result, a method that appears competitive on one benchmark family may fail to retain that position once the problem structure changes.

This has an important consequence for benchmark design. Claims about practical method quality should be based on portfolios of structurally distinct problems rather than on isolated demonstrations. In particular, the present results support difficulty-at-small-sizes benchmarking, where instances remain classically meaningful while still exposing different failure modes of near-term quantum methods. From this perspective, the value of a benchmark suite such as QOBLIB is not only that it contains hard instances, but that it prevents overgeneralization from a narrow class of favorable formulations.

A second implication is methodological. Since method rankings are conditional rather than absolute, comparisons should be framed less as searches for a u niversally best NISQ optimizer and more as attempts to identify which algorithmic features remain effective under which structural regimes. This shifts the benchmarking goal from winner selection to regime characterization, which is more informative for both hardware-facing evaluation and future method development.

6.2 Qubit compression versus practical hardware performance

The cross-problem results show that compression is useful but not sufficient. PCE and QRAO reduce circuit width substantially for several problem families, but practical performance depends on whether the compressed representation also leads to favorable compiled circuits and reliable

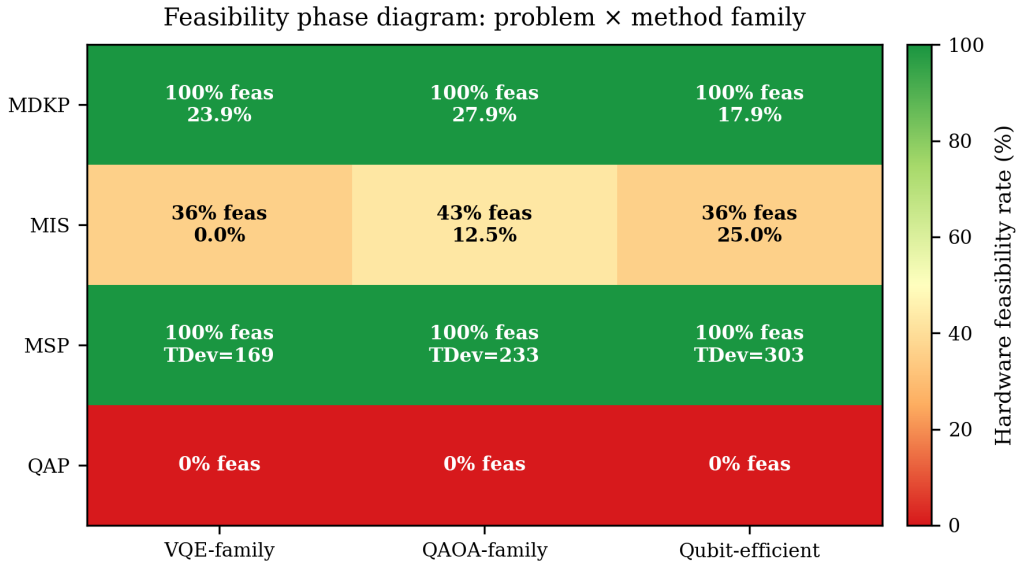

Figure 7. Feasibility phase diagram. Cell colour indicates the fraction of hardware runs that returned feasible solutions for each (problem, method-family) pair. Cell annotation reports the median hardware gap to BKS among feasible runs (TDev for MSP, for which a target-deviation metric is appropriate). MDKP and MSP remain universally feasible because their QUBO formulations are unconstrained and every bitstring is classically feasible; MIS exhibits the sharp feasibility cliff documented in Section 5.3; QAP is uniformly infeasible across all seven methods and all eleven instances.

recovery. Figure 8 plots circuit width against recovered hardware quality and shows that lower qubit count does not by itself predict better outcomes.

The main implication is that width reduction must be evaluated jointly with the distortions it may introduce elsewhere. Compressed encodings can alter the effective optimization landscape, increase decoding sensitivity, or shift difficulty from qubit count to recovery quality after measurement. They may also remain vulnerable to compilation-induced overhead once the reduced pre-transpiled circuit is mapped to a specific backend. As a result, the relevant practical question is not whether a method uses fewer qubits, but whether the width reduction survives the full path from encoding to executed circuit to recovered solution.

This point matters because qubit count is often the most visible headline metric in quantum optimization studies. The present benchmark suggests that such reporting can be misleading when presented in isolation. A lower-width method may be more runnable yet less competitive in recovered hardware quality, while a larger-width method may still be preferable if its encoding, circuit structure, and decoding pipeline are better aligned with the backend. For this reason, claims of practical advantage from qubit-efficient formulations should be supported by hardware-realized solution quality, compilation diagnostics, and recovery robustness rather than by width reduction alone.

6.3 The simulator–hardware gap

The simulator results provide controlled algorithmic references, but the hardware runs show how those references change after compilation, routing, calibration variability, and finite-shot execution are introduced.

This has an important methodological consequence. Simulator results should not be interpreted as direct evidence of near-term deployability, but as one stage in a layered evaluation workflow. In that workflow, simulation can help rule out clearly weak formulations, estimate baseline sensitivity, and guide candidate selection, but claims about practical robustness should be reserved for methods that remain competitive after execution on real hardware. The relevant object of evaluation is therefore not the algorithmic circuit alone, but the executed circuit together with its backend-specific realization.

More broadly, the simulator–hardware gap changes how progress should be interpreted in quantum optimization. Improvement in idealized simulation is scientifically useful, but it is not sufficient evidence that a method has advanced the practical frontier. A formulation that performs well before transpilation yet fails systematically after mapping to hardware should be understood as algorithmically interesting but operationally immature. For this reason, simulator studies

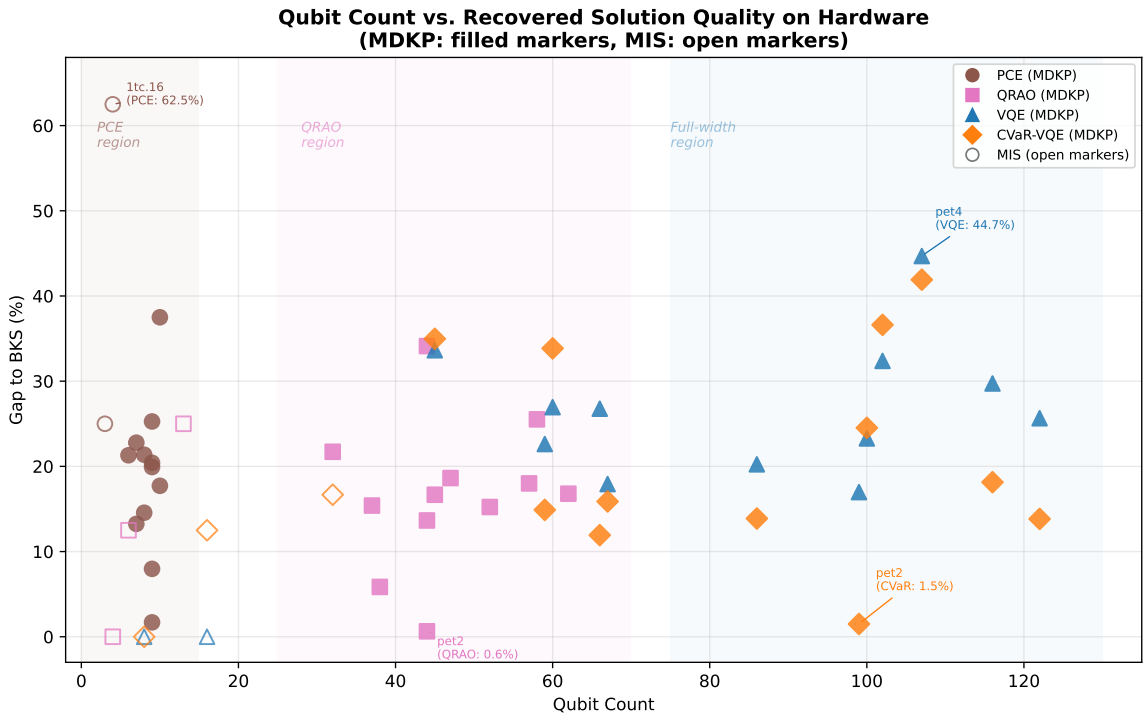

Figure 8. Qubit count versus recovered hardware solution quality for MDKP and MIS. Filled markers denote MDKP results and open markers denote MIS results, with regions indicating PCE, QRAO, and full-width formulations. The scatter shows that lower qubit count does not by itself guarantee better recovered hardware performance: qubit-efficient methods often enable access to smaller-width executions, but their achieved gaps vary substantially, while some larger-width formulations remain competitive or superior on selected instances. The plot thus illustrates that qubit compression is an access-enabling resource reduction, not a standalone predictor of final hardware solution quality.

remain necessary, but they should be paired with hardware-facing diagnostics whenever the claim concerns practical near-term capability.

6.4 Compilation and execution as first-class benchmark dimensions

A central implication of the benchmark is that compilation and execution should be treated as transformation stages that can materially change the identity of a quantum optimization method in practice. Two approaches that appear similar at the algorithmic level may cease to be comparable after transpilation if one incurs substantially greater routing overhead, deeper compiled circuits, or higher exposure to backend-specific error channels. From this perspective, practical benchmarking should evaluate not only the nominal formulation, but also how strongly that formulation degrades when mapped to hardware.

This shifts the interpretation of algorithmic performance. Algorithmic-level resource counts remain useful because they describe the intended structure of a method, but they are not sufficient to characterize deployability. The more informative question is how much of the algorithmic advantage survives compilation and execution. In near-term settings, this survival rate may be more consequential than the original circuit specification itself, especially when differences in compiled depth, two-qubit gate counts, or job robustness dominate the final quality of recovered solutions.

The broader methodological consequence is that benchmark studies should distinguish clearly between algorithmic design efficiency and hardware-realized efficiency. Conflating the two can lead to overstated claims, particularly for methods whose nominal compactness weakens after routing or whose execution behavior is unstable across backends. Treating compilation and execution as first-class benchmark dimensions therefore does more than add engineering detail: it changes what counts as convincing evidence in near-term quantum optimization.

6.5 Implications for future quantum optimization benchmarks

Beyond the specific methods and problems studied here, the benchmark has broader methodological implications. First, future benchmark studies should move beyond reporting only the best objective value obtained by a method. For constrained combinatorial problems, feasibility

Table 20. Summary decision table for near-term gate-based quantum optimization, based on the empirical regimes documented in this benchmark.

If your problem has...	Consider...	Avoid...
< 60 qubits with sparse quadratic couplings (small packing, MIS)	VQE or CVaR-VQE with EfficientSU2 of moderate repetition count; Runtime Estimator objective evaluation at `resilience_level=2`, with final candidate recovery evaluated separately from raw/default sampling	The tested standard, MA-QAOA, and WS-QAOA implementations when compiled two-qubit-gate counts exceed the empirical fidelity budget
60–120 qubits	PCE for width reduction; full-width VQE when depth permits	QAOA if exact assignment constraints are needed ($p \geq 2$ pushes N_{2Q} above 20 000)
Large permutation or assignment structure (QAP, QAP-like)	Classical solver (Gurobi, CPLEX, Concorde)	All tested quantum methods at current scale; hardware infeasibility is structural
Balancing or target-matching constraints (MSP-style)	Full-width VQE or CVaR-VQE; retain the richer ansätze	Aggressive qubit compression via PCE or QRAO at large instance sizes (recovery quality degrades)
A need to demonstrate hardware execution	Always report transpiled N_{2Q}, median backend ε_{2Q}, estimated F, Estimator mitigation settings, final-sampling configuration, and classical recovery protocol alongside the optimization result	Simulator-only claims about practical advantage; hardware execution can reshape the ranking

must be reported explicitly. For hardware studies, circuit width (qubits) alone is insufficient; transpiled circuit size, two-qubit gate burden, and execution robustness are also necessary for meaningful interpretation. Without these additional dimensions, it is difficult to distinguish between nominal algorithmic promise and practical hardware viability.

Second, future benchmarks should continue to include structurally diverse problem families. The present results show that conclusions derived from one class do not transfer reliably to others. A method that appears strong on graph-based problems may behave very differently on dense assignment problems or on balancing-type formulations. This diversity is not incidental; it is essential for assessing whether a quantum optimization strategy is genuinely general-purpose or only well matched to a narrow structural regime.

Third, the results suggest that the most informative near-term benchmarking question is not which method is globally best, but which trade-offs are currently dominant. In the present study, these trade-offs include width versus recovered quality, algorithmic design versus compiled execution cost, and simulator promise versus hardware robustness. Framing benchmarks in terms of these trade-offs may be more scientifically useful than searching for a single winning algorithm family in a regime where hardware constraints still dominate.

6.6 Practitioner guidelines for near-term deployment

The empirical patterns documented in Sections 5.2–5.8 support a compact decision table that practitioners can use to select quantum optimization methods under current hardware constraints. Table 20 is not intended as a definitive recommendation, but as a summary of the trade-offs we observed; it should be updated as hardware improves.

Two meta-level observations follow from Table 20. First, the most useful decision is rarely between two quantum methods but between a quantum method and a strong classical baseline on the specific instance size of interest. At all sizes tested in this benchmark, classical solvers such as CPLEX reach provable optimality for all MDKP, MIS, and MSP instances within seconds to minutes, and near-optimal feasible QAP solutions in minutes. The value of the quantum benchmark is not in producing a better objective value but in characterizing the execution pipeline. Second, once the fidelity budget is fixed by backend calibration, circuit width (qubits) is only one component of deployability: the product $N_{2Q} \cdot \varepsilon_{2Q}$, the cumulative noise exposure, is the more informative figure of merit, and practitioners should optimize for it rather than for qubit count

alone.

6.7 Hardware roadmap and forward-looking implications

The fidelity thresholds derived in Sec. 4.13 are anchored to the current generation of IBM Heron processors and should move as gate fidelities, connectivity, and supported circuit depths improve. IBM's published roadmap projects deeper single-processor circuits through continued gate-fidelity improvements and richer connectivity through long-range couplers [44, 45]. Such progress could expand the region in which QAOA-family circuits can be tested. The counterfactual audit in Sec. 4.13.3 shows, however, that topology-level two-qubit-gate reductions of approximately 20% are insufficient for the representative historical circuits studied here. Progress for these instances will require hardware improvement together with more substantial reductions in algorithmic cost-layer complexity, routing overhead, or parameterized-circuit depth.

However, dense assignment problems such as QAP are unlikely to become accessible through hardware scaling alone. Their compiled two-qubit-gate counts remain far above the present execution regime, so progress on this class will require both hardware improvements and encoding or compilation strategies that reduce compiled circuit size by more than a constant factor.

These observations underscore that the numerical thresholds reported here are not universal. The broader evaluation protocol—circuit width, transpiled depth, transpiled N_{2Q}, estimated fidelity, error-mitigation settings, and hardware-realized gap—is intended to remain useful as the underlying hardware numbers move.

6.8 Scope and limitations

This study is intentionally empirical and should be interpreted within that scope. The benchmark does not establish asymptotic superiority of one quantum optimization family over another, nor does it claim a practical quantum advantage over strong classical optimization methods. The tested instances remain limited by the capabilities of current hardware, and the reported results are shaped by present-day device noise, limited circuit depth, and finite execution budgets.

The MPS simulations provide an execution-consistent shot-based reference under the stated Aer configuration; they are not intended as an exhaustive comparison against all scalable classical simulation approaches. Alternative methods, including other tensor-network strategies, Pauli-propagation techniques, Gibbs-state approximations, and symmetry-aware simulators, may be advantageous in different circuit, entanglement, and noise regimes. The targeted validation in Appendix E establishes bond-cap and truncation-threshold stability for selected large MDKP VQE-family circuits, but does not constitute a universal convergence guarantee across every benchmark family, ansätze, or optimizer trajectory.

In addition, the benchmark compares representative fixed-budget implementations of each method family rather than exhaustively optimized versions of every possible variant. The recovered artifacts use a common upper cap of 200 objective evaluations, but realized stopping behavior differs across methods: many VQE-family, PCE, and QRAO runs reach the cap, whereas some QAOA-style runs terminate earlier with an optimizer-success status. Because the archived artifacts do not retain function, parameter, or gradient tolerance values, this study does not claim that every reported run reaches a common numerical convergence tolerance.

The real-hardware campaign also involves backend heterogeneity. Because queue times and backend availability made a full single-device campaign impractical, some method–instance combinations were executed on different compatible IBM processors. Backend identity, transpiled resource metrics, and execution metadata are reported for each run, but residual differences in calibration, topology, routing overhead, and execution window may contribute to cross-backend variation. The hardware results should therefore be read as execution-realistic end-to-end outcomes rather than as a controlled same-device estimate of the isolated algorithmic effect.

A reduced multi-seed simulator check further shows that initialization can materially affect decoded quality for representative VQE and warm-start QAOA instances. The headline tables should therefore be interpreted as outcomes of the documented fixed-budget protocol rather than as optimizer-independent best-case performance for each method family. Different ansätze, optimizers, or decoding strategies could improve performance in specific cases. Constraint penalties were not tuned against hardware outcomes in this study: they were fixed analytically at QUBO construction time using Eq. (6). Alternative penalty constructions may alter conditioning and practical variational optimization behavior, even when they preserve the same constrained optimum. The protocol audit and seed-sensitivity evidence are reported in Appendix C.

With these caveats in mind, the main conclusion of the discussion is clear: practical performance in gate-based quantum optimization is governed by a coupled interaction between algorithm family,

encoding strategy, compilation overhead, and hardware noise. Benchmarking studies that ignore any one of these layers risk overstating the practical value of algorithmic-level improvements.

7 Conclusion

We presented a comparative benchmark of gate-based quantum optimization methods across four classically hard 0–1 combinatorial problem families: MDKP, MIS, QAP, and MSP. By evaluating variational, QAOA-style, and qubit-efficient approaches under a shared protocol spanning both simulation and real hardware, the study provides a unified view of current near-term performance across structurally distinct problem classes.

The main empirical conclusion is that practical performance is determined by the interaction between problem structure, encoding strategy, compilation overhead, backend noise, and decoding. Algorithmic qubit count and simulator performance are therefore incomplete indicators of hardware deployability. A method that is attractive at the algorithmic level may become ineffective after routing and basis decomposition, while a compressed encoding is useful only when the resulting compiled circuit and recovery procedure remain robust.

Beyond the specific benchmark outcomes, the study argues that compilation and execution diagnostics should be treated as first-class evaluation dimensions in quantum optimization. Reporting circuit width (qubits), transpiled depth, two-qubit gate count, estimated fidelity, feasibility, and hardware-realized solution quality makes it possible to distinguish algorithmic promise from operational deployability.

The fidelity analysis developed here is hardware-window dependent, but the evaluation framework is intended to remain useful as devices improve. As gate fidelities, connectivity, and supported circuit depths increase, the numerical boundary between executable and noise-dominated regimes will move. The same protocol can therefore be used to track whether future algorithmic and hardware advances translate into measurable improvements on structurally diverse optimization problems.

Overall, the benchmark provides a reproducible empirical baseline and a diagnostic framework for interpreting near-term quantum optimization results under realistic execution constraints.

Appendix

The appendices provide the detailed formulation, protocol, simulator, compilation, hardware-diagnostic, classical-baseline, and reproducibility evidence supporting the benchmark. They are organized in the same progression as the main paper: formulation and penalty construction; optimization and method-specific recovery; simulator validation and results; compilation and hardware diagnostics; matched controls; and reproducibility and classical reference data.

Appendix A reports instance-level QUBO structural descriptors, including encoded width, coupling density, mean interaction degree, coefficient dynamic range, source metadata, and the direct-QAP feasible-space geometry. Appendix B documents the automatic instance-specific penalty construction, the selected penalty values, and a representative classical penalty-sensitivity audit.

Appendix C verifies the nominal fixed-budget variational-optimization protocol against retained benchmark records and reports the reduced initialization-sensitivity and current-PCE optimizer-resource diagnostics. Appendix D gives the mathematical formulation of Pauli Correlation Encoding (PCE), including its correlator-based reconstruction rule and the shared feasibility-preserving local-refinement procedure used after native method-specific recovery. The appendix describes available PCE enhancement mechanisms for methodological completeness, but the reported benchmark PCE runs use the single-pass protocol documented in Appendix C.

Appendix E documents the Aer MPS simulator configuration, execution environment, and targeted bond-cap and truncation-threshold stability audit for representative large MDKP VQE-family circuits. Appendix F reports the compilation-only counterfactual audit for representative bound QAOA-family circuits under historical, SWAP-aware, fractional-gate, and topology-only conditions. Appendix G provides the numerical pre-/post-transpilation source data underlying Figure 4. Appendix H provides a compact reference for the acronyms and table notation used throughout the manuscript.

Appendix I reports the full shot-based simulator results for MDKP, MIS, QAP, and MSP. Appendices J– M provide the corresponding problem-wise hardware diagnostics, including backend identity, algorithmic-level and transpiled circuit resources, and execution-robustness records for the VQE-style, QAOA-style, and encoding-based method families. Appendix N reports the matched uniform-random best-shot control for low-fidelity QAOA-family hardware runs, preserving the recorded trajectory-level candidate-selection and shared one-round local-refinement procedure.

Appendix O records the software stack, Runtime mitigation provenance, final-sampling configuration, and the master method–instance–backend fidelity and outcome table. Appendix P reports the classical Gurobi and CPLEX baseline results used to interpret the quantum solution-quality metrics. Finally, Appendix Q reports simulator resource usage by problem and method, including algorithm-level qubit count, circuit depth, total gate count, two-qubit-gate count, parameter count, and runtime.

A Instance-Level Structural Metrics

This appendix reports formulation-level descriptors for the QUBOs used in the benchmark. The purpose is to make explicit that nominal problem size alone does not capture the structural differences among MDKP, MIS, QAP, and MSP. For each instance, we characterize QUBO width, coupling density, interaction degree, coefficient dynamic range, penalty scale, source metadata, and, where analytically available, feasible-space geometry. The family-level summaries below and the instance-level tables reported in this appendix provide the structural descriptors used in the analysis.

For a QUBO with N_Q binary variables and m_Q unique nonzero off-diagonal couplings, coupling density is defined as

$$\rho_Q = \frac{2m_Q}{N_Q(N_Q-1)}. \tag{14}$$

The corresponding mean interaction degree is

$$\bar{d}_Q = \frac{2m_Q}{N_Q}, \tag{15}$$

and coefficient dynamic range is defined over the absolute values of nonzero QUBO coefficients as

$$R_Q = \frac{\max_{i\le j:Q_{ij}\neq 0}|Q_{ij}|}{\min_{i\le j:Q_{ij}\neq 0}|Q_{ij}|}. \tag{16}$$

A.1 Problem-family summary

The benchmark contains qualitatively different encoded structures. MIS is sparse because its quadratic interactions are induced by the input graph. MDKP and MSP contain moderate-to-high density introduced by capacity, slack, and target-balancing penalties. QAP is structurally distinct because its direct assignment encoding combines dense flow-distance interactions with row-and-column one-hot constraints.

Table 21. Family-level structural summary of the QUBOs used in the benchmark. Dynamic range is computed from absolute nonzero QUBO coefficients.

Problem	Instances	Width range	Density range	Median density	Median degree	Dynamic-range range
MDKP	12	45–122	0.260–0.756	0.678	42.5	8.53×10^3–6.75×10^5
MIS	7	8–128	0.095–0.269	0.181	6.0	9–129
QAP	11	100–144	0.293–1.000	0.818	95.4	1.07×10^5–2.21×10^{10}
MSP	8	48–156	0.549–0.681	0.589	58.7	9.86×10^4–1.70×10^6

We do not report a single cross-family landscape-hardness scalar based on solution degeneracy or local-minimum counts. Exact enumeration depends on the problem-specific objective and neighborhood definition, and it is not directly comparable across packing, graph, permutation, and target-allocation formulations. Instead, this appendix reports directly computable formulation descriptors for all instances and the exact feasible-space fraction for QAP, where the latter is directly relevant to the observed feasibility barrier.

A.2 QAP feasibility geometry

The direct QAP formulation uses binary assignment variables $x_{ij} \in 0, 1$, where $x_{ij} = 1$ indicates assignment of facility i to location j. An n-facility QAP therefore has n^2 binary variables, while exactly $n!$ bitstrings correspond to valid permutations. The feasible fraction of the binary hypercube is

$$\frac{n!}{2^{n^2}}. \tag{17}$$

For the smallest QAPLIB instances selected for this benchmark, `tai10a` and `tai10b`, this fraction is $10!/2^{100} \approx 10^{-23.54}$. For the tested $n = 12$ instances, it is $12!/2^{144} \approx 10^{-34.67}$. Thus, even the smallest selected direct-QAP instances have an extremely sparse feasible assignment manifold.

These structural values do not imply that QAP is impossible in simulation. The simulator results show a meaningful distinction among method families: PCE returns feasible candidates on several QAP instances, although with large optimality gaps, whereas VQE and CVaR-VQE remain infeasible. This suggests that compressed PCE reconstruction can retain partial access to the assignment manifold under noise-free execution, but it does not remove the underlying difficulty caused by dense couplings, broad coefficient scales, and sparse permutation feasibility.

B QUBO Penalty Provenance and Sensitivity Audit

This appendix documents the constraint-penalty construction used for every benchmark instance. The purpose is to distinguish analytical constraint encoding from hardware-level parameter tuning. Penalties were selected once at QUBO-construction time, before quantum execution, and were not modified by method family, backend, optimizer outcome, or hardware performance.

B.1 Automatic penalty selection

All constrained models are converted through the Qiskit Optimization `QuadraticProgramToQubo` pipeline, using `LinearEqualityToPenalty` or `LinearInequalityToPenalty` as appropriate. The converter selects a single instance-specific penalty

$$\lambda = 1 + (U_{\text{lin}} - L_{\text{lin}}) + (U_{\text{quad}} - L_{\text{quad}}), \tag{18}$$

where the bounds are evaluated on the objective before the corresponding constraint-elimination stage. The added unit margin ensures that the selected penalty exceeds the modeled pre-penalty objective range. For the integer-valued constraint residuals used in the present binary and slack-expanded formulations, any nonzero violation has squared penalty at least one.

No QUBO normalization is applied after conversion. The resulting penalized QUBO is passed directly to `to_ising()` for direct methods or to the method-specific PCE and QRAO encoders. Consequently, all methods receive the same original penalized QUBO, and the relative scale between objective and constraint terms is preserved.

Table 22. QAP direct-encoding feasibility geometry and structural descriptors. All listed QAP hardware runs are infeasible. Simulator outcomes differ: PCE returns feasible candidates on several instances, whereas VQE and CVaR-VQE remain infeasible; see Appendix I.3.

Instance	n	N_Q	$\log_{10}(\lvert\mathcal{F}\rvert/2^{N_Q})$	Density	Mean degree	Dynamic range
chr12a	12	144	−34.668	0.293	41.9	1.19×10^6
chr12b	12	144	−34.668	0.293	41.9	1.19×10^6
chr12c	12	144	−34.668	0.293	41.9	1.19×10^6
had12	12	144	−34.668	1.000	143.0	2.49×10^5
nug12	12	144	−34.668	0.731	104.5	1.07×10^5
rou12	12	144	−34.668	0.987	141.2	5.09×10^6
scr12	12	144	−34.668	0.513	73.3	2.18×10^5
tai10a	10	100	−23.543	0.964	95.4	1.68×10^7
tai10b	10	100	−23.543	0.818	81.0	1.37×10^8
tai12a	12	144	−34.668	0.974	139.3	4.13×10^7
tai12b	12	144	−34.668	0.838	119.8	2.21×10^{10}

Table 23. Instance-level penalty values selected by the automatic converter rule. Every listed value equals one plus the corresponding pre-penalty objective bound range. No post-conversion coefficient normalization is applied.

MDKP instance	λ_K	Value	MIS instance	λ_{MIS}	Value
hp1	λ_K	5,124	1tc.8	λ_{MIS}	9
hp2	λ_K	6,451	1tc.16	λ_{MIS}	17
pb1	λ_K	4,796	1tc.32	λ_{MIS}	33
pb2	λ_K	5,326	1tc.64	λ_{MIS}	65
pb4	λ_K	182,685	1dc.64	λ_{MIS}	65
pb5	λ_K	4,022	1et.64	λ_{MIS}	65
pet2	λ_K	125,895	1dc.128	λ_{MIS}	129
pet3	λ_K	5,166			
pet4	λ_K	8,656			
pet5	λ_K	15,496			
pet6	λ_K	14,724			
pet7	λ_K	22,498			

B.2 Classical sensitivity audit

A formulation-level sensitivity audit was performed on representative instances MDKP `hp1`, MIS `1tc.32`, QAP `tai10a`, and MSP `ms_seed0_prod3`. The reported penalty was multiplied by

$$\kappa \in \{0.25,\ 0.5,\ 0.75,\ 1.0,\ 1.25,\ 2.0,\ 4.0\},$$

while holding the objective, binary encoding, variable ordering, and normalization policy fixed. Each scaled QUBO was solved classically using Gurobi with a 10-second time limit, and the decoded candidate was checked against the original constraints independently of QUBO energy.

For MIS `1tc.32`, every tested multiplier, including $\kappa = 0.25$, yields a certified feasible QUBO optimum matching the classical reference independent-set size of 12. This is consistent with the direct unit-weight MIS sufficiency condition $\lambda_{MIS} > 1$ and confirms that the automatic $\lambda_{MIS} = 33$ choice is conservative.

For MDKP `hp1`, QAP `tai10a`, and MSP `ms_seed0_prod3`, the 10-second classical solves return feasible incumbents at the reported penalty but do not certify QUBO optimality. Accordingly, these rows are not used as evidence that the reported penalties are minimal, tight, or uniquely optimal. They serve only as a transparent diagnostic showing that the sensitivity sweep did not reveal an immediate feasibility failure at the tested incumbent level. The principal justification for the reported penalties remains the converter's analytical pre-penalty objective-bound construction.

C Optimization Protocol Verification and Sensitivity Analysis

This appendix documents the fixed-budget variational-optimization protocol used throughout the benchmark, verifies its realized execution against retained benchmark records, and reports reduced diagnostics for initialization sensitivity and optimizer-resource interpretation. The primary benchmark is a single-execution, fixed-protocol comparison for each method–instance configuration; it is not an exhaustive hyperparameter search or an estimate averaged over all possible initializations. Table 25 summarizes the protocol and realized execution records, Table 26 reports the reduced initialization-sensitivity study, and Table 27 separates optimizer-iteration counts from realized objective-evaluation cost for a current-PCE diagnostic.

Table 24. Instance-level QAP and MSP penalty values selected by the automatic converter rule.

QAP instance	λ_Q	Value	MSP instance	λ_M	Value
chr12a	λ_Q	5.955985×10^6	ms_seed0_prod2	λ_M	1,963
chr12b	λ_Q	5.955985×10^6	ms_seed0_prod3	λ_M	6,193
chr12c	λ_Q	5.955985×10^6	ms_seed0_prod4	λ_M	11,775
had12	λ_Q	2.492410×10^5	ms_seed0_prod5	λ_M	19,045
nug12	λ_Q	1.071850×10^5	ms_seed1_prod2	λ_M	2,061
rou12	λ_Q	4.073476×10^7	ms_seed1_prod3	λ_M	6,053
scr12	λ_Q	7.845993×10^6	ms_seed1_prod4	λ_M	12,947
tai10a	λ_Q	1.682441×10^7	ms_seed1_prod5	λ_M	20,613
tai10b	λ_Q	2.054462×10^8			
tai12a	λ_Q	4.125248×10^7			
tai12b	λ_Q	1.102967×10^{10}			

Table 25. Aggregate verification of the nominal optimization protocol using 262 retained benchmark records. The planned 200-evaluation limit is an upper bound, not a fixed realized cost for every execution.

Audit quantity	Value
Saved benchmark records audited	262
Records with `budget_reached`	149
Records with `optimizer_success`	113
Recorded optimizer	COBYLA
Optimizer implementation	`scipy.optimize.minimize`
SciPy version	1.15.3
Planned optimizer-iteration cap	200
Planned objective-evaluation cap	200
Objective shots per evaluation	1,000
Final-sampling shots, where retained	1,000
Function/parameter/gradient tolerances	not retained

C.1 Nominal protocol and execution-record verification

All benchmark method–instance configurations were evaluated under the nominal shot-based variational-optimization protocol described in Section 4.5. To provide an auditable account of its realized use, we reviewed 262 retained benchmark result records. For each recoverable record, the audit captures the problem family, instance, execution mode, method, ansatz metadata, optimizer, initialization metadata, objective-shot count, final-sampling-shot count, planned budget, realized objective evaluations, termination status, final-parameter selection rule, post-processing rule, and replayability status.

The retained records consistently identify COBYLA, invoked through `scipy.optimize.minimize` in SciPy 1.15.3, as the benchmark optimizer. The nominal protocol specifies a maximum of 200 optimizer iterations and 200 objective evaluations. Objective-evaluation metadata record 1,000 shots per evaluation, and separately retained final-sampling metadata record 1,000 shots where available. Recorded initialization metadata specify uniform parameter initialization over $[0, 2\pi]$. The benchmark runner retains the parameter vector associated with the best observed objective value before applying method-specific reconstruction or rounding, feasibility handling, and post-processing.

Table 25 summarizes the aggregate audit. The planned 200-evaluation budget is an upper bound rather than a requirement that every execution consume exactly 200 objective evaluations.

Of the 262 audited records, 149 reached the planned evaluation cap and 113 returned an `optimizer_success` status before reaching that cap. Because the retained records do not preserve explicit function, parameter, or gradient tolerances, `optimizer_success` is used only as the status returned by the optimization framework. It is not interpreted as evidence of tolerance-based convergence, local optimality, or global optimality.

The audit includes 33 retained PCE hardware records. Their stored optimizer-budget fields specify the same nominal cap of 200, while realized objective/circuit-evaluation counts are 124, 184, or 200 according to whether the run returned before the cap or exhausted the available budget. The retained PCE benchmark source path uses COBYLA.

C.2 Reduced initialization-sensitivity study

The main benchmark reports one primary protocol execution per method–instance configuration. To assess the practical sensitivity of this choice to parameter initialization, we conducted a reduced

Table 26. Reduced initialization-sensitivity study. Each row summarizes three independent parameter initializations under the nominal 200-evaluation production protocol. For MDKP and MIS, lower decoded optimality gap is better.

Problem	Inst./method	Seeds	Evals.	Status	Best gap (%)	Median gap (%)	Worst gap (%)
MDKP	`hp1` / VQE	3	200, 200, 200	budget reached	20.07	24.40	24.63
MIS	`1tc.32` / WS-QAOA	3	63, 70, 75	optimizer success	8.33	16.67	50.00
MIS	`1tc.16` / current PCE	3	200, 200, 200	budget reached	62.50	62.50	62.50

Table 27. Reduced current-PCE SLSQP diagnostic. Realized objective evaluations, rather than nominal optimizer iterations, are reported as the relevant cross-method cost metric. This diagnostic uses the current reproducible PCE implementation and is not an exact replay of the historical Brickwork-PCE hardware artifacts.

Problem	Instance	Max. iter.	Median n_{fev}	Succ.	Cap hit	Best gap	Median gap	Worst gap	Feas.
MIS	`1tc.8.txt`	100	616	1.00	0.00	25.0	25.0	25.0	1.00
MIS	`1tc.8.txt`	200	616	1.00	0.00	25.0	25.0	25.0	1.00
MIS	`1tc.16.txt`	100	2,590	0.00	1.00	62.5	62.5	62.5	1.00
MIS	`1tc.16.txt`	200	5,105	0.00	1.00	62.5	62.5	62.5	1.00
QAP	`nug12.dat`	100	7,690	0.00	1.00	–	–	–	0.00
QAP	`nug12.dat`	200	15,317	0.00	1.00	–	–	–	0.00

simulator study using three independent parameter initializations for three representative cases:

- MDKP `hp1` with VQE;
- MIS `1tc.32` with warm-start QAOA;
- MIS `1tc.16` with the current reproducible PCE implementation.

The study uses initialization seeds 1103, 4409, and 7703. Each run uses the same Aer MPS configuration, nominal 200-evaluation cap, 1,000-shot objective budget, reconstruction or rounding procedure, and post-processing pipeline as the corresponding benchmark protocol. Each seed produces one final production-style sampling result; the study therefore measures initialization-induced variation under the stated protocol, rather than separately estimating variance from repeated final-sampling draws.

Table 26 reports the resulting best, median, and worst decoded gaps across the three tested initializations. For MDKP and MIS, lower decoded optimality gap is better.

The VQE and warm-start-QAOA cases show that decoded solution quality can be materially initialization-sensitive. In particular, the three warm-start-QAOA runs returned `optimizer_success` after 63, 70, and 75 objective evaluations, but their decoded gaps ranged from 8.33% to 50.00%. The selected current-PCE case produced identical decoded gaps across the three tested initializations, although all three runs exhausted the nominal 200-evaluation budget. These results support interpreting the primary benchmark values as representative outcomes of a stated fixed-budget protocol rather than as optimizer-independent best-case values.

C.3 PCE optimizer-resource diagnostic

Optimizer iteration counts are not directly comparable across method families, because different optimizers can require different numbers of objective evaluations per iteration. To make this distinction concrete, we performed a reduced SLSQP diagnostic using the current reproducible PCE implementation on MIS `1tc.8`, MIS `1tc.16`, and QAP `nug12`. This diagnostic is not an exact replay of the historical Brickwork-PCE benchmark runs and is not used to validate their reported performance. Its sole purpose is to illustrate why realized objective evaluations, rather than nominal optimizer iterations, are the appropriate cross-method cost metric.

Table 27 reports the median number of objective evaluations, optimizer-success frequency, cap-hit frequency, decoded quality, and feasibility rate for SLSQP limits of 100 and 200 iterations.

For MIS `1tc.8`, SLSQP terminates successfully at both iteration limits, with median 616 objective evaluations and an unchanged median decoded gap of 25.0%. For MIS `1tc.16`, increasing the SLSQP cap from 100 to 200 iterations increases the median objective-evaluation count from 2,590 to 5,105 without changing the median decoded gap of 62.5%. For QAP `nug12`, the corresponding median objective-evaluation counts increase from 7,690 to 15,317, while no feasible decoded solution is recovered at either cap. These results reinforce the use of realized objective evaluations, rather than optimizer iterations alone, as the relevant cross-method budget measure.

C.4 Scope and interpretation

The analyses in Tables 25, 26, and 27 do not constitute a complete multi-seed or budget-doubling rebenchmark over all method–instance combinations. They instead provide targeted evidence on three issues raised by the benchmark protocol: realized budget consumption, sensitivity to initialization, and the non-comparability of optimizer iterations across optimization methods.

Accordingly, the manuscript reports realized objective evaluations and termination statuses where available, avoids tolerance-based convergence claims when the corresponding metadata were not retained, and interprets headline results as outcomes of the documented fixed-budget protocol. The results should not be read as optimizer-independent best-case performance estimates for each algorithmic family.

D Pauli Correlation Encoding: Formulation and Enhancements

This appendix provides the mathematical details of the Pauli Correlation Encoding (PCE) method used in the benchmark, including the QUBO-based loss formulation, the parameterized quantum ansätze, and the dynamic perturbation and multi-reoptimization strategy that we introduce as enhancements to the original PCE framework [5].

D.1 Encoding principle

PCE maps a combinatorial optimization problem with $m = \mathcal{O}(n^k)$ binary variables onto only n qubits, where k is a user-selected integer controlling the compression order. The encoding leverages k-body Pauli correlations rather than assigning one qubit per variable as in standard QAOA or VQE encodings.

Concretely, the m binary decision variables $x = \{x_i\}_{i\in[m]}$ are associated with a subset of Pauli strings Π_i (excluding the n-fold identity) via

$$x_i = \operatorname{sgn}\big(\langle \Pi_i \rangle\big) \quad \text{for all } i \in [m], \tag{19}$$

where $\langle \Pi_i \rangle = \langle \Psi | \Pi_i | \Psi \rangle$ is the expectation value of Π_i with respect to the parameterized quantum state $|\Psi(\theta)\rangle$.

The parameters θ are optimized variationally to minimize a non-linear loss function whose first term relaxes the binary sign function into a smooth hyperbolic tangent:

$$\mathcal{L} = \sum_{(i,j)\in E} W_{ij} \tanh\big(\alpha\langle \Pi_i \rangle\big) \tanh\big(\alpha\langle \Pi_j \rangle\big) + \mathcal{L}^{(\mathrm{reg})}. \tag{20}$$

The regularization term

$$\mathcal{L}^{(\mathrm{reg})} = \beta\,\nu \left[\frac{1}{m} \sum_{i=1}^{m} \tanh\big(\alpha\langle \Pi_i \rangle\big)^2 \right]^2 \tag{21}$$

penalizes large correlator magnitudes, keeping the optimizer within the correlator domain where all bitstring solutions are representable. The parameter ν is set using the Polják–Turzík bound [48] for Max-Cut problems, while β is typically fixed at $\frac{1}{2}$.

D.2 QUBO-based loss formulation

For general QUBO problems (beyond Max-Cut), we replace the graph-based loss with a formulation native to the QUBO objective $\min_{\mathbf{x}\in\{0,1\}^n} \mathbf{x}^\top Q\,\mathbf{x} + \mathbf{c}^\top \mathbf{x} + \text{offset}$, where $Q \in \mathbb{R}^{n\times n}$ is a symmetric cost matrix and $\mathbf{c} \in \mathbb{R}^n$ contains linear coefficients. The updated loss function is

$$\begin{aligned} \mathcal{L} = &\sum_{(i,j)\in E} Q_{ij} \tanh\big(\alpha\langle \pi_i \rangle\big) \tanh\big(\alpha\langle \pi_j \rangle\big) \\ &+ \sum_{i=1}^{m} c_i \tanh\big(\alpha\langle \pi_i \rangle\big)^2 + \mathcal{L}^{(\mathrm{reg})}, \end{aligned} \tag{22}$$

with the regularization parameter ν set via the Frobenius norm of Q:

$$\nu = c \cdot \sqrt{\textstyle\sum_{i,j} Q_{ij}^2}\,. \tag{23}$$

This formulation avoids the intermediate conversion to weighted Max-Cut that is otherwise required to apply the original PCE loss, thereby broadening the method's applicability to arbitrary QUBO instances.

D.3 Quantum ansätze

The parameterized circuit $|\Psi(\boldsymbol{\theta})\rangle$ uses a *Brickwork* architecture consisting of alternating layers of single-qubit rotation gates (R_X, R_Y, R_Z) and two-qubit R_{XX} entangling gates arranged in a staggered brick-like pattern. This structure ensures full qubit connectivity within each layer pair while keeping the circuit depth linear in the number of layers.

D.4 Dynamic perturbation and multi-reoptimization

To reduce the risk of premature convergence to local minima, we introduce a multi-phase re-optimization strategy that iteratively perturbs the trained circuit parameters.

At each re-optimization round r, a candidate parameter vector is generated as

$$\tilde{\theta} = \theta + \Delta_r + \Delta_d \,, \tag{24}$$

where the random component $\Delta_r \sim \mathcal{N}\big(0,\, [P'(1+f/5)]^2\, I\big)$ is scaled by both a perturbation factor P' and a failure counter f that tracks consecutive rounds without improvement, and the directional component $\Delta_d = P' \cdot \mathrm{sgn}(T)$ biases the search along the historical trend T.

The perturbation factor is amplified every third round ($P' = E \cdot P$, with exploration factor E) and decayed by a factor $\delta < 1$ upon improvement. If the failure counter exceeds a restart threshold f_{restart}, the parameters are reinitialized uniformly in $[-\pi, \pi]$. For intermediate stagnation levels, the algorithm applies either weighted blending toward the best-known solution or a stronger adaptive perturbation.

D.5 Native PCE reconstruction and shared local refinement

PCE converts its compressed quantum representation into a binary decision vector through the correlator-sign reconstruction rule in Eq. (19). This reconstruction is specific to PCE and is the method's native decoding operation; it is not a separate classical local-search advantage.

After native decoding, the benchmark applies the same single one-pass feasible local-improvement routine to the decoded candidate produced by every quantum method. Thus, PCE, VQE, CVaR-VQE, QAOA, MA-QAOA, WS-QAOA, and QRAO all receive the same final refinement stage after their respective native decoding or rounding procedures. The routine evaluates the prescribed local-swap neighborhood for the underlying problem formulation and accepts only moves that improve the original objective while preserving feasibility.

For PCE, the shared local-improvement stage starts from the binary candidate obtained through Eq. (19). It does not introduce recursive PCE re-optimization, additional variational training rounds, or a PCE-exclusive search budget. The benchmark therefore reports PCE as part of the same end-to-end hybrid quantum–classical evaluation protocol used for all compared quantum methods. The distinction between PCE-specific reconstruction and the shared local-improvement stage is important: the former is required to decode the compressed correlator representation, whereas the latter is a common post-processing rule applied uniformly across method families.

E MPS Validation and Simulator Reproducibility

This appendix documents the matrix-product-state (MPS) simulator configuration and a targeted stability audit for the large MDKP VQE-family circuits most relevant to the negative simulator–hardware gap discussed in the main text. The purpose of the audit is to test whether the production MPS reference is sensitive to bond-dimension restriction or truncation-threshold choices.

E.1 Software and execution environment

All validation runs used Python 3.10.16, Qiskit 2.3.0, and Qiskit Aer 0.17.2. The calculations were performed on an Apple M3 Pro CPU system with 12 CPU cores and 36 GB physical memory; no GPU acceleration was used. Aer was run with the `matrix_product_state` method on CPU in double precision. The production MPS configuration used adaptive uncapped bond dimension,

$$\texttt{matrix_product_state_max_bond_dimension=None}, \tag{25}$$

with truncation enabled at threshold

$$\epsilon_{\text{trunc}} = 10^{-16}. \tag{26}$$

Table 28. Targeted MPS stability audit for representative large MDKP VQE-family circuits. Each setting uses 20 independent final-sampling repetitions with 1,000 shots per repetition. TVD is the empirical total-variation distance relative to the production uncapped MPS setting, computed from the aggregated 20,000-shot empirical distributions. $\chi_{\max}$ denotes the requested MPS bond-dimension cap; "uncapped" denotes `matrix_product_state_max_bond_dimension=None`. Raw feasible mass is measured before classical recovery. All decoded repetitions were feasible.

Case	Setting	$\chi_{\max}$	ϵ_{trunc}	TVD	Raw feas. mass	Mean gap (%)	Best gap (%)
CVaR-VQE/`pet2`	production	uncapped	10^{-16}	0	0.6419	11.27 ± 6.15	0.21
	restrictive cap	32	10^{-16}	0.04635	0.6418	11.27 ± 6.15	0.21
	converged cap	64	10^{-16}	0	0.6419	11.27 ± 6.15	0.21
	conservative cap	128	10^{-16}	0	0.6419	11.27 ± 6.15	0.21
	uncapped threshold test	uncapped	10^{-12}	0	0.6419	11.27 ± 6.15	0.21
	uncapped threshold test	uncapped	10^{-8}	0.00135	0.6421	11.27 ± 6.15	0.21
VQE/`hp1`	production	uncapped	10^{-16}	0	0.6036	18.69 ± 4.93	9.98
	restrictive cap	33	10^{-16}	0.00585	0.6034	18.69 ± 4.93	9.98
	converged cap	128	10^{-16}	0	0.6036	18.69 ± 4.93	9.98
	conservative cap	256	10^{-16}	0	0.6036	18.69 ± 4.93	9.98
	uncapped threshold test	uncapped	10^{-12}	0	0.6036	18.69 ± 4.93	9.98
	uncapped threshold test	uncapped	10^{-8}	0.00035	0.6036	18.69 ± 4.93	9.98

E.2 Validation protocol

We selected two large MDKP circuits that contribute directly to the negative simulator–hardware gap: the 99-qubit CVaR-VQE circuit for `pet2` and the 60-qubit VQE circuit for `hp1`. The validation used the archived final parameter vectors and the legacy R_Y plus circular-entanglement circuit specification reflected by the stored run artifacts. For each selected case, the variational parameters, QUBO instance, circuit construction, final sampling budget, candidate-selection procedure, and decoder were fixed to the original protocol. Only the MPS bond-dimension cap and truncation threshold were changed.

Each setting used 20 final-sampling repetitions with 1,000 shots per repetition, giving 20,000 shots per setting. The same set of 20 sampling seeds was used across all settings within a case. For each setting, we recorded the empirical sampled total-variation distance (TVD) relative to the production uncapped MPS setting,

$$\mathrm{TVD}(\hat{p}, \hat{q}) = \frac{1}{2} \sum_{z} |\hat{p}(z) - \hat{q}(z)| \,, \tag{27}$$

where $\hat{p}$ and $\hat{q}$ are the empirical distributions formed by aggregating the 20 sampled repetitions. We also recorded raw feasible-sample mass before recovery, decoded optimality-gap statistics, best recovered gap, and the fraction of final-sampling repetitions that produced a feasible decoded solution.

For `pet2`, the production uncapped MPS run reached $\chi_{\text{obs}} = 64$. We compared the production setting against a deliberately restrictive cap of 32, a converged cap of 64, a conservative cap of 128, and uncapped threshold relaxations to 10^{-12} and 10^{-8}. For `hp1`, the production run reached $\chi_{\text{obs}} = 66$. We compared against a deliberately restrictive cap of 33, a converged cap of 128, a conservative cap of 256, and the same two threshold relaxations.

E.3 MDKP MPS stability results

Table 28 reports the complete validation results. The explicitly converged and conservative caps reproduce the production sampled distributions exactly for both cases. The 10^{-12} threshold relaxation also reproduces the production result exactly. The more aggressive 10^{-8} threshold causes only small empirical TVD values, 0.00135 for CVaR-VQE/`pet2` and 0.00035 for VQE/`hp1`, without changing decoded solution quality. All 20 decoded repetitions were feasible for every listed setting.

The restrictive-cap controls demonstrate that the audit can detect harmful bond restriction. For CVaR-VQE/`pet2`, cap 32 produces sampled TVD 0.04635 relative to the production setting. For VQE/`hp1`, cap 33 produces sampled TVD 0.00585. These deviations disappear once the cap is increased to the converged or conservative setting. Thus, for the two representative large MDKP VQE-family circuits examined here, the production adaptive MPS configuration is stable to the tested bond-cap and truncation settings.

E.4 Scope of the validation

The establishes stability of the MPS reference for the selected large MDKP VQE-family circuits. It does not constitute an exact-statevector comparison, which is not practical at 60 and 99 qubits, nor

does it establish equivalent convergence for every problem family, ansätze, or optimizer trajectory in the benchmark. It tests the more specific question relevant to the MDKP noise-penalty discussion: whether the final simulator references for representative high-width VQE-family cases are sensitive to plausible bond-dimension or truncation choices. For these cases, the answer is negative.

F QAOA-Family Compilation Counterfactual Audit

This appendix evaluates whether compilation changes alone could move representative QAOA-family circuits from the strongly noise-dominated regime into the empirical signal-preserving regime identified in the main text. The analysis is compilation-only: algorithmic problem encodings, QAOA depth, and final bound parameter vectors are fixed, no parameters are retrained, and no additional quantum-hardware experiments are performed.

F.1 Representative circuits and compilation conditions

The audit includes 12 representative bound circuits: standard QAOA, MA-QAOA, and WS-QAOA for MDKP `hp1`, MIS `1tc.32`, QAP `tai10a`, and MSP `ms20`. The MSP experiment is mapped to the generated `ms_seed0_prod3` instance retained in the saved benchmark artifacts.

Each circuit is compiled under four conditions:

1. **Historical baseline:** reconstructed from saved hardware-artifact metadata using the historical heavy-hex compilation workflow.
2. **SWAP-aware Heron surrogate:** connectivity-aware SABRE initial layout and routing on a Heron-like heavy-hex surrogate.
3. **Fractional-gate Heron surrogate:** bound-circuit compilation that preserves R_{ZZ} structure where possible on the same Heron-like topology.
4. **SWAP-aware Nighthawk surrogate:** the same connectivity-aware routing procedure on a topology-only square-lattice Nighthawk surrogate.

The SWAP-aware surrogate uses a heuristic connectivity-aware SABRE layout and routing configuration. It is not an optimal-routing or SAT-proved lower bound. The Nighthawk compilation is topology-only: no Nighthawk calibration data, backend noise model, or hardware execution is used. Fractional-gate rows are also resource counterfactuals only. They are not directly comparable with the original mitigated hardware campaign because they were not executed under the original ZNE/probabilistic-error-amplification workflow.

F.2 Metrics

For each compilation condition, we record algorithmic-level two-qubit-gate count, transpiled two-qubit-gate count, SWAP count, two-qubit depth, total depth, and the same conservative gate-count fidelity proxy used elsewhere in the paper. For fractional-gate rows, this quantity is denoted $\widetilde{F}_{\text{gate}}$ because it is a resource proxy and not a calibrated fractional-gate process-fidelity estimate.

F.3 Results

Table 29 reports the full representative audit. Across all 12 circuits, square-lattice Nighthawk topology gives the largest median two-qubit-gate reduction, 19.8%, relative to reconstructed historical compilation. Fractional-gate Heron compilation yields a median reduction of 4.1%. The tested SWAP-aware Heron surrogate instead increases median two-qubit-gate count by 12.0%, illustrating that a generic connectivity-aware routing heuristic does not necessarily improve on the historical compiled routes.

Most importantly, no circuit crosses either $F_{\text{est}} \geq 10^{-3}$ or $F_{\text{est}} \geq 10^{-2}$ under any counterfactual. The observed reductions are therefore insufficient to return the selected historical QAOA-family circuits to the empirical signal-preserving regime. This supports a conclusion about the tested standard QAOA, MA-QAOA, and WS-QAOA implementations and their reported circuit scales; it does not rule out other mixers, fixed-schedule QAOA variants, specialized routing methods, or future hardware. Figure 9 visualizes the corresponding post-transpilation two-qubit-gate counts and gate-count fidelity proxies for all four compilation conditions.

Table 29. Representative bound QAOA-family compilation counterfactuals. N_{2Q} denotes transpiled two-qubit-gate count. H is reconstructed historical heavy-hex compilation; S is the SWAP-aware Heron surrogate; F is fractional-gate Heron compilation; N is the topology-only square-lattice Nighthawk surrogate. No listed circuit reaches $F_{\text{est}} \geq 10^{-3}$ or $F_{\text{est}} \geq 10^{-2}$ under any condition.

Problem	Method	Instance	N_{2Q}^{H}	N_{2Q}^{S}	N_{2Q}^{F}	N_{2Q}^{N}	Best reduction	Best proxy
MDKP	QAOA	hp1	22,621	24,918	21,153	18,075	20.1%	1.77×10^{-102}
MDKP	MA-QAOA	hp1	22,019	24,918	21,153	18,075	17.9%	1.77×10^{-102}
MDKP	WS-QAOA	hp1	23,114	24,918	21,153	18,075	21.8%	1.71×10^{-102}
MIS	QAOA	1tc.32	935	969	765	720	23.0%	2.91×10^{-5}
MIS	MA-QAOA	1tc.32	915	969	765	720	21.3%	2.91×10^{-5}
MIS	WS-QAOA	1tc.32	911	969	765	720	21.0%	2.91×10^{-5}
QAP	QAOA	tai10a	79,041	95,754	81,444	65,244	17.5%	0
QAP	MA-QAOA	tai10a	79,027	95,754	81,444	65,244	17.4%	0
QAP	WS-QAOA	tai10a	76,532	90,610	81,444	60,100	21.5%	0
MSP	QAOA	ms20	38,936	43,968	37,668	31,656	18.7%	2.21×10^{-178}
MSP	MA-QAOA	ms20	39,302	43,968	37,668	31,656	19.5%	2.21×10^{-178}
MSP	WS-QAOA	ms20	39,227	43,968	37,668	31,656	19.3%	2.21×10^{-178}

Table 30. Pre- and post-transpilation two-qubit-gate counts. Values are medians across QAOA, MA-QAOA, and WS-QAOA for the stated representative instance. The expansion factor is $N_{2Q}^{\text{transpiled}}/N_{2Q}^{\text{algorithm}}$. Recorded SWAP counts are routing metadata and should not be interpreted as an additive decomposition of final two-qubit-gate count.

Problem	Instance	N_{2Q}^{alg}	N_{2Q}^{trans}	Expansion	Median recorded SWAPs
MDKP	hp1	3,765	22,621	6.01×	5,030
MIS	1tc.32	204	915	4.49×	169
QAP	tai10a	14,310	79,027	5.52×	16,802
MSP	ms20	6,300	39,227	6.23×	8,876

G QAOA-Family Transpilation Expansion

This appendix provides the numerical source data behind Figure 4. It separates algorithm-level two-qubit-gate counts from the backend-native transpiled counts for representative bound depth-3 QAOA-family circuits. The analysis uses the same historical compilation rows as the QAOA counterfactual audit, but considers only the original reported hardware-transpilation pathway. Figure 10 visualizes the circuit-level expansion factors across all 12 representative QAOA-family circuits.

The complete circuit-level data, including circuit width, QAOA depth, algorithm-level two-qubit-gate count, transpiled two-qubit-gate count, recorded SWAP count, backend, optimization level, and historical-compilation metadata, are included in the reproducibility artifact.

H Acronym and Table-Notation Reference

Table 31 provides a quick reference for the abbreviations and compact table notation used throughout the manuscript and appendices. Acronyms are grouped by their role in the benchmark rather than listed alphabetically, so that problem classes, algorithm families, execution settings, and result-table quantities can be identified quickly.

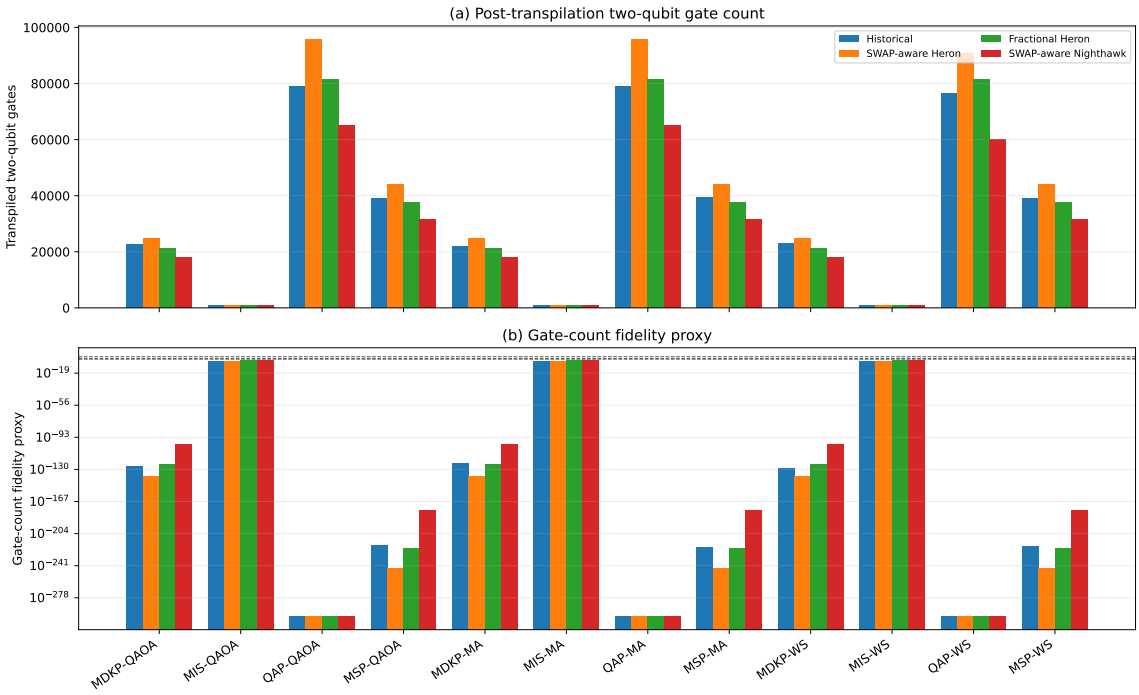

Figure 9. Compilation-only counterfactual audit for 12 representative bound QAOA-family circuits. **Top:** post-transpilation two-qubit-gate counts under reconstructed historical compilation, a SWAP-aware Heron surrogate, fractional-gate Heron compilation, and a topology-only SWAP-aware Nighthawk surrogate. **Bottom:** corresponding conservative gate-count fidelity proxies. The dashed reference lines indicate the benchmark diagnostic thresholds $F_{\text{est}} = 10^{-2}$ and $F_{\text{est}} = 10^{-3}$. No circuit crosses either threshold under any tested counterfactual. Fractional-gate values are resource proxies only and were not executed under the original ZNE/probabilistic-error-amplification workflow.

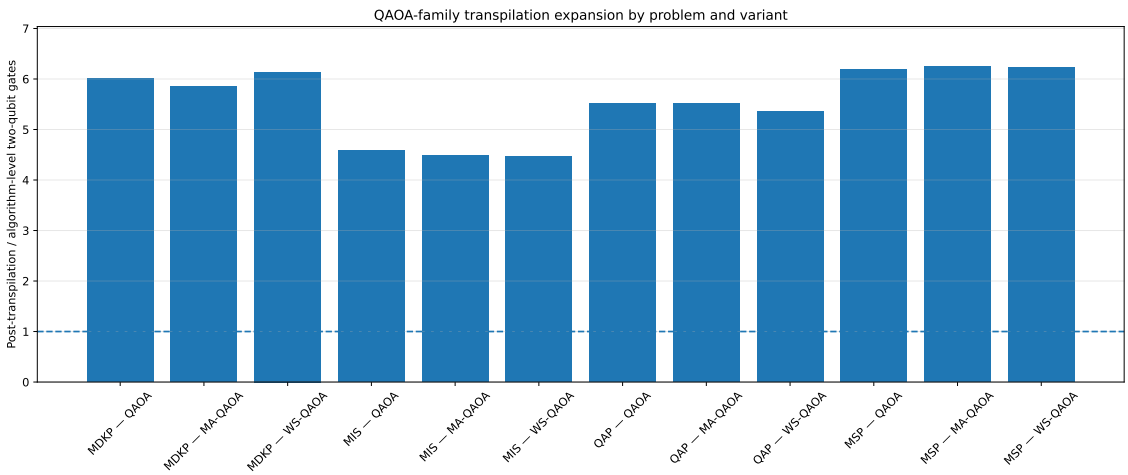

Figure 10. QAOA-family transpilation expansion factors for the 12 representative circuits in Figure 4. The dashed line at one indicates no expansion. Every circuit shows a post-transpilation two-qubit-gate count between 4.47 and 6.24 times its algorithm-level count.

Table 31. Acronym and table-notation reference. Full terms are given at first use in the main text; this table is intended as a compact reader aid for the benchmark results and supplementary diagnostics.

Category	Abbreviation	Meaning and use in this study
Problem class	MDKP	Multi-Dimensional Knapsack Problem: a packing problem with multiple capacity constraints.
Problem class	MIS	Maximum Independent Set: selection of the largest set of mutually nonadjacent graph vertices.
Problem class	QAP	Quadratic Assignment Problem: assignment of facilities to locations under quadratic flow–distance costs.
Problem class	MSP	Market Share Problem: allocation problem evaluated against prescribed market-share targets.
Problem formulation	QUBO	Quadratic Unconstrained Binary Optimization: the common binary quadratic representation used before conversion to an Ising-type cost Hamiltonian.
Reference metric	BKS	Best-known solution or value used as the classical reference target in the result tables.
MSP metric	TDev	Total absolute deviation from the prescribed market-share targets; lower values indicate better target matching.
MSP metric	MDev	Maximum single-category deviation from the prescribed market-share targets.
Variational method	VQE	Variational Quantum Eigensolver.
Risk-sensitive method	CVaR	Conditional Value-at-Risk: lower-tail objective used here with confidence level $\alpha = 0.25$.
Risk-sensitive method	CVaR-VQE	Conditional Value-at-Risk Variational Quantum Eigensolver.
Alternating-operator method	QAOA	Quantum Approximate Optimization Algorithm.
QAOA variant	MA-QAOA	Multi-Angle Quantum Approximate Optimization Algorithm.
QAOA variant	WS-QAOA	Warm-Start Quantum Approximate Optimization Algorithm.
Qubit-efficient method	PCE	Pauli Correlation Encoding: a compressed representation that reconstructs binary variables from measured Pauli correlators.
Qubit-efficient method	QRAO	Quantum Random Access Optimization: a quantum random-access-code-based optimization method with classical rounding and recovery.
Encoding primitive	QRAC	Quantum Random Access Code: the compressed coding primitive underlying the QRAO implementation.
Simulation method	MPS	Matrix Product State: the tensor-network simulation method used for the shot-based AerSimulator reference runs.
Hardware term	QPU	Quantum Processing Unit.
Compilation metric	2Q / N_{2Q}	Two-qubit gates / transpiled two-qubit-gate count. N_{2Q} is used in the process-fidelity diagnostic.
Fidelity diagnostic	F_{est}	Estimated process-fidelity proxy computed from transpiled two-qubit-gate count and representative backend error data.
Error mitigation	ZNE	Zero-Noise Extrapolation: estimator-side gate-noise mitigation used through IBM Runtime resilience settings.
Error mitigation	TREX	Twirled Readout Error eXtinction: readout-error mitigation used through IBM Runtime resilience settings.
Classical optimizer	SLSQP	Sequential Least Squares Programming: the classical optimizer used for the PCE variational objective.
Benchmark resource	QOBLIB	Quantum Optimization Benchmarking Library.
Table notation	Q / D / G / P	Respectively, circuit qubit count, circuit depth, total gate count, and number of variational parameters in the simulator-resource tables.
Solver status	OPT	Solver status indicating that a proven optimal solution was obtained.
Near-term regime	NISQ	Noisy Intermediate-Scale Quantum: the current regime of non-fault-tolerant quantum processors considered in this study.

I Simulator-Based Results

This appendix collects the full simulator-based performance tables for each benchmark problem family. These results serve as controlled reference points against which hardware-induced degradation can be measured: because the Qiskit AerSimulator (matrix product state backend, shot-based evaluation) removes queueing, calibration drift, and device-specific noise, performance differences between simulator and hardware runs isolate the cost of compilation and execution on real devices.

I.1 MDKP simulator results

Table 32 reports simulator-based performance for PCE, VQE, and CVaR-VQE on the MDKP benchmark instances. QAOA-based methods were excluded from the simulator comparison because their evaluation cost was prohibitively high even at minimal circuit depths on the dense MDKP QUBO instances. Under controlled simulation, all three methods return feasible solutions on every instance except VQE on `pb4`. Comparing these gaps with the hardware results in Section 5.2 reveals how transpilation and backend noise reshape the method ranking.

Table 32. MDKP simulator results for PCE, VQE, and CVaR-VQE. QAOA-based methods were too computationally expensive to simulate even at minimal depths. **Vars.**: number of binary variables in the QUBO formulation. For `pb4`, VQE does not return a feasible solution (gap reported as ∞).

			PCE			VQE		CVaR-VQE	
Inst.	**Opt.**	**Vars.**	**Q**	**Feas.**	**Gap**	**Feas.**	**Gap**	**Feas.**	**Gap**
hp1	3418	60	7	Yes	20.88	Yes	39.76	Yes	20.59
hp2	3186	67	8	Yes	38.38	Yes	12.34	Yes	21.78
pb1	3090	59	7	Yes	14.04	Yes	19.94	Yes	23.43
pb2	3186	66	8	Yes	14.37	Yes	19.49	Yes	22.78
pb4	95168	45	6	Yes	32.91	No	∞	Yes	39.38
pb5	2139	116	10	Yes	11.87	Yes	4.25	Yes	33.34
pet2	87061	99	9	Yes	28.19	Yes	41.07	Yes	30.37
pet3	4015	102	9	Yes	15.56	Yes	4.98	Yes	34.74
pet4	6120	107	9	Yes	50.98	Yes	66.58	Yes	48.44
pet5	12400	122	10	Yes	22.74	Yes	33.23	Yes	53.15
pet6	10618	86	9	Yes	33.84	Yes	12.50	Yes	40.41
pet7	16537	100	9	Yes	15.87	Yes	43.46	Yes	46.47

I.2 MIS simulator results

Table 33 reports simulator-based performance on the MIS instances. In contrast to the hardware results (Section 5.3), most methods achieve zero or near-zero gap on the smallest instances and retain feasibility across a wider range. This indicates that the sharp feasibility cliff observed on hardware is driven primarily by compilation overhead and backend noise rather than by algorithmic limitations at these scales.

Table 33. MIS simulator results for PCE, VQE, CVaR-VQE, QAOA, and MA-QAOA. In contrast to the hardware results (Section 5.3), most methods perform well on small instances in simulation, indicating that the hardware feasibility breakdown is driven by compilation and noise rather than algorithmic limitations at these scales.

		PCE			VQE		CVaR-VQE		QAOA	
Inst.	**Opt.**	**Q**	**Feas.**	**Gap**	**Feas.**	**Gap**	**Feas.**	**Gap**	**Feas.**	**Gap**
1tc.8	4	3	Yes	25.00	Yes	0.00	Yes	0.00	Yes	0.00
1tc.16	8	4	Yes	50.00	Yes	0.00	Yes	0.00	Yes	0.00
1tc.32	12	6	Yes	41.67	Yes	8.33	Yes	8.33	Yes	16.67
1tc.64	20	8	No	∞	No	∞	No	∞	No	∞
1et.64	18	8	No	∞	No	∞	No	∞	No	∞
1dc.64	10	8	No	∞	No	∞	No	∞	No	∞
1dc.128	16	10	No	∞	No	∞	No	∞	No	∞

I.3 QAP simulator results

Table 34 reports simulator-based performance on the QAP instances. The results provide an instructive contrast to the complete hardware infeasibility reported in Section 5.4: PCE is the only method that returns feasible solutions, albeit with large optimality gaps (15–235%), while VQE and CVaR-VQE remain infeasible even under noise-free conditions. This confirms that QAP's

dense permutation structure is inherently difficult for standard variational methods regardless of hardware effects.

Table 34. QAP simulator results for VQE, PCE, and CVaR-VQE. VQE and CVaR-VQE are infeasible on all instances (gap reported as –). PCE returns feasible solutions on all tested instances, albeit with large optimality gaps.

			VQE		PCE			CVaR-VQE	
Inst.	**Opt.**	**Vars.**	**Feas.**	**Gap**	**Q**	**Feas.**	**Gap**	**Feas.**	**Gap**
chr12a	9552	144	No	∞	11	Yes	234.75	No	∞
chr12b	9742	144	No	∞	11	Yes	15.47	No	∞
chr12c	11156	144	No	∞	11	Yes	66.82	No	∞
nug12	578	144	No	∞	11	Yes	35.98	No	∞
rou12	235528	144	No	∞	11	Yes	26.30	No	∞
scr12	31410	144	No	∞	11	Yes	71.30	No	∞
tai12a	224416	144	No	∞	11	Yes	29.78	No	∞
tai12b	39464925	144	No	∞	11	Yes	22.90	No	∞

I.4 MSP simulator results

Table 35 reports simulator-based performance on the Market Share Problem instances. Even in simulation, residual deviations from the target allocation remain non-trivial, reflecting the inherent difficulty of the balancing constraints rather than hardware noise alone.

Table 35. MSP simulator results for PCE, VQE, and CVaR-VQE. **TDev**: total absolute deviation from target split. **MDev**: maximum single-product deviation. Even in simulation, large residual deviations are observed, partly because the optimal objectives are small integers.

			PCE			VQE		CVaR-VQE	
Inst.	**Opt.**	**Q**	**TDev**	**MDev**	**Match**	**TDev**	**MDev**	**TDev**	**MDev**
ms20	3	7	3	3	No	3	2	5	3
ms30	2	8	18	12	No	12	8	15	10
ms40	1	10	35	15	No	25	12	20	9
ms50	0	11	72	28	No	55	22	48	18
ms21	3	7	5	4	No	4	3	3	2
ms31	3	8	20	14	No	10	6	12	8
ms41	1	10	38	16	No	28	14	22	10
ms51	1	11	78	30	No	60	25	50	20

J Hardware Diagnostics: MDKP

This appendix reports circuit compilation statistics and execution robustness diagnostics for all seven methods evaluated on the MDKP benchmark. For each method we provide two tables: a *circuit compilation* table reporting algorithmic-level and post-transpilation metrics (qubits, depth, total gates, two-qubit gates, and parameters) per backend, and an *execution robustness* table reporting shot budget, evaluation count, job success rates, latency statistics, and wall-clock time. These diagnostics contextualize the solution quality results in Section 5.2 by quantifying the hardware-induced overheads that shape practical performance.

J.1 MDKP: VQE-style methods

Tables 36 and 37 report compilation and execution diagnostics for VQE. Tables 38 and 39 report the corresponding diagnostics for CVaR-VQE.

Table 36. MDKP (VQE): circuit and compilation statistics. Logical metrics (qubits, depth, gates, two-qubit gates, parameters) and post-transpilation metrics per backend.

		Logical					Transpiled		
Inst.	**Backend**	**Q**	**D**	**G**	**2Q**	**P**	**D**	**G**	**2Q**
hp1	ibm_fez	60	185	480	180	240	731	1740	180
hp1	ibm_torino	60	185	480	180	240	731	1740	180
hp2	ibm_fez	67	206	536	201	268	1068	2356	338
hp2	ibm_torino	67	206	536	201	268	934	2161	279
pb1	ibm_fez	59	182	472	177	236	1015	2247	363
pb1	ibm_torino	59	182	472	177	236	985	2160	328
pb2	ibm_fez	66	203	528	198	264	1074	2356	344
pb2	ibm_torino	66	203	528	198	264	964	2196	295
pb4	ibm_fez	45	140	360	135	180	818	1707	270
pb4	ibm_torino	45	140	360	135	180	735	1636	249
pb5	ibm_fez	116	353	928	348	464	1403	3364	348
pb5	ibm_torino	116	353	928	348	464	2083	4766	847
pet2	ibm_fez	99	302	792	297	396	1236	2962	326
pet2	ibm_torino	99	302	792	297	396	1269	3032	354
pet3	ibm_fez	102	311	816	306	408	1284	3078	347
pet3	ibm_torino	102	311	816	306	408	1268	3009	324
pet4	ibm_fez	107	326	856	321	428	1405	3349	410
pet4	ibm_torino	107	326	856	321	428	1519	3640	516
pet5	ibm_fez	122	371	976	366	488	1508	3589	384
pet5	ibm_torino	122	371	976	366	488	2380	5355	1016
pet6	ibm_fez	86	267	1032	258	688	1035	3391	390
pet6	ibm_torino	86	267	1032	258	688	935	3237	336
pet7	ibm_fez	100	309	1200	300	800	919	3497	300
pet7	ibm_torino	100	309	1200	300	800	919	3497	300

Table 37. MDKP (VQE): execution robustness summary. Shots per evaluation, number of evaluations, job success counts, latency statistics, and wall-clock time.

Inst.	**Shots**	**Evals**	**Jobs (ok/fail)**	**Med. Lat. (s)**	**P95 Lat. (s)**	**Time (min)**
hp1	1000	200	200/0	8.534	13.958	43.128
hp2	1000	200	200/0	8.500	14.251	42.111
pb1	1000	200	200/0	8.492	13.914	36.385
pb2	1000	200	200/0	8.505	14.894	41.330
pb4	1000	200	200/0	8.546	14.318	37.562
pb5	1000	200	200/0	8.949	19.649	44.451
pet2	1000	200	200/0	8.548	18.904	42.780
pet3	1000	200	200/0	8.670	14.169	38.936
pet4	1000	200	200/0	9.000	52.542	87.149
pet5	1000	200	200/0	9.106	104.800	104.926
pet6	1000	200	200/0	8.700	14.409	41.173
pet7	1000	200	200/0	8.712	14.797	44.246

Table 38. MDKP (CVaR-VQE): circuit and compilation statistics. Logical metrics (qubits, depth, gates, two-qubit gates, parameters) and post-transpilation metrics per backend.

		Logical					Transpiled		
Inst.	**Backend**	**Q**	**D**	**G**	**2Q**	**P**	**D**	**G**	**2Q**
hp1	ibm_torino	60	185	480	180	240	731	1740	180
hp2	ibm_marrakesh	67	206	536	201	268	1068	2356	338
hp2	ibm_torino	67	206	536	201	268	929	2162	279
pb1	ibm_marrakesh	59	182	472	177	236	972	2153	327
pb1	ibm_torino	59	182	472	177	236	972	2124	314
pb2	ibm_marrakesh	66	203	528	198	264	1080	2354	344
pb2	ibm_torino	66	203	528	198	264	964	2196	295
pb4	ibm_marrakesh	45	140	360	135	180	970	1993	369
pb4	ibm_torino	45	140	360	135	180	812	1803	309
pb5	ibm_marrakesh	116	353	928	348	464	1403	3364	348
pb5	ibm_torino	116	353	928	348	464	2104	4838	876
pet2	ibm_torino	99	302	792	297	396	1259	3016	347
pet3	ibm_torino	102	311	816	306	408	1268	3009	324
pet4	ibm_torino	107	326	856	321	428	1452	3485	459
pet5	ibm_torino	122	371	976	366	488	2619	5963	1227
pet6	ibm_torino	86	263	688	258	344	1170	2720	332
pet7	ibm_torino	100	305	800	300	400	1211	2900	300

Table 39. MDKP (CVaR-VQE): execution robustness summary. Shots per evaluation, number of evaluations, job success counts, latency statistics, and wall-clock time.

Inst.	Shots	Evals	Jobs (ok/fail)	Med. Lat. (s)	P95 Lat. (s)	Time (min)
hp1	1000	200	200/0	19.270	21.626	57.458
hp2	1000	200	200/0	19.692	26.366	66.246
pb1	1000	200	200/0	19.580	21.897	59.023
pb2	1000	200	200/0	19.790	45.706	75.479
pb4	1000	200	200/0	8.630	24.464	42.742
pb5	1000	200	200/0	8.974	25.054	52.700
pet2	1000	200	200/0	8.763	41.798	66.312
pet3	1000	200	200/0	8.470	13.788	35.619
pet4	1000	200	200/0	8.828	14.489	43.222
pet5	1000	200	200/0	8.894	14.097	41.606
pet6	1000	200	200/0	8.678	14.505	39.838
pet7	1000	200	200/0	8.504	9.147	37.156

J.2 MDKP: QAOA-style methods

Tables 40–41 report diagnostics for QAOA, Tables 42–43 for MA-QAOA, and Tables 44–45 for WS-QAOA. The most notable compilation effect in this family is the rapid growth of transpiled two-qubit gate counts for WS-QAOA on larger instances, where the warm-start operator introduces substantial additional entangling structure.

Table 40. MDKP (QAOA): circuit and compilation statistics. Logical metrics (qubits, depth, gates, two-qubit gates, parameters) and post-transpilation metrics per backend.

		Logical					Transpiled		
Inst.	Backend	Q	D	G	2Q	P	D	G	2Q
hp1	ibm_fez	60	220	4245	3765	6	11330	86546	22501
hp1	ibm_torino	60	220	4245	3765	6	12280	86578	22621
hp2	ibm_fez	67	248	5552	5016	6	13857	111513	28967
hp2	ibm_torino	67	248	5552	5016	6	14514	115588	30329
pb1	ibm_fez	59	216	4060	3588	6	12461	83382	21821
pb1	ibm_torino	59	216	4060	3588	6	10922	80985	20909
pb2	ibm_fez	66	244	5346	4818	6	16222	111749	29320
pb2	ibm_torino	66	244	5346	4818	6	13674	108542	28059
pb4	ibm_fez	45	177	2316	1956	6	7176	44412	11522
pb4	ibm_torino	45	177	2316	1956	6	6179	43837	11119
pb5	ibm_fez	116	383	8443	7515	6	22923	178516	46275
pb5	ibm_torino	116	383	8443	7515	6	28035	181487	47838
pet2	ibm_fez	99	321	4581	3789	6	15014	92729	24261
pet2	ibm_torino	99	321	4581	3789	6	14955	90280	23440
pet3	ibm_fez	102	335	5958	5142	6	17066	124046	32232
pet3	ibm_torino	102	335	5958	5142	6	18158	122519	31868
pet4	ibm_fez	107	355	7405	6549	6	18534	158092	41325
pet4	ibm_torino	107	355	7405	6549	6	20703	157900	41078
pet5	ibm_fez	122	408	10777	9801	6	30564	239760	63249
pet5	ibm_torino	122	408	10777	9801	6	28907	237033	61641
pet6	ibm_fez	86	311	8329	7641	6	23359	178654	47056
pet6	ibm_torino	86	311	8329	7641	6	21612	175309	45464
pet7	ibm_fez	100	364	11774	10974	6	25821	254155	65365
pet7	ibm_torino	100	364	11774	10974	6	30778	251117	64817

Table 41. MDKP (QAOA): execution robustness summary. Shots per evaluation, number of evaluations, job success counts, latency statistics, and wall-clock time.

Inst.	Shots	Evals	Jobs (ok/fail)	Med. Lat. (s)	P95 Lat. (s)	Time (min)
hp1	1000	56	56/0	16.565	22.136	19.152
hp2	1000	60	60/0	16.688	51.128	28.525
pb1	1000	49	49/0	16.204	126.202	25.526
pb2	1000	49	49/0	16.470	94.612	25.196
pb4	1000	57	57/0	15.213	112.305	29.595
pb5	1000	53	53/0	17.840	33.536	19.755
pet2	1000	63	63/0	15.675	17.464	18.786
pet3	1000	53	53/0	16.759	36.663	23.444
pet4	1000	53	53/0	17.232	65.362	24.957
pet5	1000	56	56/0	24.119	43.775	66.174
pet6	1000	51	51/0	17.597	27.909	23.111
pet7	1000	58	58/0	23.737	57.358	31.400

Table 42. MDKP (MA-QAOA): circuit and compilation statistics. Logical metrics (qubits, depth, gates, two-qubit gates, parameters) and post-transpilation metrics per backend.

		Logical					Transpiled		
Inst.	Backend	Q	D	G	2Q	P	D	G	2Q
hp1	ibm_fez	60	220	4245	3765	4125	13221	86775	22896
hp1	ibm_torino	60	220	4245	3765	4125	12323	85215	22019
hp2	ibm_fez	67	248	5552	5016	5418	16548	114826	30125
hp2	ibm_torino	67	248	5552	5016	5418	14728	114316	29687
pb1	ibm_fez	59	216	4060	3588	3942	12245	82684	21754
pb1	ibm_torino	59	216	4060	3588	3942	12517	82578	21758
pb2	ibm_fez	66	244	5346	4818	5214	13485	108642	28136
pb2	ibm_torino	66	244	5346	4818	5214	14160	110256	28448
pb4	ibm_fez	45	177	2316	1956	2226	7424	44664	11506
pb4	ibm_torino	45	177	2316	1956	2226	7190	44751	11769
pb5	ibm_fez	116	383	8443	7515	8211	23279	179959	46919
pb5	ibm_torino	116	383	8443	7515	8211	21192	178172	46025
pet2	ibm_fez	99	321	4581	3789	4383	16045	90960	23551
pet2	ibm_torino	99	321	4581	3789	4383	14688	90967	23581
pet3	ibm_fez	102	335	5958	5142	5754	17605	124917	32638
pet3	ibm_torino	102	335	5958	5142	5754	16966	122721	32058
pet4	ibm_fez	107	355	7405	6549	7191	20985	159546	41625
pet4	ibm_torino	107	355	7405	6549	7191	24080	160513	41971
pet5	ibm_fez	122	408	10777	9801	10533	29079	239213	62656
pet5	ibm_marrakesh	122	408	10777	9801	10533	27861	234668	60929
pet5	ibm_torino	122	408	10777	9801	10533	30942	244192	64103
pet6	ibm_fez	86	311	8329	7641	8157	23220	174830	45006
pet6	ibm_marrakesh	86	311	8329	7641	8157	20645	175473	45943
pet6	ibm_torino	86	311	8329	7641	8157	24555	181081	47282
pet7	ibm_marrakesh	100	364	11774	10974	11574	31645	256899	66556
pet7	ibm_torino	100	364	11774	10974	11574	27783	252845	65806

Table 43. MDKP (MA-QAOA): execution robustness summary. Shots per evaluation, number of evaluations, job success counts, latency statistics, and wall-clock time.

Inst.	Shots	Evals	Jobs (ok/fail)	Med. Lat. (s)	P95 Lat. (s)	Time (min)
hp1	1000	200	200/0	15.656	31.904	74.174
hp2	1000	200	200/0	16.204	26.851	68.616
pb1	1000	200	200/0	15.768	31.438	78.120
pb2	1000	200	200/0	16.224	81.988	127.219
pb4	1000	200	200/0	15.253	25.794	63.497
pb5	1000	200	200/0	22.260	34.752	85.626
pet2	1000	200	200/0	15.737	86.152	86.775
pet3	1000	200	200/0	16.482	195.877	245.035
pet4	1000	200	200/0	22.304	125.021	154.754
pet5	1000	200	200/0	23.493	61.140	120.356
pet6	1000	200	200/0	22.777	77.704	128.654
pet7	1000	200	200/0	24.330	72.478	127.831

Table 44. MDKP (WS-QAOA): circuit and compilation statistics. Logical metrics (qubits, depth, gates, two-qubit gates, parameters) and post-transpilation metrics per backend.

		Logical					Transpiled		
Inst.	**Backend**	**Q**	**D**	**G**	**2Q**	**P**	**D**	**G**	**2Q**
hp1	ibm_fez	60	226	4605	3765	6	11913	82642	20658
hp1	ibm_torino	60	226	4605	3765	6	11945	88193	23114
hp2	ibm_fez	67	254	5954	5016	6	14710	114305	29780
hp2	ibm_torino	67	254	5954	5016	6	14804	112124	29111
pb1	ibm_fez	59	222	4414	3588	6	12646	83889	22192
pb1	ibm_torino	59	222	4414	3588	6	11390	82514	21601
pb2	ibm_fez	66	250	5742	4818	6	15456	110628	28862
pb2	ibm_torino	66	250	5742	4818	6	13743	109202	28131
pb4	ibm_fez	45	183	2586	1956	6	7172	44994	11808
pb4	ibm_torino	45	183	2586	1956	6	8043	45132	11698
pb5	ibm_fez	116	389	9139	7515	6	21330	181673	47353
pb5	ibm_torino	116	389	9139	7515	6	24725	181525	47419
pet2	ibm_fez	99	327	5175	3789	6	14412	91265	23747
pet2	ibm_torino	99	327	5175	3789	6	12887	91099	23458
pet3	ibm_fez	102	341	6570	5142	6	17378	124527	32589
pet3	ibm_torino	102	341	6570	5142	6	16250	122289	31727
pet4	ibm_torino	107	361	8047	6549	6	20281	159973	41282
pet5	ibm_torino	122	414	11509	9801	6	30377	245792	64628
pet6	ibm_torino	86	317	8845	7641	6	20991	178066	45559
pet7	ibm_torino	100	370	12374	10974	6	27930	254296	65953

Table 45. MDKP (WS-QAOA): execution robustness summary. Shots per evaluation, number of evaluations, job success counts, latency statistics, and wall-clock time.

Inst.	**Shots**	**Evals**	**Jobs (ok/fail)**	**Med. Lat. (s)**	**P95 Lat. (s)**	**Time (min)**
hp1	1000	60	60/0	15.780	21.253	19.351
hp2	1000	56	56/0	16.218	17.868	17.124
pb1	1000	68	68/0	16.047	43.036	30.552
pb2	1000	55	55/0	16.148	22.355	18.115
pb4	1000	63	63/0	15.391	20.746	21.395
pb5	1000	58	58/0	22.204	27.670	22.251
pet2	1000	55	55/0	15.794	21.586	17.101
pet3	1000	54	54/0	16.349	71.712	24.479
pet4	1000	49	49/0	16.403	17.710	15.347
pet5	1000	55	55/0	23.262	23.984	23.728
pet6	1000	45	45/0	16.956	22.491	17.986
pet7	1000	57	57/0	23.478	25.012	25.352

J.3 MDKP: encoding-based methods

Tables 46–47 report diagnostics for PCE, and Tables 48–49 for QRAO. Despite their substantially lower circuit width, both encoding methods produce non-trivial post-transpilation circuits. In particular, PCE circuits have higher circuit depth than VQE circuits on the same instances, illustrating the trade-off between qubit compression and circuit complexity that is central to the benchmark's findings.

Table 46. MDKP (PCE): circuit and compilation statistics. Logical metrics (qubits, depth, gates, two-qubit gates, parameters) and post-transpilation metrics per backend.

		Logical					Transpiled		
Inst.	**Backend**	**Q**	**D**	**G**	**2Q**	**P**	**D**	**G**	**2Q**
hp1	ibm_torino	7	57	287	84	182	393	1493	168
hp2	ibm_torino	8	65	376	112	240	449	1979	224
pb1	ibm_torino	7	57	287	84	182	393	1493	168
pb2	ibm_torino	8	65	376	112	240	449	1979	224
pb4	ibm_torino	6	49	210	60	132	337	1086	120
pb5	ibm_fez	10	81	590	180	380	561	3135	360
pb5	ibm_torino	10	81	590	180	380	561	3135	360
pet2	ibm_fez	9	73	477	144	306	505	2529	288
pet2	ibm_torino	9	73	477	144	306	505	2529	288
pet3	ibm_fez	9	73	477	144	306	505	2529	288
pet3	ibm_torino	9	73	477	144	306	505	2529	288
pet4	ibm_fez	9	73	477	144	306	505	2529	288
pet4	ibm_torino	9	73	477	144	306	505	2529	288
pet5	ibm_fez	10	81	590	180	380	561	3135	360
pet5	ibm_torino	10	81	590	180	380	561	3135	360
pet6	ibm_fez	9	73	477	144	306	505	2529	288
pet6	ibm_torino	9	73	477	144	306	505	2529	288
pet7	ibm_fez	9	73	477	144	306	505	2529	288
pet7	ibm_torino	9	73	477	144	306	505	2529	288

Table 47. MDKP (PCE): execution robustness summary. Shots per evaluation, number of evaluations, job success counts, latency statistics, and wall-clock time.

Inst.	**Shots**	**Evals**	**Jobs (ok/fail)**	**Med. Lat. (s)**	**P95 Lat. (s)**	**Time (min)**
hp1	1000	200	200/0	8.66	14.32	40.42
hp2	1000	200	200/0	8.61	13.98	37.01
pb1	1000	200	200/0	8.62	19.32	43.53
pb2	1000	200	200/0	8.62	20.14	42.26
pb4	1000	200	200/0	8.62	14.74	41.06
pb5	1000	200	200/0	8.72	46.52	72.70
pet2	1000	200	200/0	8.75	30.59	47.60
pet3	1000	200	200/0	8.81	127.30	147.46
pet4	1000	200	200/0	8.95	73.63	71.73
pet5	1000	200	200/0	8.87	14.78	40.72
pet6	1000	200	200/0	8.96	30.31	45.87
pet7	1000	200	200/0	9.07	58.03	77.65

Table 48. MDKP (QRAO): circuit and compilation statistics. Logical metrics (qubits, depth, gates, two-qubit gates, parameters) and post-transpilation metrics per backend.

		Logical					Transpiled		
Inst.	**Backend**	**Q**	**D**	**G**	**2Q**	**P**	**D**	**G**	**2Q**
hp1	ibm_fez	38	49	415	111	304	61	871	111
hp2	ibm_fez	45	56	492	132	360	68	1032	132
pb1	ibm_fez	37	48	404	108	296	60	848	108
pb2	ibm_marrakesh	44	55	481	129	352	67	1009	129
pb4	ibm_marrakesh	32	43	349	93	256	55	733	93
pb5	ibm_marrakesh	57	68	624	168	456	80	1308	168
pet2	ibm_torino	44	55	481	129	352	162	1522	129
pet3	ibm_marrakesh	44	55	481	129	352	67	1009	129
pet4	ibm_torino	47	58	514	138	376	171	1627	138
pet5	ibm_fez	58	69	635	171	464	81	1331	171
pet5	ibm_marrakesh	58	69	635	171	464	81	1331	171
pet6	ibm_fez	52	63	569	153	416	75	1193	153
pet6	ibm_marrakesh	52	63	569	153	416	75	1193	153
pet7	ibm_fez	62	73	679	183	496	85	1423	183
pet7	ibm_marrakesh	62	73	679	183	496	85	1423	183

Table 49. MDKP (QRAO): execution robustness summary. Shots per evaluation, number of evaluations, job success counts, latency statistics, and wall-clock time.

Inst.	**Shots**	**Evals**	**Jobs (ok/fail)**	**Med. Lat. (s)**	**P95 Lat. (s)**	**Time (min)**
hp1	1000	200	200/0	30.95	66.41	237.44
hp2	1000	200	200/0	32.80	91.78	227.31
pb1	1000	200	200/0	29.60	57.16	159.12
pb2	1000	200	200/0	31.00	69.14	138.50
pb4	1000	200	200/0	24.50	37.49	95.23
pb5	1000	200	200/0	31.85	65.62	188.67
pet2	1000	200	200/0	24.80	30.16	96.92
pet3	1000	200	200/0	31.95	80.71	157.92
pet4	1000	200	200/0	28.85	50.72	115.51
pet5	1000	200	200/0	36.55	165.74	258.83
pet6	1000	200	200/0	35.30	113.99	229.84
pet7	1000	200	200/0	42.80	128.37	221.51

K Hardware Diagnostics: MIS

This appendix reports compilation and execution diagnostics for all method families on the MIS benchmark. These diagnostics are particularly important for MIS because the main results (Section 5.3) reveal a sharp feasibility cliff as instance size increases. The tables below show how transpiled circuit depth and two-qubit gate counts grow across instances and backends, providing the hardware-level context for interpreting the observed feasibility breakdown.

K.1 MIS: VQE-style methods

Tables 50–51 report diagnostics for VQE, and Tables 52–53 for CVaR-VQE.

Table 50. MIS (VQE): circuit and compilation statistics. Logical metrics (qubits, depth, gates, two-qubit gates, parameters) and post-transpilation metrics per backend.

		Logical					Transpiled		
Inst.	**Backend**	**Q**	**D**	**G**	**2Q**	**P**	**D**	**G**	**2Q**
1tc.8	ibm_fez	8	29	64	24	32	174	387	78
1tc.8	ibm_torino	8	29	64	24	32	167	328	60
1tc.16	ibm_fez	16	53	128	48	64	261	623	102
1tc.16	ibm_torino	16	53	128	48	64	257	611	102
1tc.32	ibm_fez	32	101	256	96	128	395	928	96
1tc.32	ibm_torino	32	101	256	96	128	395	928	96
1tc.64	ibm_fez	64	197	512	192	256	779	1856	192
1tc.64	ibm_torino	64	197	512	192	256	779	1856	192
1et.64	ibm_fez	64	197	512	192	256	779	1856	192
1et.64	ibm_torino	64	197	512	192	256	779	1856	192
1dc.64	ibm_fez	64	197	512	192	256	779	1856	192
1dc.64	ibm_torino	64	197	512	192	256	779	1856	192
1dc.128	ibm_fez	128	389	1024	384	512	1931	4489	657
1dc.128	ibm_torino	128	389	1024	384	512	2965	6581	1403

Table 51. MIS (VQE): execution robustness summary. Shots per evaluation, number of evaluations, job success counts, latency statistics, and wall-clock time.

Inst.	**Shots**	**Evals**	**Jobs (ok/fail)**	**Med. Lat. (s)**	**P95 Lat. (s)**	**Time (min)**
1tc.8	1000	200	200/0	8.489	14.052	33.394
1tc.16	1000	200	200/0	8.467	24.764	40.188
1tc.32	1000	200	200/0	8.522	14.119	36.399
1tc.64	1000	200	200/0	8.654	14.244	38.898
1et.64	1000	200	200/0	8.437	13.826	35.473
1dc.64	1000	200	200/0	8.437	13.952	35.324
1dc.128	1000	200	200/0	8.797	19.425	62.911

Table 52. MIS (CVaR-VQE): circuit and compilation statistics. Logical metrics (qubits, depth, gates, two-qubit gates, parameters) and post-transpilation metrics per backend.

		Logical					Transpiled		
Inst.	**Backend**	**Q**	**D**	**G**	**2Q**	**P**	**D**	**G**	**2Q**
1tc.8	ibm_marrakesh	8	29	64	24	32	170	331	60
1tc.8	ibm_torino	8	29	64	24	32	176	337	60
1tc.16	ibm_marrakesh	16	53	128	48	64	255	622	105
1tc.16	ibm_torino	16	53	128	48	64	257	610	102
1tc.32	ibm_marrakesh	32	101	256	96	128	395	928	96
1tc.32	ibm_torino	32	101	256	96	128	395	928	96
1tc.64	ibm_marrakesh	64	197	512	192	256	779	1856	192
1tc.64	ibm_torino	64	197	512	192	256	779	1856	192
1et.64	ibm_marrakesh	64	197	512	192	256	779	1856	192
1et.64	ibm_torino	64	197	512	192	256	779	1856	192
1dc.64	ibm_marrakesh	64	197	512	192	256	779	1856	192
1dc.64	ibm_torino	64	197	512	192	256	779	1856	192
1dc.128	ibm_torino	128	389	1024	384	512	2855	6213	1284

K.2 MIS: QAOA-style methods

Tables 54–55 report diagnostics for QAOA, Tables 56–57 for MA-QAOA, and Tables 58–59 for WS-QAOA. For MIS, the QAOA-style circuits grow rapidly with graph size due to the problem

Table 53. MIS (CVaR-VQE): execution robustness summary. Shots per evaluation, number of evaluations, job success counts, latency statistics, and wall-clock time.

Inst.	Shots	Evals	Jobs (ok/fail)	Med. Lat. (s)	P95 Lat. (s)	Time (min)
1tc.8	1000	200	200/0	8.723	46.214	60.812
1tc.16	1000	200	200/0	8.558	24.632	41.127
1tc.32	1000	200	200/0	13.898	41.342	98.269
1tc.64	1000	200	200/0	8.748	30.126	47.822
1et.64	1000	200	200/0	19.782	24.163	58.046
1dc.64	1000	200	200/0	19.621	21.412	59.166
1dc.128	1000	200	200/0	8.650	14.456	39.590

Hamiltonian's edge structure, and routing overhead on sparse-connectivity backends further amplifies the effective depth.

Table 54. MIS (QAOA): circuit and compilation statistics. Logical metrics (qubits, depth, gates, two-qubit gates, parameters) and post-transpilation metrics per backend.

		Logical					Transpiled		
Inst.	Backend	Q	D	G	2Q	P	D	G	2Q
1tc.8	ibm_torino	8	17	82	18	6	124	390	60
1tc.16	ibm_torino	16	29	194	66	6	442	1233	241
1tc.32	ibm_torino	32	41	460	204	6	826	4141	935
1tc.64	ibm_torino	64	66	1088	576	6	1880	18387	4600
1et.64	ibm_torino	64	76	1304	792	6	1880	18387	4600
1dc.64	ibm_fez	64	155	2141	1629	6	7823	51710	14383
1dc.64	ibm_torino	64	155	2141	1629	6	7230	50389	13924
1dc.128	ibm_fez	128	242	5437	4413	6	16655	169152	48702
1dc.128	ibm_torino	128	242	5437	4413	6	17379	171179	49279

Table 55. MIS (QAOA): execution robustness summary. Shots per evaluation, number of evaluations, job success counts, latency statistics, and wall-clock time.

Inst.	Shots	Evals	Jobs (ok/fail)	Med. Lat. (s)	P95 Lat. (s)	Time (min)
1tc.8	1000	50	50/0	13.72	14.67	13.10
1tc.16	1000	62	62/0	8.75	14.09	11.91
1tc.32	1000	56	56/0	8.74	19.46	12.35
1tc.64	1000	59	59/0	8.85	12.41	10.38
1et.64	1000	65	65/0	9.08	19.64	15.14
1dc.64	1000	59	59/0	15.02	18.49	17.88
1dc.128	1000	56	56/0	16.64	21.78	17.89

K.3 MIS: encoding-based methods

Tables 60–61 report diagnostics for PCE, and Tables 62–63 for QRAO. Although both methods compress the algorithmic-level circuit width substantially, PCE's aggressive compression (e.g., 3 qubits for an 8-variable instance) comes with high circuit depth, while QRAO uses more qubits but shallower circuits.

Table 56. MIS (MA-QAOA): circuit and compilation statistics. Logical metrics (qubits, depth, gates, two-qubit gates, parameters) and post-transpilation metrics per backend.

		Logical					Transpiled		
Inst.	**Backend**	**Q**	**D**	**G**	**2Q**	**P**	**D**	**G**	**2Q**
1tc.8	ibm_fez	8	17	82	18	66	126	383	60
1tc.8	ibm_torino	8	17	82	18	66	126	383	60
1tc.16	ibm_fez	16	29	194	66	162	375	1226	237
1tc.16	ibm_torino	16	29	194	66	162	386	1232	232
1tc.32	ibm_fez	32	41	460	204	396	735	4159	931
1tc.32	ibm_torino	32	41	460	204	396	761	4112	915
1tc.64	ibm_fez	64	66	1088	576	960	1453	13369	3265
1tc.64	ibm_torino	64	66	1088	576	960	2305	13433	3274
1et.64	ibm_fez	64	76	1304	792	1176	1903	18247	4495
1et.64	ibm_torino	64	76	1304	792	1176	2160	18341	4548
1dc.64	ibm_fez	64	155	2141	1629	2013	7006	50752	14015
1dc.64	ibm_torino	64	155	2141	1629	2013	7354	50523	13926
1dc.128	ibm_fez	128	242	5437	4413	5181	15885	166696	47824
1dc.128	ibm_torino	128	242	5437	4413	5181	17098	167445	48272

Table 57. MIS (MA-QAOA): execution robustness summary. Shots per evaluation, number of evaluations, job success counts, latency statistics, and wall-clock time.

Inst.	**Shots**	**Evals**	**Jobs (ok/fail)**	**Med. Lat. (s)**	**P95 Lat. (s)**	**Time (min)**
1tc.8	1000	200	200/0	8.96	19.74	44.73
1tc.16	1000	200	200/0	9.14	14.90	39.73
1tc.32	1000	200	200/0	9.17	24.64	44.84
1tc.64	1000	200	200/0	9.45	19.87	45.10
1et.64	1000	200	200/0	14.51	67.91	86.82
1dc.64	1000	200	200/0	15.25	20.68	58.58
1dc.128	1000	200	200/0	17.31	44.04	89.61

Table 58. MIS (WS-QAOA): circuit and compilation statistics. Logical metrics (qubits, depth, gates, two-qubit gates, parameters) and post-transpilation metrics per backend.

		Logical					Transpiled		
Inst.	**Backend**	**Q**	**D**	**G**	**2Q**	**P**	**D**	**G**	**2Q**
1tc.8	ibm_torino	8	23	130	18	6	133	405	60
1tc.16	ibm_torino	16	35	290	66	6	456	1277	237
1tc.32	ibm_torino	32	47	652	204	6	849	4159	911
1tc.64	ibm_torino	64	72	1472	576	6	6986	50824	14029
1et.64	ibm_torino	64	82	1688	792	6	6986	50824	14029
1dc.64	ibm_torino	64	161	2525	1629	6	6986	50824	14029
1dc.128	ibm_torino	128	248	6205	4413	6	17168	169184	48544

Table 59. MIS (WS-QAOA): execution robustness summary. Shots per evaluation, number of evaluations, job success counts, latency statistics, and wall-clock time.

Inst.	**Shots**	**Evals**	**Jobs (ok/fail)**	**Med. Lat. (s)**	**P95 Lat. (s)**	**Time (min)**
1tc.8	1000	64	64/0	8.56	13.77	10.59
1tc.16	1000	60	60/0	8.89	41.30	15.88
1tc.32	1000	72	72/0	8.78	22.29	15.08
1tc.64	1000	59	59/0	14.79	69.14	22.13
1et.64	1000	65	65/0	14.91	15.68	17.36
1dc.64	1000	73	73/0	14.82	35.43	26.30
1dc.128	1000	62	62/0	16.51	22.63	20.62

Table 60. MIS (PCE): circuit and compilation statistics. Logical metrics (qubits, depth, gates, two-qubit gates, parameters) and post-transpilation metrics per backend.

		Logical					Transpiled		
Inst.	**Backend**	**Q**	**D**	**G**	**2Q**	**P**	**D**	**G**	**2Q**
1tc.8	ibm_fez	3	10	22	4	18	27	61	4
1tc.8	ibm_marrakesh	3	10	22	4	18	27	61	4
1tc.16	ibm_torino	4	11	30	6	24	30	84	6
1tc.32	ibm_fez	6	13	46	10	36	36	130	10
1tc.32	ibm_marrakesh	6	13	46	10	36	36	130	10
1tc.64	ibm_torino	8	15	62	14	48	42	176	14
1et.64	ibm_fez	8	15	62	14	48	42	176	14
1et.64	ibm_marrakesh	8	15	62	14	48	42	176	14
1dc.64	ibm_fez	8	15	62	14	48	42	176	14
1dc.64	ibm_marrakesh	8	15	62	14	48	42	176	14
1dc.128	ibm_torino	10	17	78	18	60	48	222	18

Table 61. MIS (PCE): execution robustness summary. Shots per evaluation, number of evaluations, job success counts, latency statistics, and wall-clock time.

Inst.	**Shots**	**Evals**	**Jobs (ok/fail)**	**Med. Lat. (s)**	**P95 Lat. (s)**	**Time (min)**
1tc.8	1000	124	124/0	23.994	46.039	104.451
1tc.16	1000	184	184/0	28.940	56.058	113.205
1tc.32	1000	200	200/0	28.168	54.459	150.307
1tc.64	1000	200	200/0	21.708	40.302	86.065
1et.64	1000	200	200/0	27.535	53.285	136.793
1dc.64	1000	200	200/0	22.786	111.521	167.134
1dc.128	1000	200	200/0	21.618	30.380	75.589

Table 62. MIS (QRAO): circuit and compilation statistics. Logical metrics (qubits, depth, gates, two-qubit gates, parameters) and post-transpilation metrics per backend.

		Logical					Transpiled		
Inst.	**Backend**	**Q**	**D**	**G**	**2Q**	**P**	**D**	**G**	**2Q**
1tc.8	statevector_primitives	4	15	41	9	32	–	–	–
1tc.16	ibm_fez	6	17	63	15	48	48	192	15
1tc.16	ibm_marrakesh	6	17	63	15	48	48	192	15
1tc.32	ibm_fez	13	24	140	36	104	69	437	36
1tc.32	ibm_marrakesh	13	24	140	36	104	69	437	36
1tc.64	ibm_torino	23	34	250	66	184	99	787	66
1et.64	ibm_fez	23	34	250	66	184	99	787	66
1et.64	ibm_marrakesh	23	34	250	66	184	99	787	66
1dc.64	ibm_torino	25	36	272	72	200	105	857	72
1dc.128	ibm_fez	46	57	503	135	368	135	540	135
1dc.128	ibm_marrakesh	57	57	503	135	368	135	540	135

Table 63. MIS (QRAO): execution robustness summary. Shots per evaluation, number of evaluations, job success counts, latency statistics, and wall-clock time.

Inst.	**Shots**	**Evals**	**Jobs (ok/fail)**	**Med. Lat. (s)**	**P95 Lat. (s)**	**Time (min)**
1tc.8	1000	200	200/0	–	–	0.261
1tc.16	1000	200	205/0	25.771	55.854	119.435
1tc.32	1000	200	202/0	27.735	61.712	115.894
1tc.64	1000	200	202/0	22.527	23.630	83.023
1et.64	1000	200	202/0	28.560	51.449	115.114
1dc.64	1000	200	202/0	26.062	58.875	114.982
1dc.128	1000	200	201/0	31.121	52.935	160.077

L Hardware Diagnostics: QAP

This appendix reports compilation and execution diagnostics for all method families on the QAP benchmark. QAP is the most demanding problem in the study: its dense quadratic assignment structure produces the largest encoded Hamiltonians and the highest post-transpilation gate counts. These diagnostics quantify the circuit burden that underlies the complete infeasibility observed in Section 5.4 and help explain why even qubit-efficient methods cannot recover feasible solutions on current hardware for this problem class.

L.1 QAP: VQE-style methods

Tables 64–65 report diagnostics for VQE, and Tables 66–67 for CVaR-VQE. The 144-qubit circuit width required for the 12-variable QAP instances already approaches the physical capacity of the tested backends, and transpilation further amplifies circuit depth and two-qubit gate counts.

Table 64. QAP (VQE): circuit and compilation statistics. Logical metrics (qubits, depth, gates, two-qubit gates, parameters) and post-transpilation metrics per backend.

		Logical					Transpiled		
Inst.	**Backend**	**Q**	**D**	**G**	**2Q**	**P**	**D**	**G**	**2Q**
chr12a	ibm_fez	144	437	1152	432	576	2995	6706	1323
chr12b	ibm_fez	144	437	1152	432	576	2995	6706	1323
chr12c	ibm_fez	144	441	1728	432	1152	2596	7380	1218
nug12	ibm_fez	144	441	1728	432	1152	2596	7380	1218
had12	ibm_fez	144	441	1728	432	1152	2596	7380	1218
rou12	ibm_fez	144	441	1728	432	1152	2596	7380	1218
scr12	ibm_fez	144	441	1728	432	1152	2596	7380	1218
tai10a	ibm_fez	100	309	1200	300	800	919	3497	300
tai10a	ibm_torino	100	309	1200	300	800	919	3497	300
tai10b	ibm_fez	100	309	1200	300	800	919	3497	300
tai10b	ibm_torino	100	309	1200	300	800	919	3497	300
tai12a	ibm_fez	144	441	1728	432	1152	2596	7380	1218
tai12b	ibm_fez	144	441	1728	432	1152	2458	7120	1134

Table 65. QAP (VQE): execution robustness summary. Shots per evaluation, number of evaluations, job success counts, latency statistics, and wall-clock time.

Inst.	**Shots**	**Evals**	**Jobs (ok/fail)**	**Med. Lat. (s)**	**P95 Lat. (s)**	**Time (min)**
chr12a	1000	200	200/0	8.681	30.096	49.703
chr12b	1000	200	200/0	9.196	159.688	144.250
chr12c	1000	200	200/0	13.837	19.875	53.118
nug12	1000	200	200/0	9.294	19.723	63.117
had12	1000	200	200/0	14.300	41.324	89.017
rou12	1000	200	200/0	9.535	79.171	109.948
scr12	1000	200	200/0	9.242	74.311	133.229
tai10a	1000	200	200/0	9.362	31.067	62.898
tai10b	1000	200	200/0	9.286	20.099	60.371
tai12a	1000	200	200/0	14.304	41.058	74.305
tai12b	1000	200	200/0	14.039	30.613	100.887

L.2 QAP: QAOA-style methods

Tables 68–69 report diagnostics for QAOA, Tables 70–71 for MA-QAOA, and Tables 72–73 for WS-QAOA.

L.3 QAP: encoding-based methods

Tables 74–75 report diagnostics for PCE, and Tables 76–77 for QRAO. PCE compresses the 144-variable QAP instances to just 11 qubits, but the resulting circuits still fail to produce feasible solutions on hardware, illustrating that extreme qubit compression does not compensate for the dense coupling structure of QAP.

M Hardware Diagnostics: MSP

This appendix reports compilation and execution diagnostics for all method families on the Market Share Problem benchmark. Unlike QAP, all methods produce feasible solutions for MSP, so the diagnostics here help explain the variation in recovered solution quality rather than feasibility. In

Table 66. QAP (CVaR-VQE): circuit and compilation statistics. Logical metrics (qubits, depth, gates, two-qubit gates, parameters) and post-transpilation metrics per backend.

		Logical					Transpiled		
Inst.	**Backend**	**Q**	**D**	**G**	**2Q**	**P**	**D**	**G**	**2Q**
chr12a	ibm_marrakesh	144	437	1152	432	576	3026	6901	1389
chr12b	ibm_marrakesh	144	437	1152	432	576	3015	6714	1329
chr12c	ibm_marrakesh	144	437	1152	432	576	3026	6901	1389
nug12	ibm_fez	144	437	1152	432	576	3412	7473	1580
had12	ibm_marrakesh	144	437	1152	432	576	3026	6901	1389
rou12	ibm_fez	144	437	1152	432	576	3412	7473	1580
scr12	ibm_fez	144	437	1152	432	576	3412	7473	1580
tai10a	ibm_fez	100	305	800	300	400	1211	2900	300
tai10a	ibm_torino	100	305	800	300	400	1211	2900	300
tai10b	ibm_fez	100	305	800	300	400	1211	2900	300
tai10b	ibm_torino	100	305	800	300	400	1211	2900	300
tai12a	ibm_fez	144	437	1152	432	576	3412	7473	1580
tai12b	ibm_fez	144	437	1152	432	576	3412	7473	1580

Table 67. QAP (CVaR-VQE): execution robustness summary. Shots per evaluation, number of evaluations, job success counts, latency statistics, and wall-clock time.

Inst.	**Shots**	**Evals**	**Jobs (ok/fail)**	**Med. Lat. (s)**	**P95 Lat. (s)**	**Time (min)**
chr12a	1000	200	200/0	8.507	14.091	40.771
chr12b	1000	200	200/0	8.848	30.082	54.166
chr12c	1000	200	200/0	8.924	73.387	119.847
nug12	1000	200	200/0	8.680	24.723	63.019
had12	1000	200	200/0	8.816	73.071	92.513
rou12	1000	200	200/0	8.561	24.753	77.076
scr12	1000	200	200/0	8.438	13.844	42.205
tai10a	1000	200	200/0	8.557	14.621	45.653
tai10b	1000	200	200/0	8.558	14.132	42.362
tai12a	1000	200	200/0	8.543	19.417	102.043
tai12b	1000	200	200/0	8.549	14.173	50.708

Table 68. QAP (QAOA): circuit and compilation statistics. Logical metrics (qubits, depth, gates, two-qubit gates, parameters) and post-transpilation metrics per backend.

		Logical					Transpiled		
Inst.	**Backend**	**Q**	**D**	**G**	**2Q**	**P**	**D**	**G**	**2Q**
chr12a	ibm_fez	144	350	10194	9042	6	33622	297432	84111
chr12b	ibm_fez	144	383	10194	9042	6	33622	297432	84111
chr12c	ibm_fez	144	350	10194	9042	6	33622	297432	84111
nug12	ibm_marrakesh	144	581	23724	22572	6	45119	586299	158163
had12	ibm_fez	144	581	32040	30888	6	33622	297432	84111
rou12	ibm_marrakesh	144	581	31644	30492	6	45119	586299	158163
scr12	ibm_marrakesh	144	504	16992	15840	6	45119	586299	158163
tai10a	ibm_fez	100	405	15110	14310	6	21681	299467	74145
tai10a	ibm_marrakesh	100	405	15110	14310	6	35011	312712	79041
tai10a	ibm_torino	100	405	15110	14310	6	30214	308388	77265
tai10b	ibm_fez	100	405	12950	12150	6	21681	299467	74145
tai10b	ibm_marrakesh	100	405	12950	12150	6	35011	312712	79041
tai12a	ibm_fez	144	581	31248	30096	6	53641	664051	168995
tai12a	ibm_marrakesh	144	581	31248	30096	6	45119	586299	158163
tai12b	ibm_marrakesh	144	570	27024	25872	6	45119	586299	158163

Table 69. QAP (QAOA): execution robustness summary. Shots per evaluation, number of evaluations, job success counts, latency statistics, and wall-clock time.

Inst.	**Shots**	**Evals**	**Jobs (ok/fail)**	**Med. Lat. (s)**	**P95 Lat. (s)**	**Time (min)**
chr12a	1000	60	60/0	23.779	52.064	34.534
chr12b	1000	63	63/0	23.834	133.728	50.833
chr12c	1000	64	64/0	23.821	39.282	32.922
nug12	1000	53	53/0	40.163	200.741	59.933
had12	1000	62	62/0	28.894	77.350	42.513
rou12	1000	48	48/0	39.588	42.271	36.761
scr12	1000	62	62/0	40.433	93.911	55.197
tai10a	1000	54	54/0	25.504	176.651	52.640
tai10b	1000	61	61/0	24.921	31.502	29.735
tai12a	1000	55	55/0	39.530	57.626	44.326
tai12b	1000	54	54/0	39.849	43.370	45.861

Table 70. QAP (MA-QAOA): circuit and compilation statistics. Logical metrics (qubits, depth, gates, two-qubit gates, parameters) and post-transpilation metrics per backend.

		Logical					Transpiled		
Inst.	**Backend**	**Q**	**D**	**G**	**2Q**	**P**	**D**	**G**	**2Q**
chr12a	ibm_fez	144	350	10194	9042	9906	32646	297939	83724
chr12a	ibm_marrakesh	144	350	10194	9042	9906	31882	300715	84615
chr12b	ibm_fez	144	383	10194	9042	9906	32378	298821	83936
chr12b	ibm_marrakesh	144	383	10194	9042	9906	32937	298766	84276
chr12c	ibm_marrakesh	144	350	10194	9042	9906	32937	298766	84276
nug12	ibm_fez	144	581	23724	22572	23436	50753	582411	158188
nug12	ibm_marrakesh	144	581	23724	22572	23436	49186	585337	159279
had12	ibm_fez	144	581	32040	30888	23436	58958	679545	173096
had12	ibm_marrakesh	144	581	32040	30888	23436	52379	670490	169151
rou12	ibm_fez	144	581	31644	30492	23436	58958	679545	173096
rou12	ibm_marrakesh	144	581	31644	30492	23436	52379	670490	169151
scr12	ibm_fez	144	504	16992	15840	16704	46354	464930	127688
scr12	ibm_marrakesh	144	504	16992	15840	16704	40375	461528	126628
tai10a	ibm_fez	100	405	15110	14310	14910	38869	317872	81971
tai10a	ibm_marrakesh	100	405	15110	14310	14910	26862	311241	79027
tai10a	ibm_torino	100	405	15110	14310	14910	36950	312637	80095
tai10b	ibm_fez	100	405	12950	12150	12750	28807	296936	78718
tai10b	ibm_marrakesh	100	405	12950	12150	12750	27730	291243	77471
tai12a	ibm_fez	144	581	31248	30096	23436	68253	664859	170894
tai12a	ibm_marrakesh	144	581	31248	30096	23436	48566	654259	164264
tai12b	ibm_fez	144	570	27024	25872	26736	59372	635760	167992
tai12b	ibm_marrakesh	144	570	27024	25872	26736	55396	640370	168270

Table 71. QAP (MA-QAOA): execution robustness summary. Shots per evaluation, number of evaluations, job success counts, latency statistics, and wall-clock time.

Inst.	**Shots**	**Evals**	**Jobs (ok/fail)**	**Med. Lat. (s)**	**P95 Lat. (s)**	**Time (min)**
chr12a	1000	200	200/0	24.858	35.665	102.356
chr12b	1000	200	200/0	25.002	65.119	203.732
chr12c	1000	200	200/0	24.384	41.098	102.559
nug12	1000	200	200/0	43.779	103.283	232.456
had12	1000	67	67/0	47.348	73.956	65.430
rou12	1000	62	62/0	47.785	60.243	60.291
scr12	1000	200	200/0	36.732	52.809	154.193
tai10a	1000	200	200/0	29.018	45.262	114.011
tai10b	1000	200	200/0	30.108	38.175	113.757
tai12a	1000	67	67/0	48.202	54.950	62.244
tai12b	1000	200	200/0	46.908	79.634	206.645

Table 72. QAP (WS-QAOA): circuit and compilation statistics. Logical metrics (qubits, depth, gates, two-qubit gates, parameters) and post-transpilation metrics per backend.

		Logical					Transpiled		
Inst.	**Backend**	**Q**	**D**	**G**	**2Q**	**P**	**D**	**G**	**2Q**
chr12a	ibm_fez	144	356	11058	9042	6	30456	301381	84503
chr12a	ibm_marrakesh	144	356	11058	9042	6	28717	296861	82789
chr12b	ibm_fez	144	389	11058	9042	6	30456	301381	84503
chr12b	ibm_marrakesh	144	389	11058	9042	6	28717	296861	82789
chr12c	ibm_fez	144	356	11058	9042	6	30456	301381	84503
chr12c	ibm_marrakesh	144	356	11058	9042	6	28717	296861	82789
nug12	ibm_fez	144	587	24588	22572	6	50864	589536	159188
nug12	ibm_marrakesh	144	587	24588	22572	6	49604	591422	159153
had12	ibm_marrakesh	144	587	32904	30888	6	28717	296861	82789
rou12	ibm_fez	144	587	32508	30492	6	50864	589536	159188
rou12	ibm_marrakesh	144	587	32508	30492	6	49604	591422	159153
scr12	ibm_marrakesh	144	510	17856	15840	6	49604	591422	159153
tai10a	ibm_marrakesh	100	411	15710	14310	6	33740	309729	77609
tai10a	ibm_torino	100	411	15710	14310	6	26709	307357	76532
tai10b	ibm_marrakesh	100	411	13550	12150	6	33740	309729	77609
tai10b	ibm_torino	100	411	13550	12150	6	26709	307357	76532

Table 73. QAP (WS-QAOA): execution robustness summary. Shots per evaluation, number of evaluations, job success counts, latency statistics, and wall-clock time.

Inst.	Shots	Evals	Jobs (ok/fail)	Med. Lat. (s)	P95 Lat. (s)	Time (min)
chr12a	1000	49	49/0	23.849	30.497	22.715
chr12b	1000	46	46/0	25.030	51.947	27.362
chr12c	1000	63	63/0	24.938	35.776	32.358
nug12	1000	46	46/0	40.295	338.060	122.527
had12	1000	50	50/0	23.870	29.658	25.958
rou12	1000	59	59/0	40.639	55.351	61.584
scr12	1000	66	66/0	40.469	64.525	53.502
tai10a	1000	50	50/0	23.919	46.100	25.578
tai10b	1000	58	58/0	24.067	34.706	29.370

Table 74. QAP (PCE): circuit and compilation statistics. Logical metrics (qubits, depth, gates, two-qubit gates, parameters) and post-transpilation metrics per backend.

		Logical					Transpiled		
Inst.	Backend	Q	D	G	2Q	P	D	G	2Q
chr12a	ibm_fez	11	89	715	220	462	617	3817	440
chr12a	ibm_torino	11	89	715	220	462	617	3817	440
chr12b	ibm_fez	11	89	715	220	462	617	3817	440
chr12b	ibm_torino	11	89	715	220	462	617	3817	440
chr12c	ibm_fez	11	89	715	220	462	617	3817	440
chr12c	ibm_torino	11	89	715	220	462	617	3817	440
nug12	ibm_fez	11	18	86	20	66	51	245	20
nug12	ibm_marrakesh	11	18	86	20	66	51	245	20
had12	ibm_fez	11	18	86	20	66	51	245	20
had12	ibm_marrakesh	11	18	86	20	66	51	245	20
rou12	aer_simulator_mps	11	18	86	20	66	51	245	20
rou12	ibm_fez	11	18	86	20	66	51	245	20
rou12	ibm_marrakesh	11	18	86	20	66	51	245	20

Table 75. QAP (PCE): execution robustness summary. Shots per evaluation, number of evaluations, job success counts, latency statistics, and wall-clock time.

Inst.	Shots	Evals	Jobs (ok/fail)	Med. Lat. (s)	P95 Lat. (s)	Time (min)
chr12a	1000	200	200/0	13.951	63.975	81.420
chr12b	1000	200	200/0	9.171	25.250	50.613
chr12c	1000	200	200/0	9.113	30.273	45.370
nug12	1000	200	200/0	24.223	83.771	115.372
had12	1000	200	200/0	23.536	42.756	99.672
rou12	1000	200	200/0	23.337	113.295	125.164

Table 76. QAP (QRAO): circuit and compilation statistics. Logical metrics (qubits, depth, gates, two-qubit gates, parameters) and post-transpilation metrics per backend.

		Logical					Transpiled		
Inst.	Backend	Q	D	G	2Q	P	D	G	2Q
chr12a	ibm_fez	56	67	613	165	448	198	1942	165
chr12a	ibm_marrakesh	56	67	613	165	448	198	1942	165
chr12b	ibm_fez	62	73	679	183	496	216	2152	183
chr12b	ibm_marrakesh	62	73	679	183	496	216	2152	183
chr12c	ibm_fez	54	65	591	159	432	192	1872	159
chr12c	ibm_marrakesh	54	65	591	159	432	192	1872	159
nug12	ibm_fez	63	74	690	186	504	219	2187	186
had12	ibm_fez	144	155	1581	429	1152	1195	7033	1110
had12	ibm_marrakesh	144	155	1581	429	1152	1195	7033	1110
rou12	ibm_torino	132	143	1449	393	1056	1737	7659	1413
scr12	ibm_fez	60	71	657	177	480	210	2082	177
scr12	ibm_kingston	60	71	657	177	480	210	2082	177
scr12	ibm_marrakesh	60	71	657	177	480	210	2082	177

Table 77. QAP (QRAO): execution robustness summary. Shots per evaluation, number of evaluations, job success counts, latency statistics, and wall-clock time.

Inst.	Shots	Evals	Jobs (ok/fail)	Med. Lat. (s)	P95 Lat. (s)	Time (min)
chr12a	1000	200	202/0	38.992	260.216	255.781
chr12b	1000	200	202/0	36.777	50.377	139.077
chr12c	1000	200	202/0	39.006	157.909	192.154
nug12	1000	200	202/0	67.249	390.702	489.529
had12	1000	200	202/0	118.453	224.432	463.684
rou12	1000	200	202/0	107.806	139.019	403.562
scr12	1000	200	202/0	48.854	155.421	219.811

particular, the tables reveal how the balancing-constraint structure of MSP interacts differently with full-width and compressed encodings after transpilation.

M.1 MSP normalization reference bounds

The range-normalized approximation ratio $\mathrm{AR}_{\mathrm{TDev}}$ defined in Eq. (3) uses instance-specific reference bounds computed over the original MSP feasible decision domain. For each instance, we solve both the minimum and maximum total deviation, $\mathrm{TDev}^{\star}$ and $\mathrm{TDev}^{\max}$, using a classical mixed-integer optimization audit. Both bounds are certified optimal. All revised MSP result tables use the certified bounds reported in Table 78.

Table 78. Classically certified MSP reference bounds used to compute the range-normalized approximation ratio $\mathrm{AR}_{\mathrm{TDev}}$. The minimum and maximum are evaluated over the original feasible decision domain used for decoding and result evaluation.

Instance	$\mathrm{TDev}^{\star}$	$\mathrm{TDev}^{\max}$	$\mathrm{TDev}^{\max} - \mathrm{TDev}^{\star}$
ms20	3	491	488
ms30	2	1549	1547
ms40	1	2944	2943
ms50	0	4762	4762
ms21	3	515	512
ms31	3	1513	1510
ms41	1	3238	3237
ms51	1	5154	5153

M.2 MSP: VQE-style methods

Tables 79–80 report diagnostics for VQE, and Tables 81–82 for CVaR-VQE.

Table 79. MSP (VQE): circuit and compilation statistics. Logical metrics (qubits, depth, gates, two-qubit gates, parameters) and post-transpilation metrics per backend.

		Logical					Transpiled		
Inst.	Backend	Q	D	G	2Q	P	D	G	2Q
ms_seed0_prod2	ibm_fez	48	149	384	144	192	587	1392	144
ms_seed0_prod2	ibm_torino	48	149	384	144	192	587	1392	144
ms_seed0_prod3	ibm_fez	84	257	672	252	336	1019	2436	252
ms_seed0_prod3	ibm_torino	84	257	672	252	336	1019	2436	252
ms_seed0_prod4	ibm_fez	118	359	944	354	472	1532	3581	408
ms_seed0_prod4	ibm_torino	118	359	944	354	472	1979	4704	808
ms_seed0_prod5	ibm_fez	150	455	1200	450	600	3018	6901	1348
ms_seed1_prod2	ibm_fez	50	155	400	150	200	914	2069	369
ms_seed1_prod2	ibm_torino	50	155	400	150	200	796	1814	272
ms_seed1_prod3	ibm_fez	84	257	672	252	336	1019	2436	252
ms_seed1_prod3	ibm_torino	84	257	672	252	336	1019	2436	252
ms_seed1_prod4	ibm_fez	118	359	944	354	472	1532	3581	408
ms_seed1_prod4	ibm_torino	118	359	944	354	472	1979	4704	808
ms_seed1_prod5	ibm_fez	156	473	1248	468	624	3276	7592	1536

M.3 MSP: QAOA-style methods

Tables 83–84 report diagnostics for QAOA, Tables 85–86 for MA-QAOA, and Tables 87–88 for WS-QAOA. The WS-QAOA circuits are by far the largest in the benchmark due to the dense

Table 80. MSP (VQE): execution robustness summary. Shots per evaluation, number of evaluations, job success counts, latency statistics, and wall-clock time.

Inst.	Shots	Evals	Jobs (ok/fail)	Med. Lat. (s)	P95 Lat. (s)	Time (min)
ms_seed0_prod2	1000	200	200/0	8.545	13.995	39.038
ms_seed0_prod3	1000	200	200/0	8.529	13.990	41.030
ms_seed0_prod4	1000	200	200/0	8.752	14.005	41.955
ms_seed0_prod5	1000	200	200/0	8.606	26.120	51.288
ms_seed1_prod2	1000	200	200/0	8.509	14.447	39.081
ms_seed1_prod3	1000	200	200/0	8.570	14.011	40.675
ms_seed1_prod4	1000	200	200/0	8.957	20.124	51.252
ms_seed1_prod5	1000	200	200/0	8.505	14.008	45.000

Table 81. MSP (CVaR-VQE): circuit and compilation statistics. Logical metrics (qubits, depth, gates, two-qubit gates, parameters) and post-transpilation metrics per backend.

		Logical					Transpiled		
Inst.	**Backend**	**Q**	**D**	**G**	**2Q**	**P**	**D**	**G**	**2Q**
ms_seed0_prod2	ibm_marrakesh	48	149	384	144	192	587	1392	144
ms_seed0_prod2	ibm_torino	48	149	384	144	192	587	1392	144
ms_seed0_prod3	ibm_marrakesh	84	257	672	252	336	1019	2436	252
ms_seed0_prod3	ibm_torino	84	257	672	252	336	1019	2436	252
ms_seed0_prod4	ibm_marrakesh	118	359	944	354	472	1532	3581	408
ms_seed0_prod4	ibm_torino	118	359	944	354	472	1923	4661	784
ms_seed0_prod5	ibm_marrakesh	150	455	1200	450	600	3239	7428	1534
ms_seed1_prod2	ibm_marrakesh	50	155	400	150	200	894	1943	318
ms_seed1_prod2	ibm_torino	50	155	400	150	200	818	1807	272
ms_seed1_prod3	ibm_marrakesh	84	257	672	252	336	1019	2436	252
ms_seed1_prod3	ibm_torino	84	257	672	252	336	1019	2436	252
ms_seed1_prod4	ibm_marrakesh	118	359	944	354	472	1532	3581	408
ms_seed1_prod4	ibm_torino	118	359	944	354	472	1923	4661	784
ms_seed1_prod5	ibm_fez	156	473	1248	468	624	3551	7727	1621

Table 82. MSP (CVaR-VQE): execution robustness summary. Shots per evaluation, number of evaluations, job success counts, latency statistics, and wall-clock time.

Inst.	Shots	Evals	Jobs (ok/fail)	Med. Lat. (s)	P95 Lat. (s)	Time (min)
ms_seed0_prod2	1000	200	200/0	13.987	19.851	51.716
ms_seed0_prod3	1000	200	200/0	8.568	14.837	42.078
ms_seed0_prod4	1000	200	200/0	8.948	19.892	46.589
ms_seed0_prod5	1000	200	200/0	8.908	30.100	61.004
ms_seed1_prod2	1000	200	200/0	13.978	46.324	99.710
ms_seed1_prod3	1000	200	200/0	8.642	45.728	57.528
ms_seed1_prod4	1000	200	200/0	9.033	91.113	79.357
ms_seed1_prod5	1000	200	200/0	8.576	25.067	61.076

warm-start operator structure, with transpiled two-qubit gate counts exceeding 100 000 on several instances.

Table 83. MSP (QAOA): circuit and compilation statistics. Logical metrics (qubits, depth, gates, two-qubit gates, parameters) and post-transpilation metrics per backend.

		Logical					Transpiled		
Inst.	**Backend**	**Q**	**D**	**G**	**2Q**	**P**	**D**	**G**	**2Q**
ms_seed0_prod2	ibm_fez	48	177	2688	2304	6	7779	51252	13304
ms_seed0_prod2	ibm_torino	48	177	2688	2304	6	8056	51421	13467
ms_seed0_prod3	ibm_fez	84	299	6972	6300	6	17879	145758	38039
ms_seed0_prod3	ibm_torino	84	299	6972	6300	6	19016	148732	38936
ms_seed0_prod4	ibm_fez	118	411	12875	11931	6	30660	292910	76599
ms_seed0_prod4	ibm_torino	118	411	12875	11931	6	31394	292454	76264
ms_seed0_prod5	ibm_fez	150	517	20139	18939	6	48019	471852	123875
ms_seed1_prod2	ibm_fez	50	182	2845	2475	6	8795	56016	14614
ms_seed1_prod2	ibm_torino	50	182	2845	2475	6	7836	55147	14494
ms_seed1_prod3	ibm_fez	84	296	6918	6306	6	17879	145758	38039
ms_seed1_prod3	ibm_torino	84	296	6918	6306	6	19016	148732	38936
ms_seed1_prod4	ibm_fez	118	411	12875	11931	6	30660	292910	76599
ms_seed1_prod4	ibm_torino	118	411	12875	11931	6	31394	292454	76264
ms_seed1_prod5	ibm_fez	156	535	21174	19926	6	47838	504835	133151

Table 84. MSP (QAOA): execution robustness summary. Shots per evaluation, number of evaluations, job success counts, latency statistics, and wall-clock time.

Inst.	**Shots**	**Evals**	**Jobs (ok/fail)**	**Med. Lat. (s)**	**P95 Lat. (s)**	**Time (min)**
ms_seed0_prod2	1000	51	51/0	15.372	172.062	32.583
ms_seed0_prod3	1000	58	58/0	16.906	82.326	37.490
ms_seed0_prod4	1000	55	55/0	24.950	54.760	37.729
ms_seed0_prod5	1000	56	56/0	33.051	61.486	42.136
ms_seed1_prod2	1000	59	59/0	15.314	69.292	25.101
ms_seed1_prod3	1000	55	55/0	17.174	49.124	26.164
ms_seed1_prod4	1000	48	48/0	25.237	83.587	60.450
ms_seed1_prod5	1000	49	49/0	38.445	101.818	44.298

Table 85. MSP (MA-QAOA): circuit and compilation statistics. Logical metrics (qubits, depth, gates, two-qubit gates, parameters) and post-transpilation metrics per backend.

		Logical					Transpiled		
Inst.	**Backend**	**Q**	**D**	**G**	**2Q**	**P**	**D**	**G**	**2Q**
ms_seed0_prod2	ibm_torino	48	177	2688	2304	2592	8265	52094	13644
ms_seed0_prod3	ibm_fez	84	299	6972	6300	6804	19539	151739	39882
ms_seed0_prod3	ibm_torino	84	299	6972	6300	6804	17352	150102	39302
ms_seed0_prod4	ibm_fez	118	411	12875	11931	12639	30936	291142	76248
ms_seed0_prod4	ibm_torino	118	411	12875	11931	12639	31327	290871	75551
ms_seed0_prod5	ibm_fez	150	517	20139	18939	19839	44337	460244	120201
ms_seed1_prod2	ibm_fez	50	182	2845	2475	2745	8267	55586	14473
ms_seed1_prod2	ibm_torino	50	182	2845	2475	2745	9113	55648	14473
ms_seed1_prod3	ibm_fez	84	296	6918	6306	6750	19222	149753	39159
ms_seed1_prod3	ibm_torino	84	296	6918	6306	6750	18957	152431	40562
ms_seed1_prod4	ibm_fez	118	411	12875	11931	12639	30936	291142	76248
ms_seed1_prod4	ibm_torino	118	411	12875	11931	12639	31327	290871	75551
ms_seed1_prod5	ibm_fez	156	535	21174	19926	20862	44655	495541	128487
ms_seed1_prod5	ibm_marrakesh	156	535	21174	19926	20862	50183	504651	132622

M.4 MSP: encoding-based methods

Tables 89–90 report diagnostics for PCE, and Tables 91–92 for QRAO. MSP provides the most extreme width compression in the benchmark: PCE and QRAO reduce the 48–156 qubit full-width formulations to 7–11 qubits. However, the main results show that this compression does not translate into better recovered solution quality, and the compilation diagnostics here help explain why.

Table 86. MSP (MA-QAOA): execution robustness summary. Shots per evaluation, number of evaluations, job success counts, latency statistics, and wall-clock time.

Inst.	Shots	Evals	Jobs (ok/fail)	Med. Lat. (s)	P95 Lat. (s)	Time (min)
ms_seed0_prod2	1000	200	200/0	15.186	36.421	69.192
ms_seed0_prod3	1000	200	200/0	16.914	27.327	71.063
ms_seed0_prod4	1000	200	200/0	24.383	51.213	133.832
ms_seed0_prod5	1000	200	200/0	36.655	128.320	187.643
ms_seed1_prod2	1000	200	200/0	15.312	30.668	61.797
ms_seed1_prod3	1000	200	200/0	16.550	70.541	86.375
ms_seed1_prod4	1000	200	200/0	25.452	208.449	294.116
ms_seed1_prod5	1000	200	200/0	37.311	79.805	161.180

Table 87. MSP (WS-QAOA): circuit and compilation statistics. Logical metrics (qubits, depth, gates, two-qubit gates, parameters) and post-transpilation metrics per backend.

		Logical					Transpiled		
Inst.	Backend	Q	D	G	2Q	P	D	G	2Q
ms_seed0_prod2	ibm_fez	48	183	2976	2304	6	8207	52335	13434
ms_seed0_prod2	ibm_marrakesh	48	183	2976	2304	6	8017	52247	13512
ms_seed0_prod3	ibm_marrakesh	84	305	7476	6300	6	19052	150195	39227
ms_seed0_prod3	ibm_torino	84	305	7476	6300	6	18206	151219	39165
ms_seed0_prod4	ibm_marrakesh	118	417	13583	11931	6	30844	290228	75459
ms_seed0_prod4	ibm_torino	118	417	13583	11931	6	31861	290794	76190
ms_seed0_prod5	ibm_fez	150	523	21039	18939	6	46370	472119	123414
ms_seed0_prod5	ibm_marrakesh	150	523	21039	18939	6	47791	468318	122758
ms_seed1_prod2	ibm_fez	50	188	3145	2475	6	8079	55016	14116
ms_seed1_prod2	ibm_marrakesh	50	188	3145	2475	6	8356	56799	14801
ms_seed1_prod3	ibm_fez	84	302	7422	6306	6	20804	152636	40149
ms_seed1_prod3	ibm_marrakesh	84	302	7422	6306	6	19052	150195	39227
ms_seed1_prod3	ibm_torino	84	302	7422	6306	6	18206	151219	39165
ms_seed1_prod4	ibm_marrakesh	118	417	13583	11931	6	30844	290228	75459
ms_seed1_prod4	ibm_torino	118	417	13583	11931	6	31861	290794	76190
ms_seed1_prod5	ibm_marrakesh	156	541	22110	19926	6	44420	501025	130345

Table 88. MSP (WS-QAOA): execution robustness summary. Shots per evaluation, number of evaluations, job success counts, latency statistics, and wall-clock time.

Inst.	Shots	Evals	Jobs (ok/fail)	Med. Lat. (s)	P95 Lat. (s)	Time (min)
ms_seed0_prod2	1000	47	47/0	15.588	17.731	20.871
ms_seed0_prod3	1000	55	55/0	17.915	36.054	21.653
ms_seed0_prod4	1000	55	55/0	29.904	107.441	40.353
ms_seed0_prod5	1000	61	61/0	33.791	314.956	69.344
ms_seed1_prod2	1000	52	52/0	15.670	16.473	15.024
ms_seed1_prod3	1000	53	53/0	16.765	22.371	18.412
ms_seed1_prod4	1000	63	63/0	24.157	30.182	29.032
ms_seed1_prod5	1000	50	50/0	34.046	41.184	34.045

Table 89. MSP (PCE): circuit and compilation statistics. Logical metrics (qubits, depth, gates, two-qubit gates, parameters) and post-transpilation metrics per backend.

		Logical					Transpiled		
Inst.	Backend	Q	D	G	2Q	P	D	G	2Q
ms_seed0_prod2	ibm_torino	7	57	287	84	182	393	1493	168
ms_seed0_prod3	ibm_torino	8	65	376	112	240	449	1979	224
ms_seed0_prod4	ibm_torino	10	81	590	180	380	561	3135	360
ms_seed0_prod5	ibm_torino	11	89	715	220	462	617	3817	440
ms_seed1_prod2	ibm_torino	7	57	287	84	182	393	1493	168
ms_seed1_prod3	ibm_fez	8	65	376	112	240	449	1979	224
ms_seed1_prod3	ibm_torino	8	65	376	112	240	449	1979	224
ms_seed1_prod4	ibm_fez	10	81	590	180	380	561	3135	360
ms_seed1_prod4	ibm_torino	10	81	590	180	380	561	3135	360
ms_seed1_prod5	ibm_fez	11	89	715	220	462	617	3817	440
ms_seed1_prod5	ibm_torino	11	89	715	220	462	617	3817	440

Table 90. MSP (PCE): execution robustness summary. Shots per evaluation, number of evaluations, job success counts, latency statistics, and wall-clock time.

Inst.	Shots	Evals	Jobs (ok/fail)	Med. Lat. (s)	P95 Lat. (s)	Time (min)
ms_seed0_prod2	1000	200	200/0	8.792	14.989	41.288
ms_seed0_prod3	1000	200	200/0	8.527	14.136	37.539
ms_seed0_prod4	1000	200	200/0	8.560	19.221	42.853
ms_seed0_prod5	1000	200	200/0	8.771	19.698	41.875
ms_seed1_prod2	1000	200	200/0	8.690	14.561	40.588
ms_seed1_prod3	1000	200	200/0	8.768	52.741	69.656
ms_seed1_prod4	1000	200	200/0	8.778	20.076	46.427
ms_seed1_prod5	1000	200	200/0	8.941	31.443	56.768

Table 91. MSP (QRAO): circuit and compilation statistics. Logical metrics (qubits, depth, gates, two-qubit gates, parameters) and post-transpilation metrics per backend.

		Logical					Transpiled		
Inst.	**Backend**	**Q**	**D**	**G**	**2Q**	**P**	**D**	**G**	**2Q**
ms_seed0_prod2	ibm_fez	30	41	327	87	240	120	1032	87
ms_seed0_prod2	ibm_marrakesh	30	41	327	87	240	120	1032	87
ms_seed0_prod3	ibm_torino	42	53	459	123	336	156	1452	123
ms_seed0_prod4	ibm_torino	73	84	800	216	584	249	2537	216
ms_seed0_prod5	ibm_torino	84	95	921	249	672	282	2922	249
ms_seed1_prod2	ibm_fez	30	41	327	87	240	120	1032	87
ms_seed1_prod3	ibm_fez	42	53	459	123	336	156	1452	123
ms_seed1_prod3	ibm_marrakesh	42	53	459	123	336	156	1452	123
ms_seed1_prod4	ibm_fez	73	84	800	216	584	249	2537	216
ms_seed1_prod4	ibm_marrakesh	73	84	800	216	584	249	2537	216
ms_seed1_prod5	ibm_fez	85	96	932	252	680	285	2957	252
ms_seed1_prod5	ibm_marrakesh	85	96	932	252	680	285	2957	252

Table 92. MSP (QRAO): execution robustness summary. Shots per evaluation, number of evaluations, job success counts, latency statistics, and wall-clock time.

Inst.	Shots	Evals	Jobs (ok/fail)	Med. Lat. (s)	P95 Lat. (s)	Time (min)
ms_seed0_prod2	1000	200	202/0	23.565	33.261	91.169
ms_seed0_prod3	1000	200	202/0	24.884	50.117	100.389
ms_seed0_prod4	1000	200	202/0	43.719	97.333	186.746
ms_seed0_prod5	1000	200	202/0	52.110	99.067	210.891
ms_seed1_prod2	1000	200	202/0	23.350	157.532	171.703
ms_seed1_prod3	1000	200	202/0	29.245	346.852	471.645
ms_seed1_prod4	1000	200	202/0	41.341	131.894	238.789
ms_seed1_prod5	1000	200	202/0	59.588	304.199	401.842

N Matched Uniform-Random Baseline for Low-Fidelity QAOA-Family Runs

This appendix evaluates whether the decoded quality of low-fidelity QAOA-family hardware runs exceeds a matched uniform-random best-shot control. The purpose is to test the practical interpretation of the strongly noise-dominated regime without assuming that a small gate-count fidelity proxy implies a fully uniform measured output distribution.

N.1 Scope and matched-control construction

The analysis includes all 106 saved QAOA, MA-QAOA, and warm-start-QAOA hardware artifacts whose reconstructed gate-count fidelity proxy satisfies

$$F_{\text{est}} < 10^{-3}. \tag{28}$$

PCE and QRAO are excluded because their compressed encodings use distinct native reconstruction or rounding procedures; the present control addresses the low-fidelity QAOA-family interpretation specifically.

For each hardware run, the random control matches the decision-variable dimension, optimizer-trajectory batch count, shots per batch, batch-selection rule, within-batch tie-breaking rule, and shared one-round local-swap refinement used by the corresponding hardware artifact. The saved hardware path stores counts from the optimizer-evaluation batch with the lowest expectation objective and does not retain an independent final-sampling batch. Each random replicate therefore generates the same number of uniformly random bitstrings as the corresponding hardware run, grouped into the same optimizer-evaluation batches. The replicate selects the batch with the lowest mean QUBO energy, selects the lowest-QUBO-energy bitstring within that batch, and then applies the same one-round local-swap refinement used by the hardware pipeline.

Each hardware run is compared with 300 independent matched uniform-random replicates. For MDKP, MIS, and QAP, the outcome metric is optimality gap. For MSP, the outcome metric is total deviation, TDev. QAP is reported as a feasibility-only comparison because all selected hardware QAP outputs are infeasible and valid random permutations are astronomically unlikely at the available candidate budgets.

N.2 Run-level classification

For a feasible hardware outcome with a finite matched random-quality distribution, let Q_{HW} denote the final hardware metric and let $Q_{\text{rand}}^{(b)}$ denote the final metric from matched random replicate b. Since lower values are better, we define the empirical random tail fraction

$$\tau = \frac{1 + \sum_{b=1}^{300} \mathbb{I}\left[Q_{\text{rand}}^{(b)} \leq Q_{\text{HW}}\right]}{301}. \tag{29}$$

A hardware outcome is described as within the empirical random range when $0.05 < \tau < 0.95$ and as worse than the empirical random range when $\tau \geq 0.95$. The figure below displays the central 2.5–97.5% random interval for visualization, whereas the run-level classification uses the stated empirical tail-fraction rule.

A separate category is required when the hardware pipeline returns a feasible candidate but none of the 300 matched random replicates does so. Such a result does not have a finite random-quality distribution against which a standard optimality-gap comparison can be made. We therefore report it as a finite-sample feasibility exception rather than as a finite-gap outperformance or a quantum-advantage claim.

N.3 Results

Table 93 summarizes the matched control. Of the 106 low-fidelity QAOA-family hardware runs, 43 are hardware-infeasible and are therefore treated as feasibility-only comparisons. Among the 62 feasible hardware runs for which the matched random control produces a finite quality distribution, 51 lie within the empirical random range and 11 are worse than the random baseline. One additional warm-start-QAOA MIS run, `1tc.64`, is a finite-sample feasibility exception: the hardware pipeline returned a feasible candidate, whereas none of the 300 matched random replicates did.

The dominant empirical pattern is therefore not broad evidence of optimization beyond the matched random baseline. Instead, most feasible low-fidelity QAOA-family outcomes are compatible with best-of-budget random candidate selection under the same trajectory-level selection and common local-refinement protocol, or are worse than that baseline. At the same time,

Table 93. Matched uniform-random control for low-fidelity QAOA-family hardware runs. Within range" and Worse" apply only to feasible hardware runs for which the matched random control yields a finite quality distribution. "Feasibility exception" denotes a feasible hardware result with zero feasible matched random draws. QAP is feasibility-only because all selected hardware outputs are infeasible.

Problem	Method	Runs	HW feasible	Within range	Worse	Feasibility exception	HW infeasible
MDKP	MA-QAOA	12	12	9	3	0	0
MDKP	QAOA	12	12	8	4	0	0
MDKP	WS-QAOA	12	12	12	0	0	0
MIS	MA-QAOA	5	0	0	0	0	5
MIS	QAOA	5	1	1	0	0	4
MIS	WS-QAOA	5	2	1	0	1	3
MSP	MA-QAOA	8	8	7	1	0	0
MSP	QAOA	8	8	7	1	0	0
MSP	WS-QAOA	8	8	6	2	0	0
QAP	MA-QAOA	11	0	–	–	–	11
QAP	QAOA	11	0	–	–	–	11
QAP	WS-QAOA	9	0	–	–	–	9
Total	–	106	63	51	11	1	43

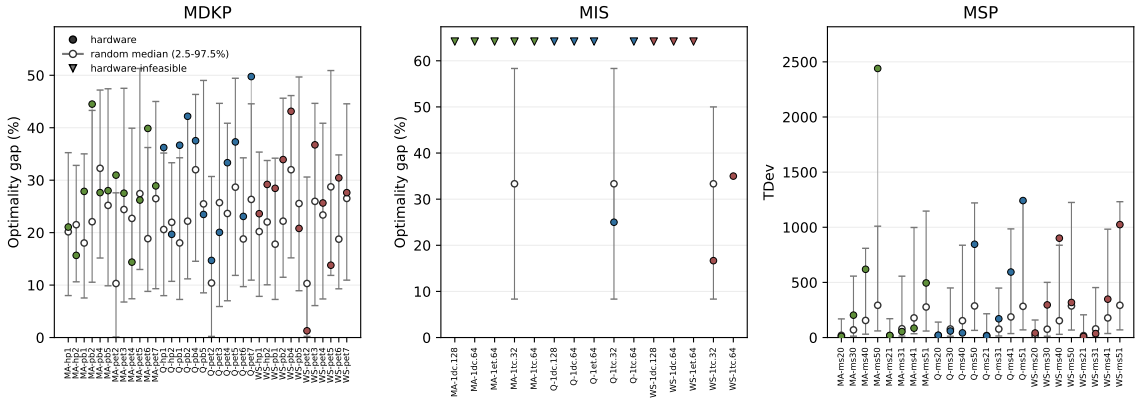

Figure 11. Matched uniform-random baseline for low-fidelity QAOA-family hardware runs. Filled circles show final hardware outcomes. Open circles show random medians, and vertical intervals show the central 2.5–97.5% range across 300 matched random replicates. Each random pool matches the original run's decision-variable dimension, optimizer-trajectory batch structure, candidate-selection rule, and one-round local refinement. MDKP and MIS report optimality gap; MSP reports TDev. Downward triangles indicate hardware-infeasible runs. QAP is omitted because all hardware outputs are infeasible and valid random permutations are astronomically unlikely at the sampled candidate budgets.

the `1tc.64` feasibility exception shows why the gate-count fidelity proxy must not be interpreted as proof that every low-fidelity output distribution is exactly uniform random. Figure 11 shows the run-level hardware outcomes relative to the matched-random medians and central empirical intervals.

The common local-refinement stage is materially active in the matched pipeline. Its scale is reported separately by problem family because MDKP and MIS use percentage optimality gap whereas MSP uses TDev. Across matched random replicates, the median pre-to-post refinement improvement is 20.56 percentage points for MDKP, 8.33 percentage points for MIS, and 6675 TDev units for MSP. These values describe the shared hybrid post-processing stage and should not be compared across problem families as a single pooled quantity.

The complete selection ledger, all 31,800 random-baseline replicates, corrected run-level classifications, and problem-level aggregate summaries are provided in the reproducibility artifact.

O Reproducibility details

O.1 Software stack and experimental window

Table 94. Software stack used for all experiments in this study.

Component	Version
Python	3.10.16
Qiskit	2.3.0
`qiskit-ibm-runtime`	0.45.1
`qiskit-aer`	0.17.2
SciPy	1.15.3
NumPy	2.2.6
CPLEX Python API	22.1.2.0
Gurobi (classical baseline)	13.0.1

O.2 Execution and Runtime mitigation scope

The execution contains 255 method–instance records: 84 MDKP, 49 MIS, 56 MSP, and 66 QAP records. All Estimator-based objective evaluations use `resilience_level=2` with 1,000 requested shots and no manually configured mitigation sub-options. In particular, the metadata does not retain custom TREX randomization settings, ZNE noise factors, extrapolator choices, twirling parameters, or dynamical-decoupling settings. These settings are therefore not reported as historical protocol facts.

Final candidate bitstrings are generated by separate SamplerV2 jobs with raw/default options and no custom sampler noise-management configuration. The ledger records raw/default final sampling for all 255 archived records. Most use 1,000 final sampling shots; a small subset follows the recorded one-shot final-sampling pathway. In all cases, final bitstrings are decoded and checked classically rather than inferred from Estimator expectation values.

Table 95. Execution summary. The table distinguishes Estimator mitigation from final SamplerV2 decoding samples.

Provenance field	Archived result
Archived method–instance records	255
Estimator resilience level	2 for all records
Estimator requested shots	1,000 for all records
Custom Estimator mitigation options	None recorded
Final sampling primitive	Separate SamplerV2
Custom Sampler noise-management options	None recorded
Final bitstrings from raw/default SamplerV2	Yes, all records
Final sampling shots	1,000 for 235 records; 1 for 20 records
Paired level-0 mitigation-overhead study	Not performed

The data does not contain paired executions of the same circuit at `resilience_level=0` and `resilience_level=2`. We therefore do not infer a circuit-specific mitigation-overhead multiplier retrospectively. Wall-clock durations are retained where available, but they combine queueing, backend availability, calibration-time variation, compilation, managed Runtime work, and ordinary execution time; they are not interpreted as a controlled mitigation-cost measurement.

Transpiler `optimization_level=3` was used for hardware-aware circuit compilation. Compilation and Runtime mitigation are distinct pipeline stages: the former determines the executable circuit, whereas the latter affects only Estimator-based expectation-value evaluation in the protocol.

O.3 Master fidelity table

Table 96 (on the following pages) reports the estimated process fidelity, hardware outcome, and simulator outcome for every method–instance–backend combination evaluated in this study.

Table 96: Complete process-fidelity estimates for every method–instance–backend combination evaluated on hardware in this benchmark. N_{2Q}: transpiled two-qubit gate count. F_{est}: estimated process fidelity under the independent-depolarizing model of Section 4.11 using the median backend ε_{2Q} during the experimental window. Sim and HW gap are reported as percentage optimality gap (or TDev for MSP) where available; '–' indicates not evaluated. Feas: Y if the hardware run returned a feasible solution, N otherwise.

Problem	Method	Instance	Backend	N_{2Q}	F_{est}	Sim gap %	HW gap %	Feas
MDKP	CVaR-VQE	hp1	ibm_torino	180	0.486	20.59	33.85	Y
MDKP	CVaR-VQE	hp2	ibm_torino	279	0.327	21.78	15.88	Y
MDKP	CVaR-VQE	pb1	ibm_torino	314	0.284	23.43	14.89	Y
MDKP	CVaR-VQE	pb2	ibm_torino	295	0.307	22.78	11.93	Y
MDKP	CVaR-VQE	pb4	ibm_torino	309	0.29	39.38	34.97	Y
MDKP	CVaR-VQE	pb5	ibm_torino	876	0.03	33.34	18.14	Y
MDKP	CVaR-VQE	pet2	ibm_torino	347	0.249	30.37	1.50	Y
MDKP	CVaR-VQE	pet3	ibm_torino	324	0.273	34.74	36.61	Y
MDKP	CVaR-VQE	pet4	ibm_torino	459	0.159	48.44	41.91	Y
MDKP	CVaR-VQE	pet5	ibm_torino	1227	0.00731	53.15	13.83	Y
MDKP	CVaR-VQE	pet6	ibm_torino	332	0.264	40.41	13.88	Y
MDKP	CVaR-VQE	pet7	ibm_torino	300	0.3	46.47	24.52	Y
MDKP	MA-QAOA	hp1	ibm_fez	22896	1.3299999999999999e-30	–	21.06	Y
MDKP	MA-QAOA	hp2	ibm_fez	30125	4.9199999999999996e-40	–	15.66	Y
MDKP	MA-QAOA	pb1	ibm_fez	21754	4.1200000000000003e-29	–	27.86	Y
MDKP	MA-QAOA	pb2	ibm_fez	28136	1.94e-37	–	44.51	Y
MDKP	MA-QAOA	pb4	ibm_fez	11506	9.69e-16	–	27.63	Y
MDKP	MA-QAOA	pb5	ibm_fez	46919	6e-62	–	28.00	Y
MDKP	MA-QAOA	pet2	ibm_fez	23551	1.8600000000000002e-31	–	30.97	Y
MDKP	MA-QAOA	pet3	ibm_fez	32638	2.5900000000000003e-43	–	27.52	Y
MDKP	MA-QAOA	pet4	ibm_fez	41625	4.85e-55	–	14.38	Y
MDKP	MA-QAOA	pet5	ibm_fez	62656	1.75e-82	–	26.21	Y
MDKP	MA-QAOA	pet6	ibm_fez	45006	1.8800000000000002e-59	–	39.87	Y
MDKP	MA-QAOA	pet7	ibm_marrakesh	66556	1.43e-87	–	28.91	Y
MDKP	PCE	hp1	ibm_torino	168	0.51	20.88	13.25	Y
MDKP	PCE	hp2	ibm_torino	224	0.407	38.38	14.56	Y
MDKP	PCE	pb1	ibm_torino	168	0.51	14.04	22.78	Y
MDKP	PCE	pb2	ibm_torino	224	0.407	14.37	21.37	Y
MDKP	PCE	pb4	ibm_torino	120	0.618	32.91	21.30	Y
MDKP	PCE	pb5	ibm_fez	360	0.339	11.87	17.72	Y
MDKP	PCE	pet2	ibm_fez	288	0.421	28.19	1.69	Y
MDKP	PCE	pet3	ibm_fez	288	0.421	15.56	7.97	Y
MDKP	PCE	pet4	ibm_fez	288	0.421	50.98	20.42	Y
MDKP	PCE	pet5	ibm_fez	360	0.339	22.74	37.50	Y

Continued on next page

Table 96 – continued from previous page

Problem	Method	Instance	Backend	N_{2Q}	F_{est}	Sim gap %	HW gap %	Feas
MDKP	PCE	pet6	ibm_fez	288	0.421	33.84	19.92	Y
MDKP	PCE	pet7	ibm_fez	288	0.421	15.87	25.27	Y
MDKP	QAOA	hp1	ibm_fez	22501	4.36e-30	–	36.22	Y
MDKP	QAOA	hp2	ibm_fez	28967	1.59e-38	–	19.68	Y
MDKP	QAOA	pb1	ibm_fez	21821	3.37e-29	–	36.67	Y
MDKP	QAOA	pb2	ibm_fez	29320	5.52e-39	–	42.18	Y
MDKP	QAOA	pb4	ibm_fez	11522	9.24e-16	–	37.53	Y
MDKP	QAOA	pb5	ibm_fez	46275	4.1499999999999996e-61	–	23.47	Y
MDKP	QAOA	pet2	ibm_fez	24261	2.2e-32	–	14.70	Y
MDKP	QAOA	pet3	ibm_fez	32232	8.760000000000001e-43	–	20.05	Y
MDKP	QAOA	pet4	ibm_fez	41325	1.1999999999999999e-54	–	33.33	Y
MDKP	QAOA	pet5	ibm_fez	63249	2.95e-83	–	37.30	Y
MDKP	QAOA	pet6	ibm_fez	47056	3.9799999999999995e-62	–	23.09	Y
MDKP	QAOA	pet7	ibm_fez	65365	5.1200000000000004e-86	–	49.76	Y
MDKP	QRAO	hp1	ibm_fez	111	0.716	–	5.85	Y
MDKP	QRAO	hp2	ibm_fez	132	0.673	–	16.67	Y
MDKP	QRAO	pb1	ibm_fez	108	0.723	–	15.40	Y
MDKP	QRAO	pb2	ibm_marrakesh	129	0.679	–	13.65	Y
MDKP	QRAO	pb4	ibm_marrakesh	93	0.756	–	21.71	Y
MDKP	QRAO	pb5	ibm_marrakesh	168	0.604	–	18.00	Y
MDKP	QRAO	pet2	ibm_torino	129	0.596	–	0.64	Y
MDKP	QRAO	pet3	ibm_marrakesh	129	0.679	–	34.12	Y
MDKP	QRAO	pet4	ibm_torino	138	0.575	–	18.63	Y
MDKP	QRAO	pet5	ibm_fez	171	0.598	–	25.52	Y
MDKP	QRAO	pet6	ibm_fez	153	0.631	–	15.23	Y
MDKP	QRAO	pet7	ibm_fez	183	0.577	–	16.79	Y
MDKP	VQE	hp1	ibm_fez	180	0.582	39.76	26.95	Y
MDKP	VQE	hp2	ibm_fez	338	0.362	12.34	17.92	Y
MDKP	VQE	pb1	ibm_fez	363	0.336	19.94	22.62	Y
MDKP	VQE	pb2	ibm_fez	344	0.356	19.49	26.77	Y
MDKP	VQE	pb4	ibm_fez	270	0.444	–	33.63	Y
MDKP	VQE	pb5	ibm_fez	348	0.351	4.25	29.73	Y
MDKP	VQE	pet2	ibm_fez	326	0.376	41.07	16.98	Y
MDKP	VQE	pet3	ibm_fez	347	0.353	4.98	32.38	Y
MDKP	VQE	pet4	ibm_fez	410	0.292	66.58	44.69	Y
MDKP	VQE	pet5	ibm_fez	384	0.315	33.23	25.65	Y
MDKP	VQE	pet6	ibm_fez	390	0.31	12.50	20.24	Y
MDKP	VQE	pet7	ibm_fez	300	0.406	43.46	23.28	Y
MDKP	WS-QAOA	hp1	ibm_fez	20658	1.11e-27	–	23.61	Y
MDKP	WS-QAOA	hp2	ibm_fez	29780	1.39e-39	–	29.19	Y
MDKP	WS-QAOA	pb1	ibm_fez	22192	1.1000000000000001e-29	–	28.45	Y

Continued on next page

Table 96 – continued from previous page

Problem	Method	Instance	Backend	N_{2Q}	F_{est}	Sim gap %	HW gap %	Feas
MDKP	WS-QAOA	pb2	ibm_fez	28862	2.19e-38	–	33.93	Y
MDKP	WS-QAOA	pb4	ibm_fez	11808	3.91e-16	–	43.13	Y
MDKP	WS-QAOA	pb5	ibm_fez	47353	1.63e-62	–	20.80	Y
MDKP	WS-QAOA	pet2	ibm_fez	23747	1.03e-31	–	1.28	Y
MDKP	WS-QAOA	pet3	ibm_fez	32589	3e-43	–	36.74	Y
MDKP	WS-QAOA	pet4	ibm_torino	41282	1.3900000000000001e-72	–	25.65	Y
MDKP	WS-QAOA	pet5	ibm_torino	64628	3.2e-113	–	13.79	Y
MDKP	WS-QAOA	pet6	ibm_torino	45559	4.98e-80	–	30.45	Y
MDKP	WS-QAOA	pet7	ibm_torino	65953	1.58e-115	–	27.62	Y
MIS	CVaR-VQE	1dc.128	ibm_torino	1284	0.00582	–	–	N
MIS	CVaR-VQE	1dc.64	ibm_torino	192	0.463	–	–	N
MIS	CVaR-VQE	1et.64	ibm_torino	192	0.463	–	–	N
MIS	CVaR-VQE	1tc.16	ibm_torino	102	0.664	0.00	12.50	Y
MIS	CVaR-VQE	1tc.32	ibm_marrakesh	96	0.749	8.33	16.67	Y
MIS	CVaR-VQE	1tc.64	ibm_torino	192	0.463	–	–	N
MIS	CVaR-VQE	1tc.8	ibm_torino	60	0.786	0.00	0.00	Y
MIS	MA-QAOA	1dc.128	ibm_fez	47824	3.96e-63	–	–	N
MIS	MA-QAOA	1dc.64	ibm_fez	14015	5.16e-19	–	–	N
MIS	MA-QAOA	1et.64	ibm_fez	4495	1.36e-06	–	–	N
MIS	MA-QAOA	1tc.16	ibm_fez	237	0.491	–	12.50	Y
MIS	MA-QAOA	1tc.32	ibm_fez	931	0.061	–	–	N
MIS	MA-QAOA	1tc.64	ibm_fez	3265	5.49e-05	–	–	N
MIS	MA-QAOA	1tc.8	ibm_fez	60	0.835	–	0.00	Y
MIS	PCE	1dc.128	ibm_torino	18	0.93	–	–	N
MIS	PCE	1dc.64	ibm_fez	14	0.959	–	–	N
MIS	PCE	1et.64	ibm_fez	14	0.959	–	–	N
MIS	PCE	1tc.16	ibm_torino	6	0.976	50.00	62.50	Y
MIS	PCE	1tc.32	ibm_fez	10	0.97	41.67	–	N
MIS	PCE	1tc.64	ibm_torino	14	0.945	–	–	N
MIS	PCE	1tc.8	ibm_fez	4	0.988	25.00	25.00	Y
MIS	QAOA	1dc.128	ibm_fez	48702	2.83e-64	–	–	N
MIS	QAOA	1dc.64	ibm_fez	14383	1.71e-19	–	–	N
MIS	QAOA	1et.64	ibm_torino	4600	9.84e-09	–	–	N
MIS	QAOA	1tc.16	ibm_torino	241	0.381	–	25.00	Y
MIS	QAOA	1tc.32	ibm_torino	935	0.024	–	25.00	Y
MIS	QAOA	1tc.64	ibm_torino	4600	9.84e-09	–	–	N
MIS	QAOA	1tc.8	ibm_torino	60	0.786	–	0.00	Y
MIS	QRAO	1dc.128	ibm_fez	135	0.667	–	–	N
MIS	QRAO	1dc.64	ibm_torino	72	0.749	–	–	N
MIS	QRAO	1et.64	ibm_fez	66	0.82	–	–	N
MIS	QRAO	1tc.16	ibm_fez	15	0.956	–	12.50	Y

Continued on next page

Table 96 – continued from previous page

Problem	Method	Instance	Backend	N_{2Q}	F_{est}	Sim gap %	HW gap %	Feas
MIS	QRAO	1tc.32	ibm_fez	36	0.897	–	25.00	Y
MIS	QRAO	1tc.64	ibm_torino	66	0.768	–	–	N
MIS	QRAO	1tc.8	sim	9	0.969	–	0.00	Y
MIS	VQE	1dc.128	ibm_fez	657	0.139	–	–	N
MIS	VQE	1dc.64	ibm_fez	192	0.562	–	–	N
MIS	VQE	1et.64	ibm_fez	192	0.562	–	–	N
MIS	VQE	1tc.16	ibm_fez	102	0.736	0.00	0.00	Y
MIS	VQE	1tc.32	ibm_fez	96	0.749	8.33	–	N
MIS	VQE	1tc.64	ibm_fez	192	0.562	–	–	N
MIS	VQE	1tc.8	ibm_fez	78	0.791	0.00	0.00	Y
MIS	WS-QAOA	1dc.128	ibm_torino	48544	3.17e-85	–	–	N
MIS	WS-QAOA	1dc.64	ibm_torino	14029	3.8e-25	–	–	N
MIS	WS-QAOA	1et.64	ibm_torino	14029	3.8e-25	–	–	N
MIS	WS-QAOA	1tc.16	ibm_torino	237	0.387	–	0.00	Y
MIS	WS-QAOA	1tc.32	ibm_torino	911	0.026	–	16.67	Y
MIS	WS-QAOA	1tc.64	ibm_torino	14029	3.8e-25	–	35.00	Y
MIS	WS-QAOA	1tc.8	ibm_torino	60	0.786	–	0.00	Y
MSP	CVaR-VQE	ms20	ibm_marrakesh	144	0.649	–	27.00	Y
MSP	CVaR-VQE	ms21	ibm_marrakesh	318	0.385	–	9.00	Y
MSP	CVaR-VQE	ms30	ibm_marrakesh	252	0.469	–	347.00	Y
MSP	CVaR-VQE	ms31	ibm_marrakesh	252	0.469	–	51.00	Y
MSP	CVaR-VQE	ms40	ibm_marrakesh	408	0.294	–	150.00	Y
MSP	CVaR-VQE	ms41	ibm_marrakesh	408	0.294	–	48.00	Y
MSP	CVaR-VQE	ms50	ibm_marrakesh	1534	0.00996	–	476.00	Y
MSP	CVaR-VQE	ms51	ibm_fez	1621	0.00767	–	565.00	Y
MSP	PCE	ms20	ibm_torino	168	0.51	–	45.00	Y
MSP	PCE	ms21	ibm_torino	168	0.51	–	52.00	Y
MSP	PCE	ms30	ibm_torino	224	0.407	–	167.00	Y
MSP	PCE	ms31	ibm_fez	224	0.51	–	185.00	Y
MSP	PCE	ms40	ibm_torino	360	0.236	–	296.00	Y
MSP	PCE	ms41	ibm_fez	360	0.339	–	317.00	Y
MSP	PCE	ms50	ibm_torino	440	0.171	–	822.00	Y
MSP	PCE	ms51	ibm_fez	440	0.267	–	845.00	Y
MSP	QAOA	ms20	ibm_fez	13304	4.37e-18	–	21.00	Y
MSP	QAOA	ms21	ibm_fez	14614	8.53e-20	–	15.00	Y
MSP	QAOA	ms30	ibm_fez	38039	2.32e-50	–	59.00	Y
MSP	QAOA	ms31	ibm_fez	38039	2.32e-50	–	170.00	Y
MSP	QAOA	ms40	ibm_fez	76599	1.1200000000000001e-100	–	42.00	Y
MSP	QAOA	ms41	ibm_fez	76599	1.1200000000000001e-100	–	594.00	Y
MSP	QAOA	ms50	ibm_fez	123875	2.31e-162	–	846.00	Y
MSP	QAOA	ms51	ibm_fez	133151	1.8199999999999999e-174	–	1242.00	Y

Continued on next page

Table 96 – continued from previous page

Problem	Method	Instance	Backend	N_{2Q}	F_{est}	Sim gap %	HW gap %	Feas
MSP	QRAO	ms20	ibm_fez	87	0.77	–	81.00	Y
MSP	QRAO	ms21	ibm_fez	87	0.77	–	99.00	Y
MSP	QRAO	ms30	ibm_torino	123	0.611	–	291.00	Y
MSP	QRAO	ms31	ibm_fez	123	0.691	–	310.00	Y
MSP	QRAO	ms40	ibm_torino	216	0.421	–	485.00	Y
MSP	QRAO	ms41	ibm_fez	216	0.523	–	509.00	Y
MSP	QRAO	ms50	ibm_torino	249	0.369	–	1120.00	Y
MSP	QRAO	ms51	ibm_fez	252	0.469	–	1150.00	Y
MSP	VQE	ms20	ibm_fez	144	0.649	–	4.00	Y
MSP	VQE	ms21	ibm_fez	369	0.33	–	215.00	Y
MSP	VQE	ms30	ibm_fez	252	0.469	–	127.00	Y
MSP	VQE	ms31	ibm_fez	252	0.469	–	12.00	Y
MSP	VQE	ms40	ibm_fez	408	0.294	–	188.00	Y
MSP	VQE	ms41	ibm_fez	408	0.294	–	273.00	Y
MSP	VQE	ms50	ibm_fez	1348	0.017	–	644.00	Y
MSP	VQE	ms51	ibm_fez	1536	0.0099	–	439.00	Y
MSP	WS-QAOA	ms20	ibm_fez	13434	2.96e-18	–	41.00	Y
MSP	WS-QAOA	ms21	ibm_fez	14116	3.81e-19	–	9.00	Y
MSP	WS-QAOA	ms30	ibm_marrakesh	39227	6.529999999999999e-52	–	296.00	Y
MSP	WS-QAOA	ms31	ibm_fez	40149	4.09e-53	–	36.00	Y
MSP	WS-QAOA	ms40	ibm_marrakesh	75459	3.45e-99	–	901.00	Y
MSP	WS-QAOA	ms41	ibm_marrakesh	75459	3.45e-99	–	348.00	Y
MSP	WS-QAOA	ms50	ibm_fez	123414	9.21e-162	–	318.00	Y
MSP	WS-QAOA	ms51	ibm_marrakesh	130345	8.33e-171	–	1024.00	Y
QAP	CVaR-VQE	chr12a	ibm_marrakesh	1389	0.015	–	–	N
QAP	CVaR-VQE	chr12b	ibm_marrakesh	1329	0.018	–	–	N
QAP	CVaR-VQE	chr12c	ibm_marrakesh	1389	0.015	–	–	N
QAP	CVaR-VQE	had12	ibm_marrakesh	1389	0.015	–	–	N
QAP	CVaR-VQE	nug12	ibm_fez	1580	0.00868	–	–	N
QAP	CVaR-VQE	rou12	ibm_fez	1580	0.00868	–	–	N
QAP	CVaR-VQE	scr12	ibm_fez	1580	0.00868	–	–	N
QAP	CVaR-VQE	tai10a	ibm_fez	300	0.406	–	–	N
QAP	CVaR-VQE	tai10b	ibm_fez	300	0.406	–	–	N
QAP	CVaR-VQE	tai12a	ibm_fez	1580	0.00868	–	–	N
QAP	CVaR-VQE	tai12b	ibm_fez	1580	0.00868	–	–	N
QAP	MA-QAOA	chr12a	ibm_fez	83724	5.670000000000001e-110	–	–	N
QAP	MA-QAOA	chr12b	ibm_fez	83936	3.0000000000000004e-110	–	–	N
QAP	MA-QAOA	chr12c	ibm_marrakesh	84276	1.0800000000000001e-110	–	–	N
QAP	MA-QAOA	had12	ibm_fez	173096	1.3700000000000001e-226	–	–	N
QAP	MA-QAOA	nug12	ibm_fez	158188	3.8899999999999996e-207	–	–	N
QAP	MA-QAOA	rou12	ibm_fez	173096	1.3700000000000001e-226	–	–	N

Continued on next page

Table 96 – continued from previous page

Problem	Method	Instance	Backend	N_{2Q}	F_{est}	Sim gap %	HW gap %	Feas
QAP	MA-QAOA	scr12	ibm_fez	127688	2.44e-167	–	–	N
QAP	MA-QAOA	tai10a	ibm_fez	81971	1.1e-107	–	–	N
QAP	MA-QAOA	tai10b	ibm_fez	78718	1.93e-103	–	–	N
QAP	MA-QAOA	tai12a	ibm_fez	170894	1.02e-223	–	–	N
QAP	MA-QAOA	tai12b	ibm_fez	167992	6.2699999999999996e-220	–	–	N
QAP	PCE	chr12a	ibm_fez	440	0.267	234.75	–	N
QAP	PCE	chr12b	ibm_fez	440	0.267	15.47	–	N
QAP	PCE	chr12c	ibm_fez	440	0.267	66.82	–	N
QAP	PCE	had12	ibm_fez	20	0.942	–	–	N
QAP	PCE	nug12	ibm_fez	20	0.942	35.98	–	N
QAP	PCE	rou12	ibm_fez	20	0.942	26.30	–	N
QAP	QAOA	chr12a	ibm_fez	84111	1.77e-110	–	–	N
QAP	QAOA	chr12b	ibm_fez	84111	1.77e-110	–	–	N
QAP	QAOA	chr12c	ibm_fez	84111	1.77e-110	–	–	N
QAP	QAOA	had12	ibm_fez	84111	1.77e-110	–	–	N
QAP	QAOA	nug12	ibm_marrakesh	158163	4.1899999999999994e-207	–	–	N
QAP	QAOA	rou12	ibm_marrakesh	158163	4.1899999999999994e-207	–	–	N
QAP	QAOA	scr12	ibm_marrakesh	158163	4.1899999999999994e-207	–	–	N
QAP	QAOA	tai10a	ibm_fez	74145	1.79e-97	–	–	N
QAP	QAOA	tai10b	ibm_fez	74145	1.79e-97	–	–	N
QAP	QAOA	tai12a	ibm_fez	168995	3.08e-221	–	–	N
QAP	QAOA	tai12b	ibm_marrakesh	158163	4.1899999999999994e-207	–	–	N
QAP	QRAO	chr12a	ibm_fez	165	0.609	–	–	N
QAP	QRAO	chr12b	ibm_fez	183	0.577	–	–	N
QAP	QRAO	chr12c	ibm_fez	159	0.62	–	–	N
QAP	QRAO	had12	ibm_fez	1110	0.036	–	–	N
QAP	QRAO	nug12	ibm_fez	186	0.572	–	–	N
QAP	QRAO	rou12	ibm_torino	1413	0.00347	–	–	N
QAP	QRAO	scr12	ibm_fez	177	0.588	–	–	N
QAP	VQE	chr12a	ibm_fez	1323	0.019	–	–	N
QAP	VQE	chr12b	ibm_fez	1323	0.019	–	–	N
QAP	VQE	chr12c	ibm_fez	1218	0.026	–	–	N
QAP	VQE	had12	ibm_fez	1218	0.026	–	–	N
QAP	VQE	nug12	ibm_fez	1218	0.026	–	–	N
QAP	VQE	rou12	ibm_fez	1218	0.026	–	–	N
QAP	VQE	scr12	ibm_fez	1218	0.026	–	–	N
QAP	VQE	tai10a	ibm_fez	300	0.406	–	–	N
QAP	VQE	tai10b	ibm_fez	300	0.406	–	–	N
QAP	VQE	tai12a	ibm_fez	1218	0.026	–	–	N
QAP	VQE	tai12b	ibm_fez	1134	0.033	–	–	N
QAP	WS-QAOA	chr12a	ibm_fez	84503	5.46e-111	–	–	N

Continued on next page

Table 96 – continued from previous page

Problem	Method	Instance	Backend	N_{2Q}	F_{est}	Sim gap %	HW gap %	Feas
QAP	WS-QAOA	chr12b	`ibm_fez`	84503	5.46e-111	–	–	N
QAP	WS-QAOA	chr12c	`ibm_fez`	84503	5.46e-111	–	–	N
QAP	WS-QAOA	had12	`ibm_marrakesh`	82789	9.410000000000001e-109	–	–	N
QAP	WS-QAOA	nug12	`ibm_fez`	159188	1.9300000000000002e-208	–	–	N
QAP	WS-QAOA	rou12	`ibm_fez`	159188	1.9300000000000002e-208	–	–	N
QAP	WS-QAOA	scr12	`ibm_marrakesh`	159153	2.14e-208	–	–	N
QAP	WS-QAOA	tai10a	`ibm_marrakesh`	77609	5.4e-102	–	–	N
QAP	WS-QAOA	tai10b	`ibm_marrakesh`	77609	5.4e-102	–	–	N

P Classical Baseline Performance

This section reports the classical baseline performance for all benchmark families considered in the paper: the Multi-Dimensional Knapsack Problem (MDKP), Maximum Independent Set (MIS), Quadratic Assignment Problem (QAP), and Market Share Problem (MSP). These results provide a classical reference for interpreting the hardware and simulator outcomes reported in the main text.

For MDKP, MIS, and QAP, we report the performance of exact Gurobi-based integer programming formulations, including the best incumbent found at termination, the final best bound, the relative optimality gap, solver status, and runtime. For MSP, we report the performance of CPLEX using the same summary metrics adopted in the main experimental workflow, namely the search effort in terms of branch-and-bound nodes and simplex/barrier iterations, together with the final gap, solution value, and runtime.

Overall, the classical baselines confirm that the selected benchmark instances span a meaningful range of difficulty. Many MDKP and MIS instances are solved to proven optimality almost immediately, providing a clean reference point for evaluating quantum solution quality. In contrast, several QAP and larger MSP instances remain substantially more challenging: some QAP instances terminate at the time limit with nonzero optimality gaps, while for MSP the larger cases reach the one-hour limit with gaps close to 1. These results support the role of the chosen benchmark families as classically meaningful testbeds rather than trivial small-scale examples.

Table 97. Classical Gurobi performance on MDKP instances. **Size**: items × dimensions. **BKS**: known optimal value from the benchmark file. **Incumbent**: best feasible solution at termination. **Bound**: final best bound. **Gap**: final relative optimality gap. **Status**: solver termination status. All listed instances were solved to proven optimality.

Inst.	Size	BKS	Inc.	Bound	Gap (%)	Status	Time (s)
hp1	28×4	3 418	3 418	3 418	0.0	OPT	0.01
hp2	35×4	3 186	3 186	3 186	0.0	OPT	0.00
pb1	27×4	3 090	3 090	3 090	0.0	OPT	0.00
pb2	34×4	3 186	3 186	3 186	0.0	OPT	0.00
pb4	29×2	95 168	95 168	95 168	0.0	OPT	0.00
pb5	20×10	2 139	2 139	2 139	0.0	OPT	0.02
pet2	10×10	87 061	87 061	87 061	0.0	OPT	0.00
pet3	15×10	4 015	4 015	4 015	0.0	OPT	0.00
pet4	20×10	6 120	6 120	6 120	0.0	OPT	0.00
pet5	28×10	12 400	12 400	12 400	0.0	OPT	0.01
pet6	39×5	10 618	10 618	10 618	0.0	OPT	0.00
pet7	50×5	16 537	16 537	16 537	0.0	OPT	0.09

Table 98. Classical Gurobi performance on MIS instances. $|V|$: number of vertices. $|E|$: number of edges. **BKS**: known optimal independent-set size. **Incumbent**: best feasible solution at termination. **Bound**: final best bound. **Gap**: final relative optimality gap. All listed instances were solved to proven optimality.

Instance	$\|V\|$	$\|E\|$	BKS	Incumbent	Bound	Gap (%)	Status	Time (s)
1dc.64	64	543	10	10	10	0.0	OPT	0.00
1dc.128	128	1 471	16	16	16	0.0	OPT	0.02
1et.64	64	264	18	18	18	0.0	OPT	0.00
1tc.8	8	6	4	4	4	0.0	OPT	0.00
1tc.16	16	22	8	8	8	0.0	OPT	0.00
1tc.32	32	68	12	12	12	0.0	OPT	0.00
1tc.64	64	192	20	20	20	0.0	OPT	0.00

Table 99. Classical Gurobi performance on QAP instances. n: number of facilities/locations. **BKS**: known optimal objective value. **Incumbent**: best feasible solution at termination. **Bound**: final best bound. **Gap**: final relative optimality gap. **Status**: solver termination status. Entries with status TL reached the imposed time limit (100 seconds) before proving optimality.

Instance	n	**BKS**	**Incumbent**	**Bound**	**Gap (%)**	**Status**	**Time (s)**
chr12a	12	9 552	9 552	9 552	0.0	OPT	0.36
chr12b	12	9 742	9 742	9 742	0.0	OPT	0.21
chr12c	12	11 156	11 156	11 156	0.0	OPT	2.00
had12	12	1 652	1 652	1 260	23.7	TL	100.00
nug12	12	578	578	578	0.0	OPT	98.41
rou12	12	235 528	235 528	131 514	44.2	TL	100.00
scr12	12	31 410	31 410	31 410	0.0	OPT	0.89
tai10a	10	135 028	135 028	135 028	0.0	OPT	5.82
tai10b	10	1 183 760	1 183 760	1 183 760	0.0	OPT	0.62
tai12a	12	224 416	224 416	142 796	36.4	TL	100.00
tai12b	12	39 464 925	39 464 894.17	39 464 894.17	0.0	OPT	11.17

Table 100. CPLEX solver performance on Market Share Problem instances. **Gap**: relative difference between incumbent and lower bound (values near 1 indicate the solver could not close the gap within the time limit). **Nodes**: branch-and-bound nodes explored. **Iters**: simplex/barrier iterations. For sizes 6×50 and above, a one-hour time limit was imposed.

Size	**Nodes**	**Iters**	**Gap**	**Sol.**	**Time (s)**
3×20	7 552	9 776	0.0	3	2.97
3×20	7 270	9 035	0.0	2	1.70
3×20	7 559	10 287	0.0	3	2.05
3×20	9 205	11 446	0.0	3	1.13
3×20	8 301	11 358	0.0	2	1.47
4×30	765 655	1 622 772	0.0	1	5.64
4×30	72 436	138 158	0.0	0	5.92
4×30	439 294	960 557	0.0	2	7.33
4×30	538 857	1 197 837	0.0	1	9.28
4×30	772 561	1 687 113	0.0	1	7.33
5×40	50 288 061	117 363 318	0.0	1	777
5×40	72 691 565	173 591 038	0.0	1	1 076
5×40	65 010 492	153 229 808	0.0	1	777
5×40	41 687 999	98 461 473	0.0	1	292
5×40	14 683 912	36 843 546	0.0	0	95
6×50	263 122 381	682 375 105	≈1	1	3 607
6×50	433 287 296	1 046 486 269	≈1	2	3 600
6×50	426 949 570	1 037 766 414	≈1	2	3 600
6×50	544 066 780	1 327 364 155	≈1	2	3 600
6×50	477 967 274	1 147 025 106	≈1	2	3 600
7×60	448 161 278	1 166 369 595	≈1	4	3 617
7×60	344 532 350	910 970 829	≈1	6	3 617
7×60	409 426 464	1 086 559 026	≈1	5	3 617
7×60	491 680 008	1 327 295 105	≈1	5	3 619
7×60	426 054 792	1 120 381 222	≈1	6	3 617

Q Simulator Resource Usage by Problem and Method

This appendix reports the computational resource usage for each method–instance combination under simulator-based evaluation. These tables complement the hardware diagnostics by providing the algorithmic-level circuit baseline before transpilation and backend-specific effects are introduced.

Q.1 MDKP resource usage

Table 101. MDKP simulator resource usage for VQE, CVaR-VQE, and PCE

Inst.	Method	Q	D	G	2Q	P	Time (min)
hp1	VQE	60	75	836	236	600	351.9
	CVaR-VQE	60	71	557	177	480	246.8
	PCE	7	336	1568	336	364	72.5
hp2	VQE	67	82	934	264	670	395.0
	CVaR-VQE	67	78	734	198	538	384.3
	PCE	8	384	2080	448	480	125.8
pb1	VQE	59	74	822	232	590	344.1
	CVaR-VQE	59	70	646	174	472	241.6
	PCE	7	336	1568	336	364	71.0
pb2	VQE	66	81	920	260	660	385.2
	CVaR-VQE	66	77	723	195	528	312.2
	PCE	8	384	2080	448	480	119.0
pb4	VQE	45	60	626	176	450	261.9
	CVaR-VQE	45	56	492	132	360	174.4
	PCE	6	288	1128	240	264	28.1
pb5	VQE	116	131	1620	460	1160	678.6
	CVaR-VQE	116	127	1273	345	928	593.7
	PCE	10	480	3320	720	760	336.5
pet2	VQE	99	114	1382	392	990	578.8
	CVaR-VQE	99	110	1086	294	792	467.2
	PCE	9	432	2664	576	612	151.3
pet3	VQE	102	117	1424	404	1020	596.4
	CVaR-VQE	102	113	1119	303	816	565.9
	PCE	9	432	2664	576	612	187.1
pet4	VQE	107	122	1494	424	1070	625.8
	CVaR-VQE	107	118	1174	318	856	517.3
	PCE	9	432	2664	576	612	175.3
pet5	VQE	122	137	1704	484	1220	713.8
	CVaR-VQE	122	133	1339	363	976	576.8
	PCE	10	480	3320	720	760	345.5
pet6	VQE	86	101	1210	340	860	502.5
	CVaR-VQE	86	97	943	255	688	477.5
	PCE	9	432	2664	576	612	198.3
pet7	VQE	100	115	1396	396	1000	584.7
	CVaR-VQE	100	111	1097	297	800	550.1
	PCE	9	432	2664	576	612	198.6

Q.2 MIS resource usage

Q.3 QAP resource usage

Q.4 MSP resource usage

Table 102. MIS simulator resource usage for VQE, CVaR-VQE, PCE, QRAO, QAOA, and MA-QAOA. Execution time is reported in seconds. M.E. denotes memory exhaustion.

Inst.	**Method**	**Q**	**D**	**G**	**2Q**	**P**	**Time (s)**
1tc.8	VQE	8	19	85	21	64	3.1
	CVaR-VQE	8	15	62	14	48	1.4
	PCE	3	144	240	48	60	0.6
	QRAO	4	11	30	6	24	1.4
	QAOA	8	12	42	12	30	15.2
	MA-QAOA	8	6	30	6	22	1.5
1tc.16	VQE	16	27	173	45	128	17.4
	CVaR-VQE	16	23	126	30	96	14.3
	PCE	4	192	464	96	112	1.9
	QRAO	6	13	54	10	34	4.3
	QAOA	16	30	114	44	70	52.4
	MA-QAOA	16	12	70	22	54	4.3
1tc.32	VQE	32	43	349	93	256	68.2
	CVaR-VQE	32	39	254	62	192	54.4
	PCE	6	288	1128	240	264	9.9
	QRAO	13	20	102	24	78	111.2
	QAOA	32	54	300	136	164	158.7
	MA-QAOA	32	20	164	68	132	11.8
1tc.64	VQE	64	75	701	189	512	248.2
	CVaR-VQE	64	71	510	126	384	186.6
	PCE	8	384	2080	448	480	34.7
	QRAO	23	30	182	44	138	310.1
	QAOA	64	105	768	384	384	702.4
	MA-QAOA	64	32	350	145	286	47.9
1et.64	VQE	62	73	679	183	496	218.5
	CVaR-VQE	62	69	494	122	372	156.2
	PCE	7	336	1568	336	364	26.8
	QRAO	24	31	190	46	144	516.6
	QAOA	62	105	978	528	450	812.8
	MA-QAOA	62	37	414	210	352	2 668.7
1dc.64	VQE	50	61	547	147	400	231.4
	CVaR-VQE	50	57	398	98	300	184.1
	PCE	7	336	1568	336	364	31.9
	QRAO	18	25	142	34	108	133.0
	QAOA	50	252	1377	818	559	M.E.
	MA-QAOA	50	86	559	409	509	3 135.2

Table 103. QAP simulator resource usage for VQE, CVaR-VQE, and PCE

Inst.	Method	Q	D	G	2Q	P	Time (min)
chr12a	VQE	144	163	2443	715	1728	1 917.5
	CVaR-VQE	144	163	2443	715	1728	777.4
	PCE	11	528	4048	880	924	537.6
chr12b	VQE	144	163	2443	715	1728	1 927.9
	CVaR-VQE	144	163	2443	715	1728	772.5
	PCE	11	528	4048	880	924	592.7
chr12c	VQE	144	163	2443	715	1728	1 910.4
	CVaR-VQE	144	163	2443	715	1728	760.2
	PCE	11	528	4048	880	924	930.5
nug12	VQE	144	163	2443	715	1728	1 947.8
	CVaR-VQE	144	163	2443	715	1728	765.6
	PCE	11	528	4048	880	924	1 169.1
rou12	VQE	144	163	2443	715	1728	1 961.6
	CVaR-VQE	144	163	2443	715	1728	796.5
	PCE	11	528	4048	880	924	1 500.4
scr12	VQE	144	163	2443	715	1728	1 906.6
	CVaR-VQE	144	163	2443	715	1728	783.4
	PCE	11	528	4048	880	924	831.4
tai12a	VQE	144	163	2443	715	1728	1 883.8
	CVaR-VQE	144	163	2443	715	1728	755.5
	PCE	11	528	4048	880	924	1 545.3
tai12b	VQE	144	163	2443	715	1728	1 911.3
	CVaR-VQE	144	163	2443	715	1728	789.0
	PCE	11	528	4048	880	924	1 206.2

Table 104. MSP simulator resource usage for VQE, CVaR-VQE, and PCE

Inst.	Method	Q	D	G	2Q	P	Time (min)
2×10 S0	VQE	50	69	845	245	600	2 135.7
	CVaR-VQE	50	69	845	245	600	1 727.8
	PCE	7	336	1568	336	364	55.4
2×10 S1	VQE	46	65	777	225	552	1 680.0
	CVaR-VQE	46	65	777	225	552	1 343.8
	PCE	7	336	1568	336	364	47.4
3×20 S0	VQE	84	103	1423	415	1008	2 050.6
	CVaR-VQE	84	103	1423	415	1008	1 358.7
	PCE	8	384	2080	448	480	164.9
3×20 S1	VQE	80	99	1355	395	960	2 494.1
	CVaR-VQE	80	99	1355	395	960	1 857.6
	PCE	8	384	2080	448	480	155.6
4×30 S0	VQE	118	137	2001	585	1416	4 283.2
	CVaR-VQE	118	137	2001	585	1416	3 629.8
	PCE	10	480	3320	720	760	504.6
4×30 S1	VQE	118	137	2001	585	1416	4 663.9
	CVaR-VQE	118	137	2001	585	1416	3 712.6
	PCE	10	480	3320	720	760	512.2
5×40 S0	VQE	154	165	1691	459	1232	6 956.9
	CVaR-VQE	154	165	1691	459	1232	5 958.5
	PCE	11	528	4048	880	924	1 029.2
5×40 S1	VQE	154	165	1691	459	1232	6 693.6
	CVaR-VQE	154	165	1691	459	1232	5 719.3
	PCE	11	528	4048	880	924	1 020.9

References

[1] Abbas A, Ambainis A, Augustino B, Bärtschi A, Buhrman H, Coffrin C J, Cortiana G, Dunjko V, Egger D J, Elmegreen B G *et al.* 2023 Quantum optimization: Potential, challenges, and the path forward Tech. rep. Los Alamos National Laboratory (LANL)

[2] Peruzzo A, McClean J, Shadbolt P, Yung M H, Zhou X Q, Love P J, Aspuru-Guzik A and O'Brien J L 2014 *Nature Communications* **5** ISSN 2041-1723 URL http://dx.doi.org/10.1038/ncomms5213

[3] Barkoutsos P K, Nannicini G, Robert A, Tavernelli I and Woerner S 2020 *Quantum* **4** 256 ISSN 2521-327X URL http://dx.doi.org/10.22331/q-2020-04-20-256

[4] Farhi E, Goldstone J and Gutmann S 2014 *arXiv preprint arXiv:1411.4028*

[5] Sciorilli M, Borges L, Patti T L, García-Martín D, Camilo G, Anandkumar A and Aolita L 2025 *Nature Communications* **16** ISSN 2041-1723 URL http://dx.doi.org/10.1038/s41467-024-55346-z

[6] Fuller B, Hadfield C, Glick J R, Imamichi T, Itoko T, Thompson R J, Jiao Y, Kagele M M, Blom-Schieber A W, Raymond R *et al.* 2024 *IEEE Transactions on Quantum Engineering* **5** 1–15

[7] Koch T, Bernal Neira D E, Chen Y, Cortiana G, Egger D J, Heese R, Hegade N N, Gomez Cadavid A, Huang R, Itoko T *et al.* 2025 *arXiv e-prints* arXiv–2504

[8] Lubinski T, Johri S, Varosy P, Coleman J, Zhao L, Necaise J, Baldwin C H, Mayer K and Proctor T 2023 *IEEE Transactions on Quantum Engineering* **4** 1–32 ISSN 2689-1808 URL http://dx.doi.org/10.1109/TQE.2023.3253761

[9] Dupont M, Sundar B, Evert B, Neira D E B, Peng Z, Jeffrey S and Hodson M J 2025 *Physical Review Applied* **23** ISSN 2331-7019 URL http://dx.doi.org/10.1103/PhysRevApplied.23.014045

[10] Brandhofer S, Braun D, Dehn V, Hellstern G, Hüls M, Ji Y, Polian I, Bhatia A S and Wellens T 2022 *Quantum Information Processing* **22** ISSN 1573-1332 URL http://dx.doi.org/10.1007/s11128-022-03766-5

[11] Li A C Y, Alam M S, Iadecola T, Jahin A, Job J, Kurkcuoglu D M, Li R, Orth P P, Özgüler A B, Perdue G N and Tubman N M 2023 *Physical Review Research* **5** ISSN 2643-1564 URL http://dx.doi.org/10.1103/PhysRevResearch.5.033071

[12] Shaydulin R, Li C, Chakrabarti S, DeCross M, Herman D, Kumar N, Larson J, Lykov D, Minssen P, Sun Y, Alexeev Y, Dreiling J M, Gaebler J P, Gatterman T M, Gerber J A, Gilmore K, Gresh D, Hewitt N, Horst C V, Hu S, Johansen J, Matheny M, Mengle T, Mills M, Moses S A, Neyenhuis B, Siegfried P, Yalovetzky R and Pistoia M 2024 *Science Advances* **10** ISSN 2375-2548 URL http://dx.doi.org/10.1126/sciadv.adm6761

[13] McDowall K, Kapourniotis T, Oliver C, Lolur P and Georgopoulos K 2026 Cross-platform benchmarking of near-term quantum optimisation algorithms (*Preprint* 2504.06885) URL https://arxiv.org/abs/2504.06885

[14] Chekuri C and Khanna S 2004 *SIAM Journal on Computing* **33** 837–851

[15] Lawler E L, Lenstra J K and Rinnooy Kan A 1980 *SIAM Journal on Computing* **9** 558–565

[16] Sahni S and Gonzalez T 1976 *Journal of the ACM* **23** 555–565

[17] Kellerer H, Pferschy U and Pisinger D 2004 *Multidimensional Knapsack Problems* (Berlin, Heidelberg: Springer Berlin Heidelberg) pp 235–283 ISBN 978-3-540-24777-7 URL https://doi.org/10.1007/978-3-540-24777-7_9

[18] Garey M R and Johnson D S 1979 *Computers and Intractability: A Guide to the Theory of NP-Completeness* (W. H. Freeman and Company)

[19] Koopmans T C and Beckmann M 1957 *Econometrica* **25** 53–76 ISSN 00129682, 14680262 URL http://www.jstor.org/stable/1907742

[20] Cornuéjols G and Dawande M 1999 *INFORMS Journal on Computing* **11** 205–210 URL https://doi.org/10.1287/ijoc.11.2.205

[21] Cerezo M, Arrasmith A, Babbush R, Benjamin S C, Endo S, Fujii K, McClean J R, Mitarai K, Yuan X, Cincio L and Coles P J 2021 *Nature Reviews Physics* **3** 625–644 ISSN 2522-5820 URL http://dx.doi.org/10.1038/s42254-021-00348-9

[22] Blekos K, Brand D, Ceschini A, Chou C H, Li R H, Pandya K and Summer A 2024 *Physics Reports* **1068** 1–66 ISSN 0370-1573 URL http://dx.doi.org/10.1016/j.physrep.2024.03.002

[23] Tilly J, Chen H, Cao S, Picozzi D, Setia K, Li Y, Grant E, Wossnig L, Rungger I, Booth G H and Tennyson J 2022 *Physics Reports* **986** 1–128 ISSN 0370-1573 URL http://dx.doi.org/10.1016/j.physrep.2022.08.003

[24] Cerezo M, Sone A, Volkoff T, Cincio L and Coles P J 2021 *Nature Communications* **12** ISSN 2041-1723 URL http://dx.doi.org/10.1038/s41467-021-21728-w

[25] Egger D J, Mareček J and Woerner S 2021 *Quantum* **5** 479 ISSN 2521-327X URL http://dx.doi.org/10.22331/q-2021-06-17-479

[26] Herrman R, Lotshaw P C, Ostrowski J, Humble T S and Siopsis G 2022 *Scientific Reports* **12** 6781

[27] McDowall K, Kapourniotis T, Oliver C, Lolur P and Georgopoulos K 2025 *arXiv preprint arXiv:2504.06885*

[28] Turati G, Dacrema M F and Cremonesi P 2023 Benchmarking adaptative variational quantum algorithms on qubo instances (*Preprint* 2308.01789) URL https://arxiv.org/abs/2308.01789

[29] Schwägerl T, Chai Y, Hartung T, Jansen K and Kühn S 2026 *Quantum Machine Intelligence* **8** ISSN 2524-4914 URL http://dx.doi.org/10.1007/s42484-026-00355-y

[30] Fréville A 2004 *European Journal of Operational Research* **155** 1–21

[31] Butenko S and Pardalos P M 2002 *Handbook of Applied Optimization* 403–413

[32] Loiola E M, de Abreu N M M, Boaventura-Netto P O, Hahn P and Querido T 2007 *European Journal of Operational Research* **176** 657–690

[33] Burkard R E, Karisch S E and Rendl F 1997 Qaplib – a quadratic assignment problem library https://coral.ise.lehigh.edu/data-sets/qaplib/ accessed: 2025-02-12

[34] Cornuejols G and Dawande M 1999 *Manufacturing and Service Operations Management* Also described in QOBLIB benchmark suite

[35] Puchinger J, Raidl G R and Pferschy U 2010 *INFORMS Journal on Computing* **22** 250–265

[36] Drake J 2015 Benchmark instances for the multidimensional knapsack problem

[37] Sloane N J A 2000 Challenge problems: Independent sets in graphs accessed: January 14, 2025 URL https://oeis.org/A265032/a265032.html

[38] Montanez-Barrera J A, Ji Y, von Spakovsky M R, Neira D E B and Michielsen K 2025 Optimizing qaoa circuit transpilation with parity twine and swap network encodings (*Preprint* 2505.17944) URL https://arxiv.org/abs/2505.17944

[39] Montañez-Barrera J A and Michielsen K 2025 *npj Quantum Information* **11** ISSN 2056-6387 URL http://dx.doi.org/10.1038/s41534-025-01082-1

[40] McDowall K, Georgopoulos K and Wallden P 2026 Spectral gap informed ramp qaoa (*Preprint* 2604.24580) URL https://arxiv.org/abs/2604.24580

[41] Lucas A 2014 *Frontiers in Physics* **2** 5

[42] Kochenberger G, Hao J K, Glover F, Lewis M, Lü Z, Wang H and Wang Y 2014 *Journal of Combinatorial Optimization* **28** 58–81

[43] Javadi-Abhari A, Treinish M, Krsulich K, Wood C J, Lishman J, Gacon J, Martiel S, Nation P D, Bishop L S, Cross A W *et al.* 2024 *arXiv preprint arXiv:2405.08810*

[44] IBM Quantum 2024 Heron r2: A 156-qubit quantum processor with TLS mitigation and enhanced coherence IBM Quantum Developer Conference announcement, November 2024. Available at https://www.ibm.com/quantum/hardware accessed during experimental window of this study

[45] IBM Quantum 2025 IBM Quantum Developer Roadmap: Nighthawk, Heron, and beyond Available at https://www.ibm.com/quantum/technology Nighthawk processor targets approximately 5000 two-qubit gates initially, with subsequent iterations projected for 7500 (2026), 10000 (2027), and 15000 (2028) gates through long-range couplers.

[46] Temme K, Bravyi S and Gambetta J M 2017 *Physical Review Letters* **119** 180509

[47] Endo S, Benjamin S C and Li Y 2018 *Physical Review X* **8** ISSN 2160-3308 URL http://dx.doi.org/10.1103/PhysRevX.8.031027

[48] Polják S and Turzík D 1986 *Journal of Combinatorial Theory, Series B* **40** 99–103